

**GEOCHEMICAL AND SPECTRAL
CHARACTERIZATION OF
HYDROTHERMAL ALTERATION
FACIES AT THE EPITHERMAL
GOLD MINERALIZATION AT
RODALQUILAR, SPAIN**

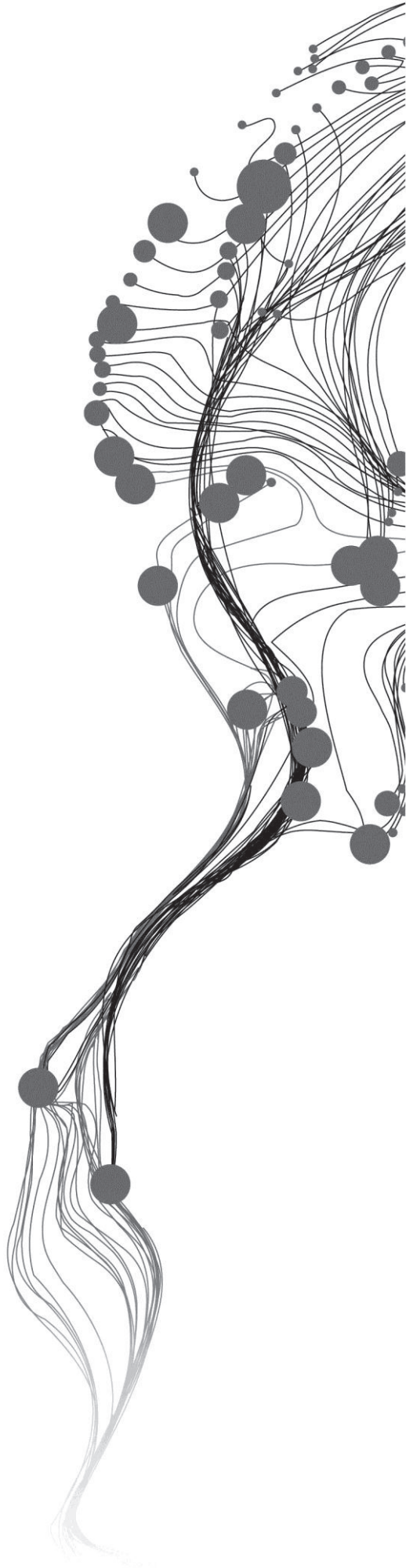
KAMINA CHOROROKA

February, 2012

SUPERVISORS:

Drs. J.B, (Boudewijn) De Smeth

Dr., F.J.A, (Frank) van Ruitenbeek



GEOCHEMICAL AND SPECTRAL CHARACTERIZATION OF HYDROTHERMAL ALTERATION FACIES AT THE EPITHERMAL GOLD MINERALIZATION AT RODALQUILAR. SPAIN

KAMINA CHOROROKA

Enschede, The Netherlands, February, 2012

Thesis submitted to the Faculty of Geo-Information Science and Earth Observation of the University of Twente in partial fulfilment of the requirements for the degree of Master of Science in Geo-information Science and Earth Observation.

Specialization: Earth Resources Exploration

SUPERVISORS:

Drs. J.B. (Boudewijn) De Smeth

Dr., F.J.A. (Frank) van Ruitenbeek

THESIS ASSESSMENT BOARD:

Prof. Dr. F.D. (Freek) van der Meer (Chair)

Dr. Mike Buxton (External Examiner, University of Delft – Dept. of Geotechnology - Civil Engineering & Geosciences)

DISCLAIMER

This document describes work undertaken as part of a programme of study at the Faculty of Geo-Information Science and Earth Observation of the University of Twente. All views and opinions expressed therein remain the sole responsibility of the author, and do not necessarily represent those of the Faculty.

ABSTRACT

Epithermal gold deposits are a type of lode mineral deposits consisting of economic concentrations of Au \pm Ag and base metals. These deposits form in a variety of host rocks from ascending hydrothermal fluids, primarily by replacement and/or by open-space filling. The present study aims to test whether direct field data of major and trace elements can be used in combination with mineralogical IR information for the exploration of the epithermal gold deposits.

89 rock-samples were available for portable XRF and ASD spectral measurements, these samples were collected in 2004 along two perpendicular traverses by ITC students over the Rodalquilar epithermal gold deposit. Rodalquilar Gold Mine forms part of the Cabo de Gata National Park area which is located close to the coast in the Almeria Province in the south-eastern part of Spain. The total area covered in this study is approximately 56 km². Fine rock powder samples for XRF analysis, were prepared by grinding the samples using a Tema disk mill and a mullite hand mortar.

Rocks in the study area range in compositions from andesite to rhyolites. Element concentrations of major and trace elements together with mineralogical information were used to study the lithological differences and alteration style/intensity on the study area. Positive correlations between SiO₂, Al₂O₃, TiO₂, Zr, and Sr are observed which is linked to the lithological association, also a positive correlation is observed between As and S which is associated with mineralization.

The portable XRF results show that Zr and Ti are the most suitable elements to discriminate andesites and rhyolites lithologies. The Silicification and Hashigushi Indices calculated from the whole rock geochemistry, proved to be most effective in delineating argillic-advanced argillic alteration styles for the epithermal deposits.

Spectral NIR detectable parameters such as kaolinite crystallinity and mineral chemistry (Al-OH position and depth) indicate the potential application of reflectance spectroscopy in the characterizing alteration and elements associations within the Rodalquilar study area. Kaolinite crystallinity shows a special pattern, whereby the highly altered mineralized areas are characterized by low value of the crystallinity index and the least altered, peripheral zone is characterized by high values of this index. It is shown also that the central part, which is the highly mineralized part of the study area, is dominated by higher depth of the Al-OH absorption feature at 2200nm as compared to the surrounding area.

The overall results indicate that by using data obtained with a portable XRF and a NIR field spectrometer, it is possible to differentiate between lithologies, different alteration styles and intensities. In addition the Zr- Ti relationship can be used to characterize different volcanic lithologies in an epithermal gold environment. setting like Rodalquilar.

ACKNOWLEDGEMENTS

First, I am grateful to Allah, the almighty God for giving me sustenance, strength and wisdom for the successful completion of my MSc program. Secondly, I would like to thank the Dutch Government, through NUFFIC for the Scholarship, which made this study possible.

My gratitude is extended to all who assisted me in completing this component of my research undertakings. Special thanks are due to my supervisors; Drs Boudewijn de Smeth and Dr. F.A.J. van Ruitenbeek. Thanks are also due to Dr. E.J.M. Carranza, Dr. T. Woldai and Dr. M.F. Noomen for their valuable instructions during my studies in AES (Exploration stream). Special thanks are also due to Drs. Tom Loran (the then AES course director) and Dr. Rossiter.

Sincere gratitude to Twigg gold (T) ltd for granting me study leave, I am indebted to Mr Benjamin Clavery Safi for proof reading and constructive comments. Gold finders of Tanzania is appreciated for its logistics supports.

To my fellow students who were never too busy to consider an idea or discuss a question – I am grateful to you all. Special thanks go out to Mohammed Abweny, Fitriani Agustin, Chandima Fernando and Sarah Herbert.

Finally, I would like to thank my family, my dear wife Zaytun and sons Tojo and Abdul, for without their support none of this would be possible.

To all, I say Thank you very much.

Kamina Chororoka.

TABLE OF CONTENTS

Abstract	i
Acknowledgements	ii
List of figures	v
List of tables	vii
1. INTRODUCTION.....	1
1.1. Background of the reserch	1
1.2. Research problem	1
1.3. Motivation.....	1
1.4. Research objectives.....	2
1.5. Research queastions.....	2
1.6. Research hypothesis.....	2
1.7. Data sets	2
1.8. Thesis outline.....	3
2. EPITHERMAL GOLD-GENERAL OVERVIEW	5
2.1. What is epithermal gold?.....	5
2.2. Geological, mineralogical and geochemical characteristics of epithermal gold.....	5
2.2.1. Conceptual model of epithermal gold	9
2.3.1. High sulphidation epithermal gold.....	10
2.3.2. Low Sulphdation deposits	10
2.4. Exploration for epithermal gold.....	11
2.5. Summary.....	12
3. THE STUDY AREA.....	13
3.1. General	13
3.2. Regional geology	13
3.3. Local geology.....	13
3.4. The Rodalqular deposit.....	15
3.5. Previous explorations/ mining works	16
3.6. Concluding remarks.....	16
4. ANALYSIS OF GEOCHEMICAL DATA	17
4.1. Overall research methodology	17
4.2. Geochemical data collection, processing and interpretation.	17
4.2.1. Univariate statistical analysis.	24
4.2.2. Mapping of Uni-elements populations.....	26
4.2.3. Multi-variate statistical analysis.	30
4.2.4. Litho geochemistry.	34
4.2.4.1.Trace elements geochemistry.	34
4.2.4.2.Alteration Indices	37
4.3. Concluding remarks.....	41
5. ANALYSIS OF ASD SPECTRAL DATA FOr IDENTIFICATION OF ALTERATION MINERALOGY.....	43
5.1. IR spectra data collection, processing and interpretation	43
5.2. The reflectance properties of minerals.....	44
5.3. Identified minerals and their diagnostic absorption features.....	46
5.3.1. Kandite minerals group.....	47

5.3.2. Smectite	49
5.3.3. Sulphate group	50
5.3.4. Illite-Sericite-Muscovite group	50
5.3.5. Pyrophyllite group	51
5.4. Distribution of alteration minerals.....	55
5.5. Concluding remarks.	55
6. DATA INTEGRATION	57
6.1. Introduction.....	57
6.2. Mineralization.....	57
6.3. Alterations.....	59
6.4. Lithology.	62
6.5. Geochemical parameters in relation to ASD parameters.....	63
6.5.1. Alteration indices and Al-OH absorption features	63
6.5.2. Lithology and Al-OH absorption features	64
6.6. Concluding remarks	65
7. CONCLUSIONS AND RECOMMENDATIONS.....	67
7.1. Conclusion	67
7.2. Recommendations.	68
List of references	69
Appendices.....	73

LIST OF FIGURES

Figure 2.1: A and B .Epithermal gold deposits. Showing characteristics geological, mineralogical and geochemical for low and high sulphidation epithermal deposits.....	7
Figure 2.2: (A) Temperature and pH range of hydrothermal mineral phases in epithermal system: (B) Simplified scheme of distribution of hydrothermal minerals in low and high sulphidation epithermal systems.	8
Figure 2.3: Graph to illustrate schematically the various processes deduced for volcanic-hydrothermal and geothermal systems, and the respective environments of high-sulfidation and low-sulfidation	9
Figure 2.4: Section through a typical high-sulfidation orebody	10
Figure 2.5: Schematic section that generalizes patterns of alteration in a low-sulfidation system.....	11
Figure 3.1: Location map of study area, showing simplified geology of the area. After Arribas, 1995.....	14
Figure 3.2: A simplified geological Map of Rodalquilar, after Arribas, 1995.....	15
Figure 4.1: Flow chart of the methodology followed in this research.	17
Figure 4.2: Location map of Rodalquilar showing the two traverse of samples.	19
Figure 4.3: Plots of ITC Niton PXRF (Horizontal) against Utrecht lab XRF results (Vertical) for some elements.....	22
Figure 4.4: Thompson and Howarth plots of duplicate measurements	23
Figure 4.5: Exploratory data analysis. Histograms (both non transformed and Clr transformed)	25
Figure 4.6: Histograms of Clr transformed data for As and S	26
Figure 4.7: Histograms of Clr transformed data for Zn and Pb.....	27
Figure 4.8: Geochemical map of As and S distribution within Rodalquilar gold deposits.....	28
Figure 4.9: Geochemical map of Zn distribution within Rodalquilar gold deposit.....	29
Figure 4.10: Components plot of the scores for the Clr transformed data.....	31
Figure 4.11: A, B and C scatter plots of factor1 against factor2, factor3 and factor4 respectively.....	32
Figure 4.12: A and B Geochemical map of factor 1 and factor 3, representing lithology and mineralization respectively.....	33
Figure 4.13: TiO ₂ vs. Al ₂ O ₃ for Arriba’s 1995 dataset left and Niton readings right.....	35
Figure 4.14: Zr/TiO ₂ vs. SiO ₂ for Arribas 1995 dataset, left and Niton readings right.....	35
Figure 4.15: Zr (ppm) vs. Al ₂ O ₃ % for Arribas 1995 dataset, left and Niton readings right.	36
Figure 4.16: Zr (ppm) vs. TiO ₂ % for Arribas 1995 dataset, left and Niton readings right.....	36
Figure 4.17: Box plot and modified box plot, left and right respectively, for Arriba’s 1995 dataset.	38
Figure 4.18: Plot of conventional alteration box plot overlaid to modified alteration box plot data from Arribas.....	39
Figure 4.19: Plots of modified alteration box plot index (A) and (B) grouped by lithology type and by dominant mineralogy respectively compared to Silicified versus Hashigushi	40
Figure 5.1: ASD FieldSpec Pro diagram.....	43
Figure 5.2: Spectra signature diagram. The width of the black bars indicate the relative widths of absorption bands (adapted from Clark, 1999)	45
Figure 5.3: Spectra showing kandite minerals group observed , Kaolinite A and Halloysite B.....	47
Figure 5.4: Spatial variation of dominant mineralogy overlaid on the alteration Map of Aster band ratio modified after Arribas 1990 alteration Map	48
Figure 5.5: Spectra of montmorillonite observed in the study area	49
Figure 5.6: Plots of the crystallinity of illite and muscovite (A), grouped by dominant mineralogy, and crystallnityof illite and muscovite (B) grouped by secondary mineralogy	50
Figure 5.7: Spectra of pyrophyllite mineral observed within the study area	51

Figure 5.8: Spectra of sulphate minerals, K-Alunite and alunite (A) and illite-sericite-muscovite minerals, illite and muscovite (B).....	52
Figure 5.9: Histogram of alteration minerals grouped by lithology	52
Figure 5.10: Minerals observed in the area, grouped according to their host rocks, based on the interpretations of the dominant minerals.....	53
Figure 5.11: A location plot showing dominant mineralogy overlain to geological map of the study area..	54
Figure 6.1: Box plot of geochemical parameters associated to mineralization related to dominant spectrally detectable mineralogy	57
Figure 6.2: The spatial variation of scores of factor3 related to hydrothermal alteration. The plot shows a clear zonation of alteration intensity within Rodalquilar gold deposit.	58
Figure 6.3: Scatter plot of As versus S within Rodalquilar gold deposit, grouped by the dominant spectrally detectable mineralogy. Plot shows no proper trend between As and S with the alteration mineralogy.	59
Figure 6.4: (A). Hashigushi (HI) index overlaid to HyMap ratio color composite image of the area. (B) Silicified (SI) indices overlying the HyMap ratio color-composite ..	61
Figure 6.5: Scatter plots of geochemical elements which are useful in discriminating the lithology within the Rodalquilar gold deposit.....	62
Figure 6.6: Factor3 geochemical map overlying the HyMap ratio color-composite image.....	63
Figure 6.7: Scatter Plots of modified Ishikawa index (AI) versus wavelength position of Al-OH absorption feature near 2200 nm(left) and modified CCPI index versus wavelength position of Al-OH absorption feature near 2200 nm (right).....	64
Figure 6.8: Box plots of Al-OH features , depth of Al-OH absorption feature in nm (right) and wavelength position near 2200 (nm) (left) , grouped by lithology.....	65
Figure 6.9: Point Map of depth of Al-OH overlying the geological map of the area.	65

LIST OF TABLES

Table 2.1: Geochemical associations of epithermal gold deposits.	6
Table 4.1: Calibration correction factors for some of the elements , to improve the data quality of Niton readings.....	22
Table 4.2: Correlation matrix of the Clr transformed data.	30
Table 4.3: Factor scores of the clr transformed data.	31
Table 4.4: Samples from Arriba’s 1995.Showing chemical composition of selected rocks types representative of the study area.....	34
Table 5.1: ASD Fieldspec Pro instrument specifications.....	43
Table 5.2: Spectra parameters of kaolinite , a subset of samples observed to have kaolinite as the dominant mineralogy.....	49

1. INTRODUCTION

1.1. Background of the research

Mineral resources exploration is a multi-stage activity, from small scale to large scale, which at last stage will lead to the selection of the sites as targets for drilling. At small regional scale level, idea is to delineate general zones, which may be of potential interest for a selected type of mineral deposit, usually on broad geological considerations, regional geological maps and information from RS data and airborne geophysics.

At medium scale, parts of the general zones are selected for more detailed follows-up exploration based on evidence from geological mapping, geochemical/ geophysical surveys and the location of known mineral occurrences.

At large scale, in this case, the deposit scale, this involves more detailed work such as trenching, and drilling.

1.2. Research problem

Despite some impressive advances in exploration technology in the last decades, chances of discovering new mineral deposits are getting restricted. With the increasing demand for energy and raw materials, the gap between available resources and future needs have been narrowed; this is because almost all resources are being exploited. Most easy and outcropping deposits have already been discovered, thus exploration these days is focused on searching for covered deposits using indirect geophysical and geochemical methods. Mining and exploration companies throughout the world have to direct their exploration activities towards more integrated techniques. Modern exploration is mainly preoccupied with defining the footprints of known deposits and with integrating various techniques such as hyperspectral RS data with geology for the efficient identification and detection of favourable terrain.

In this thesis, research is conducted using the existing geological and imagery information, in combination with geochemical and mineralogical information from rock powder of the Rodalquilar area. The results are expected to enhance the information about data integration in mineral exploration.

1.3. Motivation

Portable X-ray Fluorescence (PXRF) is a new in situ chemical analysis technique, and is usually applied in both geochemical research at geological outcrop scale and heavy metal pollution assessment in soil. Recent studies (Peinado, Ruano, González, & Molina, 2010), have proved that PXRF is a convenient, quick, reliable, non-destructive and cost-effective tool for in situ measurements of polluted soils and on rocks. The use of PXRF has been applied elsewhere for mineral exploration (Xia et al., 2011). So far nothing has been published on use of PXRF on area of known mineralization although many exploration and mining companies, such as my own, Twigg Gold (T) ltd, In Tanzania, have been using PXRF for the identification of mineralized and non-mineralized Ni laterites zones

Few published studies using PXRF on epithermal deposits do exist that examine the whole-rock geochemistry of altered rocks (Warren, Simmons, & Mauk, 2007), This became the prior interest and motivation for the proposed project. PXRF will be applied to study the whole rock geochemistry of the proposed Rodalquilar study area. This research aims at examining the effectiveness of an integrated approach of geochemical data with spectral mineralogical compositions, together with virtually interpreted.

1.4. Research objectives

The objectives of this research are to test whether a technique such portable XRF combined with VNIR-SWIR spectrometry (ASD- Fieldspec) can be used to:

1. Determine different lithological composition of the volcanic rocks
2. Determine the hydrothermal alteration styles and
3. Determine which elements measured by portable XRF can be used to characterize the lithology in the Rodalquilar epithermal alteration system

Ideally, we want to test whether direct field data of major and trace elements can be used in combination with mineralogical IR information for the exploration of the epithermal gold deposits.

1.5. Research questions

1. Can different lithologies be deduced from the whole rock geochemistry using the PXRF in Rodalquilar area?
2. Can different alteration styles be deduced by using the PXRF in Rodalquilar?
3. Which elements measured by PXRF can be used to characterize the lithology in the Rodalquilar epithermal alteration system?

1.6. Research hypothesis

1. By the application of both major and trace elements from the whole rock geochemistry, it is possible to deduce different lithological composition of the volcanic rocks.
2. It is possible to deduce different alteration styles from the whole rock geochemistry.

1.7. Data sets

The following material, data sources and software programmes were available for processing and analysis in this research:

- Geological map (1:25,000)

Scanned from the original map by Arribas (1993). Mapa Geologico del Distrito Minero de Rodalquilar, Almeria. Map digitization was done in May 2006.

- Rocks and powder samples

A total of 89 rocks and powder samples were available for analysis. These samples were collected by ITC staffs and students during the field work on the area in 2005. All rocks and powder were analysed for mineralogical (ASD) and for trace and major elements (XRF- both soil and mining mode).

- Hymap, Aster Imagery and DEM data.

Satellite imagery, Hymap imagery (126 spectral bands) with the spatial resolution of 4m, Aster VNIR (15m resolution), SWIR (30m resolution), TIR (90m resolution) and STRM and Aster DEM of 90m and 25m respectively, were available for aiding the analysis. Hymap imagery was used for the data integration, while Aster imagery was used for the visualization of the spatial distribution of the alteration mineralogy.

1.8. Thesis outline

This thesis is divided into 3 parts, chapters 1, 2 and 3 covers the first part. Next chapters 4, 5 and 6 are about data analysis. Conclusion and recommendations are explained in the last chapter (Chapter 7).

First part starts with information of the thesis in chapter 1, followed by literature review presented in chapter 2. Chapter 3 describes the study area and previous works in the area. Data analysis is explained in the next part, chapter 4 dealing with geochemical analysis, chapter 5 dealing with the spectral analysis, while chapter 6, deals with the integration of geochemical and spectral data... The last part, which is chapter 7, deals with the conclusions and recommendations, arises from this research Chapter title

This is Body Text style. Use this for the body text. Font Garamond 11. This is Body Text style. Use this for the body text. This is Body Text style..

2. EPITHERMAL GOLD-GENERAL OVERVIEW

2.1. What is epithermal gold?

Epithermal Au deposits are a type of lode mineral deposits consisting of sometimes economic concentrations of Au ± Ag and base metals (Taylor, 2007). These deposits form in a variety of host rocks from ascending hydrothermal fluids, primarily by replacement (i.e. by solution and reprecipitation), or by open-space filling (e.g. veins, breccias, pore spaces). The form of deposits originating by open-space filling typically reflects that of the structural control of the hydrothermal fluids (planar vs. irregular fractures, etc.). In Pacific areas (Corbett, 2002), studies show that localized mineralization, is a result of many combined factors such as type, distribution and zoning of hydrothermal alteration coupled with observations of deposit form, texture and mineralogy.

2.2. Geological, mineralogical and geochemical characteristics of epithermal gold.

Hydrothermal alteration is a complex process involving mineralogical, chemical and textural changes, resulting from the interaction of hot aqueous fluids with the rocks through which they circulate, under evolving physico-chemical conditions. Alteration can take place under magmatic subsolidus conditions by the action and infiltration of supercritical fluids into a rock mass. (Pirajno, 2008)

Hydrothermal mineral phases that develop in epithermal systems are a function of temperature, pressure, rock type, nature of the circulating fluids (such as pH, activities of CO₂, H₂S) and water/rock ratios. Hydrothermal alteration in epithermal systems can be considered in terms of interaction of (1) acidic fluids; (2) near-neutral chloride fluids; and (3) alkaline fluids (Fig. 2). The recognition of mineral assemblages is crucial in distinguishing low-sulphidation, high-sulphidation, intermediate sulphidation and alkalic types of epithermal systems. (Pirajno, 2008).

The epithermal deposits are mostly of Tertiary to Quaternary in age. This type of gold systems have been reviewed by (Dill, 2010), who distinguished them based on the sulphidation states of their primary sulphide assemblages and grouped them into two general types; high sulphidation- and low sulphidation deposits.

High sulphidation deposits (Alunite-Kaolinite epithermal deposits) are widely distributed in volcanic arcs worldwide. These range from structurally controlled, deeper seated to shallow hosted or breccia controlled (Robert, 2007), regionally high sulphidation lies within calc-alkaline volcanic arcs dominated by andesitic volcanism, while on local scale, they tend to associate with felsic subvolcanics. Mineralization in high sulphidation is mainly dominated by pyrite-rich sulphide assemblages, such as pyrite, enargite-luzonite and chalcopyrite, (Robert, 1997).

Low sulphidation epithermal deposits (Adularia-sericite epithermal deposits), consists of subvertical banded and breccia veins of quartz associated with Chalcedony. They are mostly found on volcano-plutonic continental and island arcs at convergent plate margins. Published studies, (Robert, 2007) indicate that low sulphidation deposits, at deposit scale, are normally hosted on volcanic units, but can also be hosted on their basements. Quartz, adularia and Mn-carbonate, with pyrite, Electrum and high-Fe sphalerite are typical minerals for this kind of deposits. The associated metals include Au, Ag, Sb, Hg, Pb, Zn and Cu. The mineralization is typically vertically zoned and they grade moving downward. Recent studies (Mixa, Dobes, Zacek, Lukes, & Quintanilla, 2011), suggests a multi stage hydrothermal processes in some low sulphidation deposits.

Epithermal deposits are well documented especially along active volcanic arcs e.g. in Indonesia , (Gemmell, 2007), where whole rock analysis was applied to study the altered rocks at the Gosowong epithermal Au-Ag deposit in Halmahera, Indonesia. The applied techniques demonstrate the ability to evaluate altered volcanic rocks suites, ranging from mafic to felsic composition; it can also provide information about both geochemical and mineralogical information relevant to Au-Ag mineralization, and hence proved to be very useful for providing a set of exploration vectors to mineralisation in prospecting area(s).

An understanding of hydrothermal alterations is of great importance, as it provides insight into origin of ore fluids, as well as chemical and physical attributes of the ore deposit formation.(Reed, 1997). Alteration zones in epithermal systems are commonly larger than the related ore deposit, hence consequently, the recognition of mineralogical and geochemical zonation within area of alteration may provide a basis for developing vectors to the ore deposits, which is very important for mineral exploration

Elsewhere, work by (Warren et al., 2007) at the El Penon epithermal deposit in northern Chile show that hydrothermal alteration records the effect of fluid-rock interactions, which are expressed as compositional changes that can be recognized in the chemistry of the rock. However, few studies of epithermal deposits exist that examine the whole-rock geochemistry of hydrothermally altered rocks related to epithermal deposits.

Table 2.1: Geochemical associations of epithermal gold deposits.

	Low Sulphidation	High Sulphidation
Anomalously high	Au ,Ag ,As ,Sb ,Hg ,Zn ,Pb ,Se ,K, Ag/Au	Au,Ag,As,Cu,Sb,Bi,Hg,Te,Sn,Pb, Mo , Te/Se
Anomalously low	Cu,Te/Se	K, Zn ,Ag/Au

Generalized chemical signatures between the two types can be used as a guide towards designing the geochemical survey.

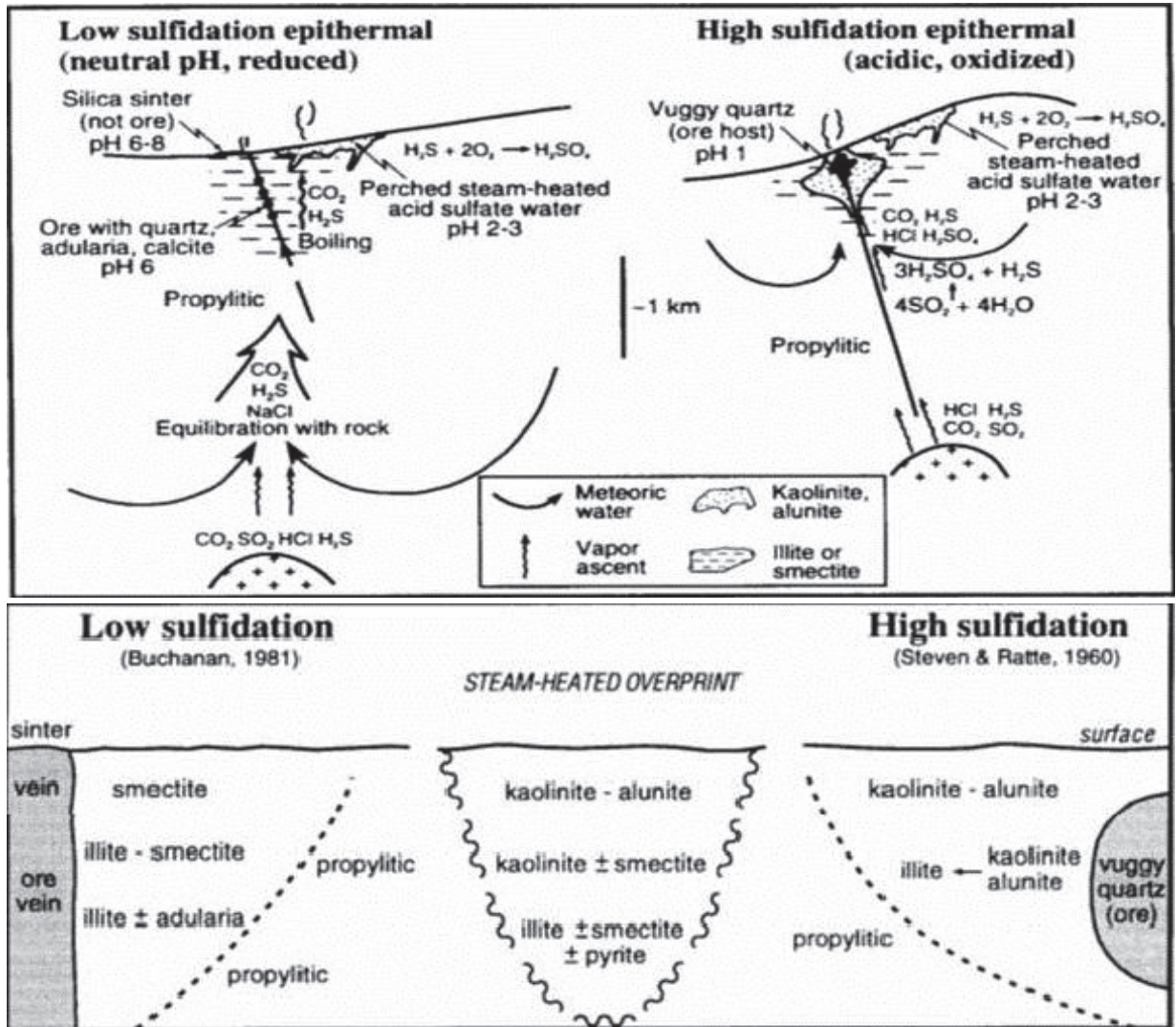


Figure 2.1: A and B .Epithermal gold deposits. Showing characteristics geological, mineralogical and geochemical for low and high sulphidation epithermal deposits. After (Noel C. White, 1995) et al.

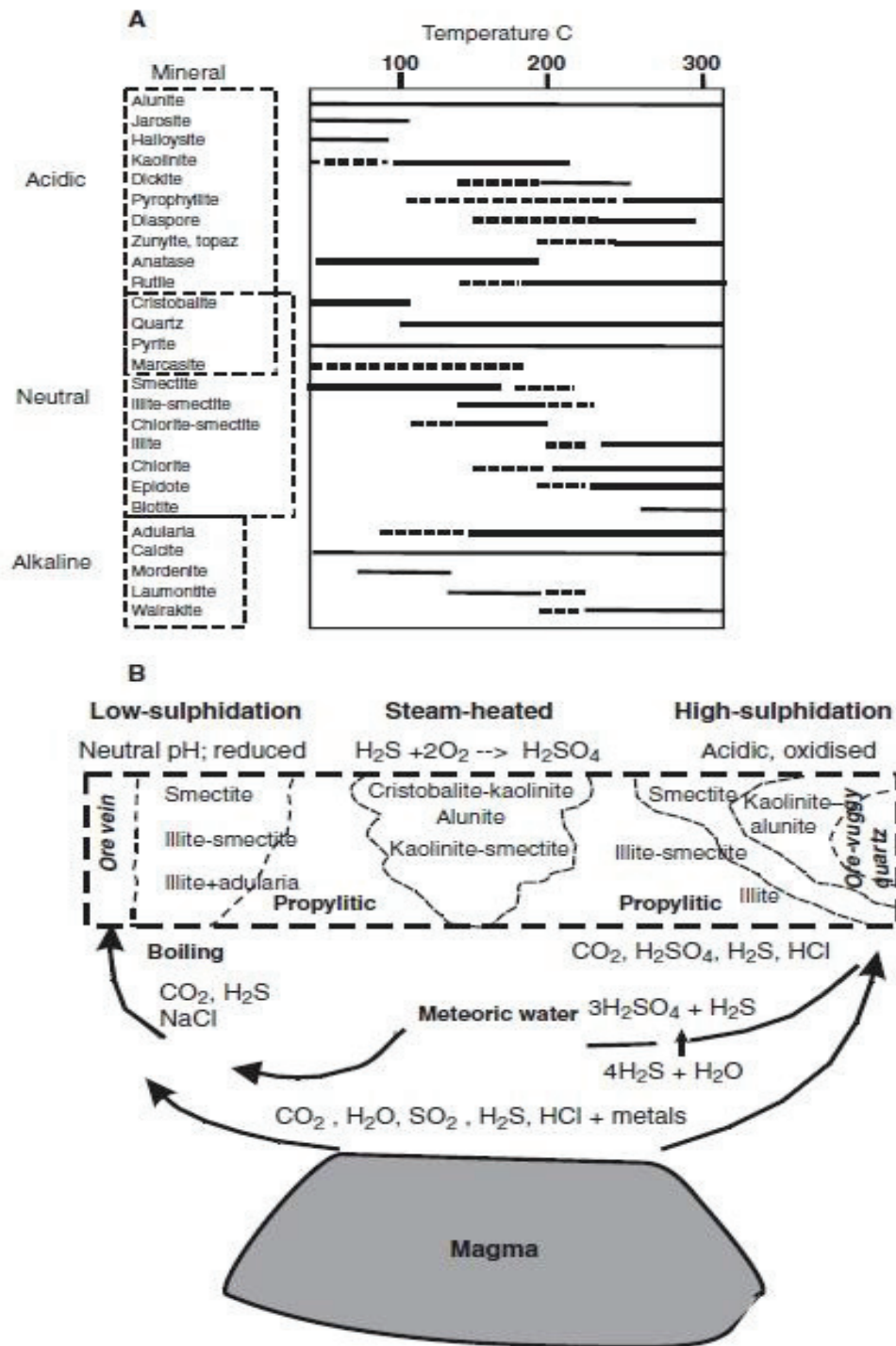


Figure 2.2: (A) Temperature and pH range of hydrothermal mineral phases in epithermal system: (B) Simplified scheme of distribution of hydrothermal minerals in low and high sulphidation epithermal systems. After (Hedenquist, ANTONIO ARRIBAS R., & GONZALEZ-URIEN, 1996)

2.2.1. Conceptual model of epithermal gold

The term epithermal is used in field exploration studies to describe Au ± Ag ± Cu deposits formed in magmatic arc environments (including rift systems) at elevated crustal settings, most typically above the level of formation of porphyry Cu-Au deposits (typically < 1 km), in many instances epithermal deposits may be associated with subvolcanic intrusions. (Corbett, 2002)

Geologist and prospectors has recognized the association between gold mineralization with volcanism and geothermal hot spring activities. The relationship is a result of hot magma eruption, in which the volcanic rocks are produced, together with the hot fluids, responsible for the transport of gold and other associated metals. The hot fluids produced, in other hand are considered to be the source of the gold itself (Morgan Poliquin, 2011). The hot fluids are produced at depth below the surface under extreme temperature and pressure, and when rising to the surface, these fluids mix with surface waters and when in contact with the country rocks, they change the composition of the rocks, the process known as alteration. (White and Hedenquist 1990)

On reaching the surface, hot fluids, breach the surface, making all epithermal precious metal deposits to be characterized by the presence of hydrothermal alteration of wall rock. Based on the dominant hydrothermal alteration and sulphide assemblages (as a result of paths taken by the magma as it rises) , the volcanic –hosted epithermal precious metal deposits, can be classified into two main subtypes, high and low sulphidation epithermal deposits, gold is largely precipitated from 2.5 kilometres depth to surface in both subtypes. (Richard H. Silitoe 2003)

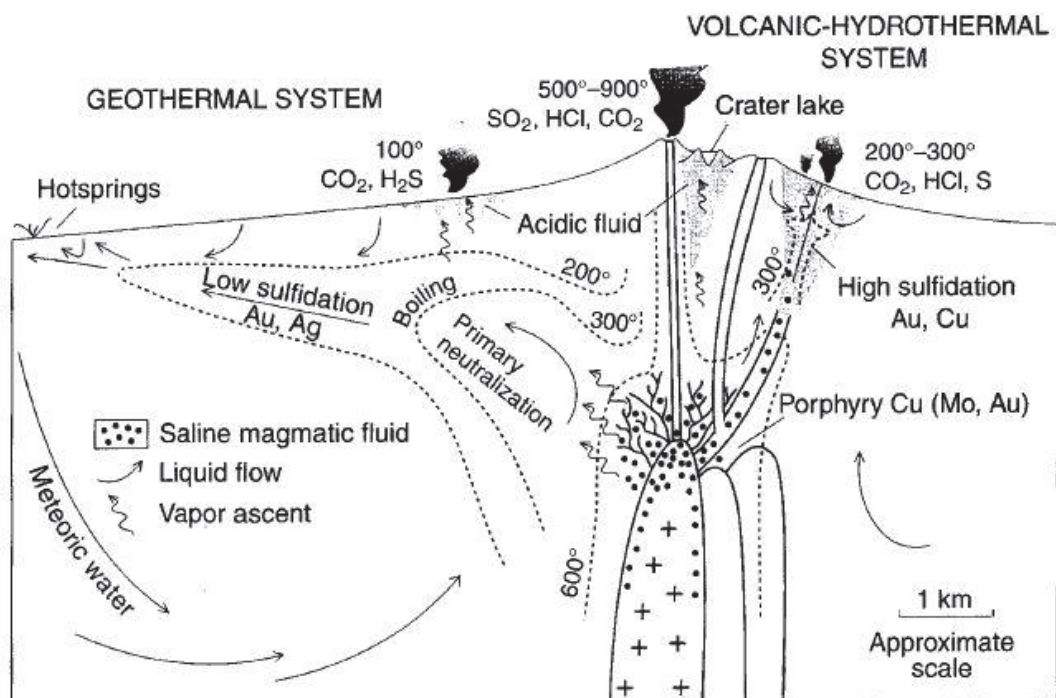


Figure 2.3: Graph to illustrate schematically the various processes deduced for volcanic-hydrothermal and geothermal systems, and the respective environments of high-sulfidation and low-sulfidation styles of epithermal ore deposits relative to the intrusive engine.(after Hedenquist, 1996)

2.3.1. High sulphidation epithermal gold

High sulphidation epithermal deposits are formed from the oxidized acidic fluids generated in the magmatic hydrothermal system, with little wall-rock interaction at depth, as these fluids are rising to the surface. SO₂ and HCl vapor are absorbed by the ground water causing SO₂ to decompose to H₂SO₄ and H₂S followed by dissociation of the H₂SO₄ and HCl, resulting into hot and highly acidic oxidized solutions, which in turn react with wall-rock (and leach them) at shallow depth (H.Macdonald, 2007)

High-sulphidation epithermal gold deposits are characterized by disseminated ore bodies, which are located in highly altered and leached zones. In high sulphidation system gold is transported mainly as a chloride complex, and precipitates as a result of dilution or cooling.

High sulphidation epithermal gold systems are dominated by massive vuggy quartz as a result of leaching at low pH. The massive vuggy silica may be cut by the massive to banded sulphide veins consisting of pyrite and enargite. High grade ore bodies within the high sulphidation epithermal system are provided by the localized veining and or brecciation (Noel C. White, 1995)

Alunite, kaolinite, picillite and propylite are common in high sulphidation epithermal system, as they are stable under acidic condition, with quartz as the principle gangue mineral. Lateral and vertical variation is observed within the high sulphidation epithermal systems, where the orebodies are surrounded by the mineral assemblages typical of less acid conditions, as the effect of acidic water is reduced by the reaction with the host rocks (H.Macdonald, 2007)

Alteration in a high-sulphidation system:

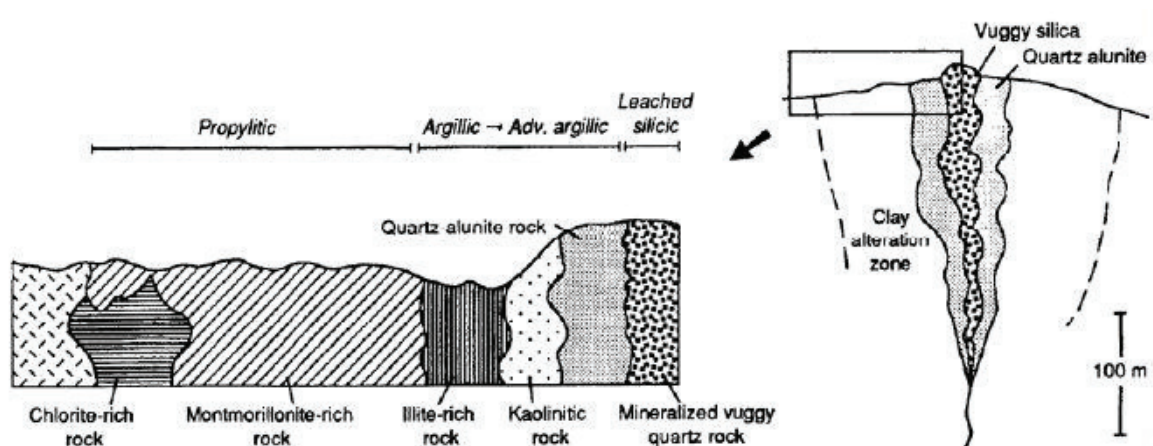


Figure 2.4: Section through a typical high-sulphidation orebody, showing the upward-flaring zone of the silicic core and the characteristic alteration zonation. (after Hedenquist 1996)

2.3.2. Low Sulphidation deposits

Low sulphidation epithermal gold deposits are formed from reduced near-neutral pH fluids with large meteoric water inputs. Studies by (Werner F, 1981) indicated that these fluids which are circulating, have absorbed acid magmatic gases such as CO₂, SO₂, and HCl at great depth. The interaction between such fluids with deep seated rocks, results into reduced environments and thus developing a near neutral pH.

CO₂ and H₂S-rich vapor are generated at shallow depth by the near-neutral pH solutions, resulting in ore association. On rising up, these vapors condense forming the steam of heated acid-sulphate which has higher pH. Lastly, the solubility of the gold decreases as a result of loss of H₂S in the system causing the precipitation of the gold. (H. Macdonald, 2007)

In low sulphidation epithermal systems ores are texturally diverse in banded, crustiform quartz and chalcedony veins, indicating multi episode of hydrothermal mineral deposition (Corbett, 2002)

The ores in low epithermal system are associated with adularia and calcite minerals, which are typical of least acidic conditions, although in some instances the calcite (which is formed as a result of boiling) may be replaced by quartz, when the system cools (Noel C. White, 1995).

Alteration in a low –sulphidation system:

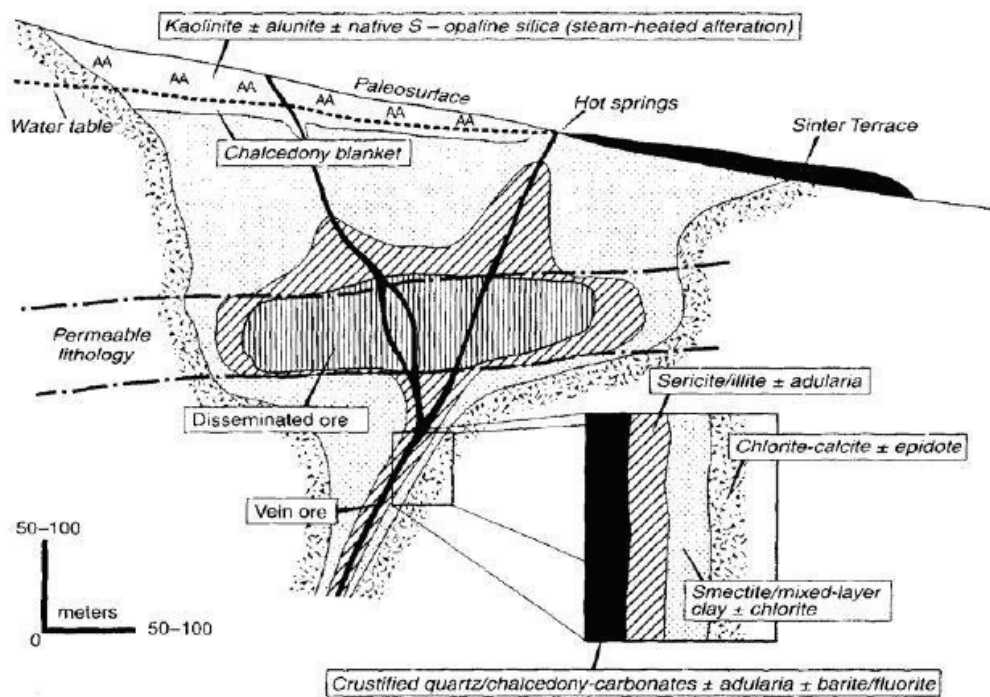


Figure 2.5: Schematic section that generalizes patterns of alteration in a low-sulphidation system, showing the variable form with increasing depth, and the typical alteration zonation. (after Hedeinquest et al. 1996)

2.4. Exploration for epithermal gold

In current practice, recognition and exploration for epithermal gold should rely more on geological and hydrothermal environments of mineralization, rather than on the set of temperature –pressure limits. This new approach is very important, as it has been shown that even ,Sediment-hosted, Carlin-type gold deposits, also appears to have been formed in epithermal environments, only that they are genetically distinct. It is reported also, that some of the Archean gold deposits were also emplaced at shallow levels, long time after volcanism. (Misra, 1999)

Exploration for epithermal gold deposits is a comprehensive approach, involves application of methodologies to assess the geological characteristics (tectonic. structure settings, petrological association, mode of occurrences, geochronology etc. etc.) , mineralogical and geochemical characteristics (mineral assemblages, mineral/rock chemical compositions) and geophysical characteristics (e.g. electrical and magnetic properties) (Taylor, 2007). Understanding these processes, in combination with the hydrothermal processes and its products is the basis for the exploration of epithermal gold. Geology can be applied for the recognition of veins and hydrothermal alteration patterns, vein texture and mineralogy. Geochemistry can be applied for shallow indicator elements and anomalous related to mineralized structures, while geophysics can be applied at both shallow and deep levels. Geophysics is very effective but only at prospects scale. Geologic understanding is the base for all interpretations.

Epithermal gold deposits, are the deposits which are formed by the ascending waters at shallow to moderate depth (<1.5 km), and low temperatures (50°-200°). Epithermal deposits are mainly associated with the intrusives or volcanic rocks. Two styles of epithermal gold mineralisation are primarily distinguished; high and low sulphidation, which evolve through dramatically differing hydrothermal fluid paths. The distinction between varying styles of epithermal gold mineralisation, identified from ore, alteration and gangue mineralogy, can be of significant benefit to the explorationist.

Distinguishing between the two subtypes is very important, simply because , although, they both show broadly similar alteration mineralogy, the distribution of the alteration zones are quite different, and the economic mineralization, in both cases, are localized in different parts of the systems. In high-sulphidation epithermal system, ore is closely associated or lies within the zone of highest acidic alteration, and typically is surrounded by mineral assemblages which are indicating less acidic conditions. Contrally to that, in low-sulphidation epithermal systems, the ore is mainly associated with the least acidic alteration, which is recognized by the presence of adularia and calcite or illite.(Misra, 1999)

In addition epithermal gold mineralization can be subjected to supergene enrichment processes when exposed to near surface. Epithermal gold deposits are among the economically important deposits, contributing about 5% of the world production.

2.5. Summary

Epithermal gold deposits, are the deposits which are formed by the ascending waters at shallow to moderate depth (<1.5 km), and low temperatures (50°-200°). Epithermal deposits are mainly associated with the intrusives or volcanic rocks. Two styles of epithermal gold mineralisation are primarily distinguished; high and low sulphidation, which evolve through dramatically differing hydrothermal fluid paths. The distinction between varying styles of epithermal gold mineralisation, identified from ore, alteration and gangue mineralogy, can be of significant benefit to the explorationist.

Distinguishing between the two subtypes is very important, simply because , although, they both show broadly similar alteration mineralogy, the distribution of the alteration zones are quite different, and the economic mineralization, in both cases, are localized in different parts of the systems. In high-sulphidation epithermal system, ore is closely associated or lies within the zone of highest acidic alteration, and typically is surrounded by mineral assemblages which are indicating less acidic conditions. Contrally to that, in low-sulphidation epithermal systems, the ore is mainly associated with the least acidic alteration, which is recognized by the presence of adularia and calcite or illite.(Misra, 1999)

In addition epithermal gold mineralization can be subjected to supergene enrichment processes when exposed to near surface. Epithermal gold deposits are among the economically important deposits, contributing about 5% of the world production.

Epithermal gold deposits have relatively higher grades and amenability to cheaper open pit mining, with the possibility of applying heap-leach for the extraction of gold, making the deposits favored targets for exploration.

3. THE STUDY AREA

3.1. General

The Study area (Rodalquilar Gold Mine) forms part of the Cabo de Gata National Park area which is located in the south-eastern part of Spain (figure1). It is located on the Topographic Map Sheet: Fernan Perez 1046-III. It is bound by the following UTM coordinates: - East: 588000, West: 579000, North: 4083000 and South: 4076000.Coordinate System, ED 1950 UTM zone 30N (datum European 1950) the total area covered in this study is approximately 56 square km. The study area is accessed by all-weather tarred and hard gravel roads.

3.2. Regional geology

The Rodalquilar area is located in the Betics region in south-eastern Spain. The area is situated in the Internal Betic zone, which is composed largely of pre-Neogene thrust sheet complexes of metamorphosed sedimentary rocks (Huibregtse, van Alebeek et al. 1998) volcanic rocks in the area are products of Neogene magmatism due to collision between the Iberian and African plates (Duggen 2005). The volcanic rocks which extends for several kilometres to the Mediterranean sea, in the western part are comprising of regionally extensive rhyolites to dacitic ash-flow tuffs (Rytuba et al., 1990)

The Rodalquilar caldera complex consists of two nested calderas (Rodalquilar and Lomilla). These calderas have resulted from an eruption of the rhyolitic Cinto ash-flow tuff from the magma chamber, consisting of a composite ash-flow sheet of six cooling units in its outfloor facies and a thick sequence of interbedded ash-flows and breccias in its intracaldera facies (Rytuba, Arribas et al. 1990). Volcanic rocks in the Rodalquilar caldera complex are intensely altered and are associated with epithermal gold-alunite deposits and base-precious metal (Pb-Zn-Ag-Au) (Arribas, et al., 1995)

3.3. Local geology

Volcanic rocks in the Cabo de Gata volcanic field range in composition from pyroxene andesine to rhyolite range in age from about 15 to 7 Ma (Queralt, 1996)

Within the Rodalquilar caldera four volcanic complexes are identified (Rytuba et al., 1990). The first complex consists of pyroxene andesites. The second one consists of hornblende-bearing andesites. Third complex comprises of dacites and rhyolite and the fourth complex consists of dark pyroxenes andesites. The Rodalquilar caldera is an oval-shaped collapse structure that was developed in an order andesites volcanic field composed of stratovolcanoes and cones. Repeated volcanic events occurred within the Rodalquilar caldera. Large inclusion of Cinto ash-flow tuff, are common in outcrops of Lazaras rhyodacite tuff in the western margin of Rodalquilar caldera. The last volcanic event in the area, which is not related to caldera volcanism, is the fourth-complex pyroxene andesites flows and breccias. The volcanogenic complexes are overlain by younger calcareous and fossiliferous limestone (Arribas et al., 1995).

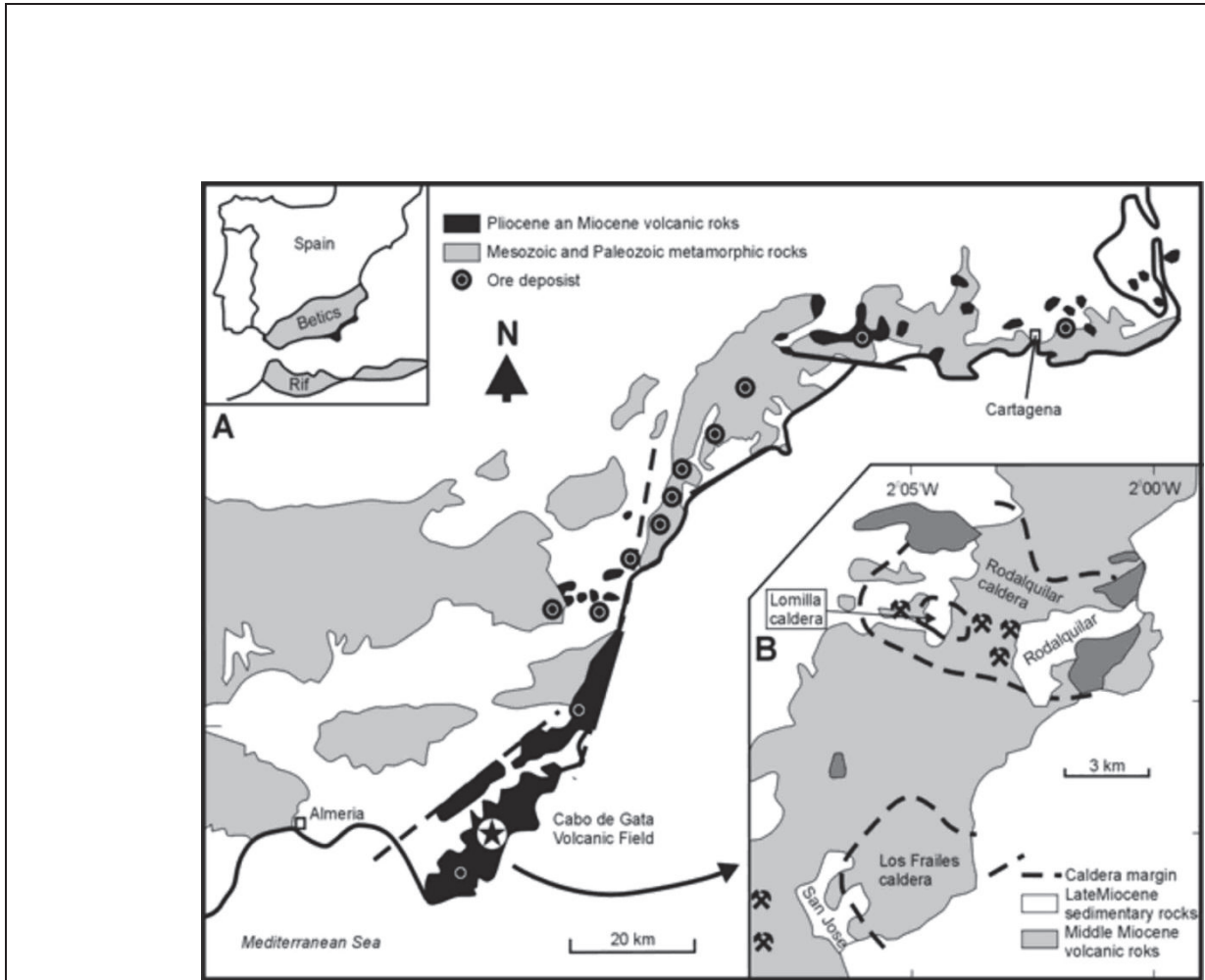


Figure 3.1: Location map of study area, showing simplified geology of the area. After Arribas, 1995

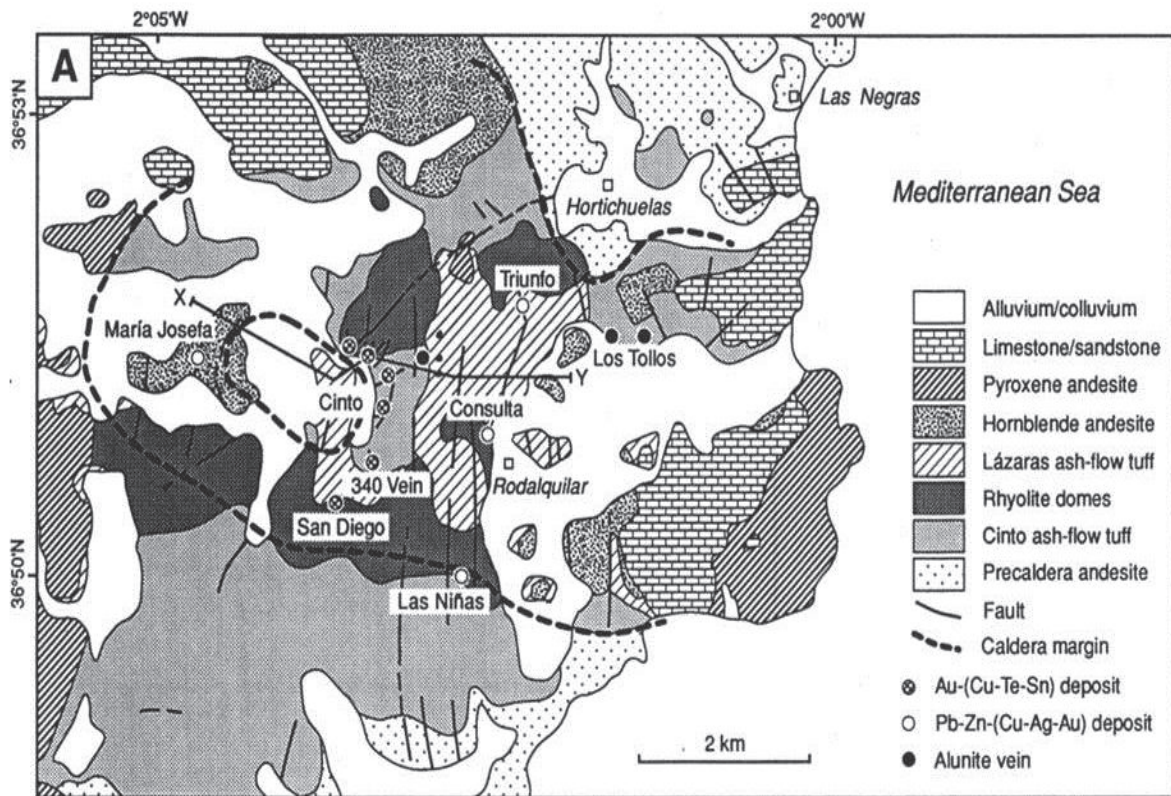


Figure 3.2: A simplified geological Map of Rodalquilar, after Arribas, 1995

3.4. The Rodalquilar deposit

The Rodalquilar Au-deposit, in Almeria province south-east Spain, (Arribas et al., 1995) is a high sulphidation epithermal gold deposit with specific alteration zonation (Oopen, Friedrich, & Vogt, 1989), The zoning occurs around gold bearing vein structures, grading from proximal advanced argillic via an argillic into a more regionally developed prophylic distal alteration zone. Gold-bearing silicified ore deposits are widely spread in the volcanic complex near the village of Rodalquilar. These deposits were formed as a result of the hydrothermal alteration related to volcanic activity during the Miocene time. Mapping of these alteration zones, and other physico-chemical properties of the deposit, by remote sensing imagery is possible as demonstrated by (Bedini, van der Meer, & van Ruitenbeek, 2009) and (Estifanos, 2006). Ore deposits within the Rodalquilar consist of both low-sulphidation Pb-Zn-(Cu-Ag-Au) quartz veins and the most economically high-sulphidation Au-(Cu-Te-Sn) ores. (Queralt, 1996) showed that the mineralized zones at the Rodalquilar/Cinto caldera complex are characterized by a suite of intensive alterations of the volcanic host rocks. The Pb Zn quartz veins occur in the periphery of the Cinto caldera, see fig 5.11

3.5. Previous explorations/ mining works

Mining history at Rodalquilar epithermal gold deposit can be traced back to 1880s where epithermal Pb-Zn-Ag veins were exploited. It was until around 1880 where gold was discovered in the same ores, followed soon later by the discovery of gold in quartz veins near Rodalquilar, 15 km south-western San Jose, in which small alunite workings existed (Arribas et al., 1995)

Mining activities at Rodalquilar continued until 1966, and later on they had to stop after the exhausting of the high grade hydrothermal breccias.

More information about the exploration and mining activities within the Rodalquilar epithermal gold deposit can be accessed at <http://www.faydon.com/Gold/Gold.html>.

3.6. Concluding remarks

The study area, Rodalquilar deposit, is one of the most studied examples of caldera-related epithermal Au mineralization in Europe. The complex hydrothermal alteration assemblages associated with this deposit is typical of high-sulphidation system. Several studies on the area cover many aspects of geology, petrology, ore genesis, mineral exploration, environmental aspects, all the way to remote sensing and GIS. (Arribas et al., 1995; Bedini et al., 2009; Oepen et al., 1989; Rytuba et al., 1990). Rodalquilar epithermal gold deposit is associated with large scale alteration of volcanic rocks (which are not deformed), and which show zoning and have the alteration minerals dominated by alunite, kaolinite, pyrophyllite and illite. The Rodalquilar area is sparsely vegetated.

The Rodalquilar gold deposit is located within the area of intense acid sulphate alteration, and it is localized in ring, fault and fractures present in the area. The availability of information from these diverse studies, the presence of alteration minerals and the fact that, the rocks are not deformed and the area is sparsely vegetated, make the study area an ideal place to conduct the current research.

4. ANALYSIS OF GEOCHEMICAL DATA

4.1. Overall research methodology

The Rodalquilar area is selected as the stud area to test research hypothesis and the related research questions regarding the use of portable XRF in mineral exploration for the epithermal gold deposits. The overall research methodologies followed in this research are shown in the flow sheet figure below. (Figure 4.1)

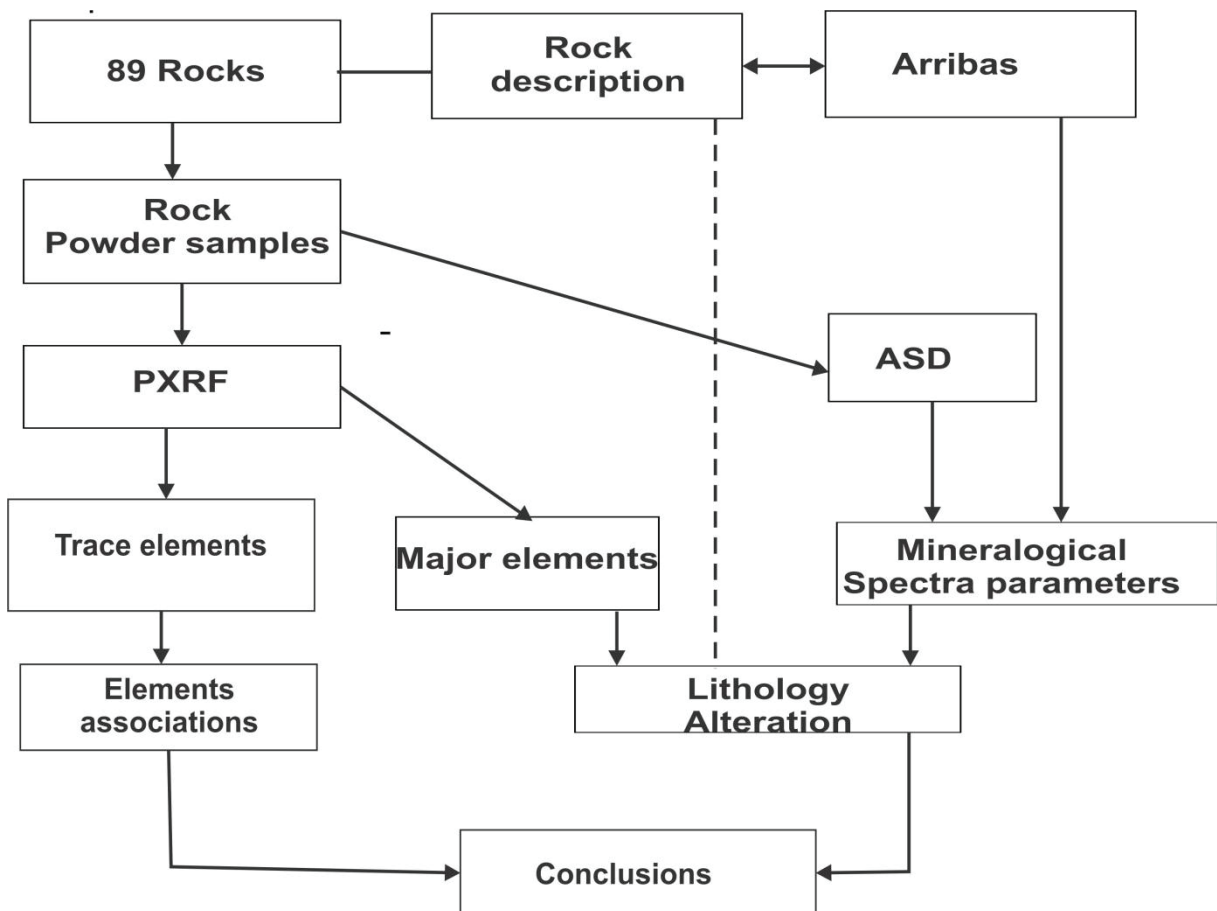


Figure 4.1: Flow chart of the methodology followed in this research.

4.2. Geochemical data collection, processing and interpretation.

For this study 89 rock-samples were available which were collected over two traverses collected in 2004 by ITC students. In appendix 1 a simple field classification of the material is given together with the sample location coordinates obtained by GPS. The sample locations in relation to the Rodalquilar ore deposit are given in fig. No. 4.2. Rock powders samples were prepared by grinding part of the samples using a Tema

disk mill and a mullite hand mortar to obtain fine rock powder for chemical analysis by PXRF methods. Sample size reduction require such preparation to affect one or more of the following:

- (1) reduction of the sample to a size that is more conveniently transported;
- (2) increase the sample surface area to enhance the efficiency of subsequent chemical attack;
- (3) homogenize the sample to ensure that a smaller subsample is representative of the entire sample.

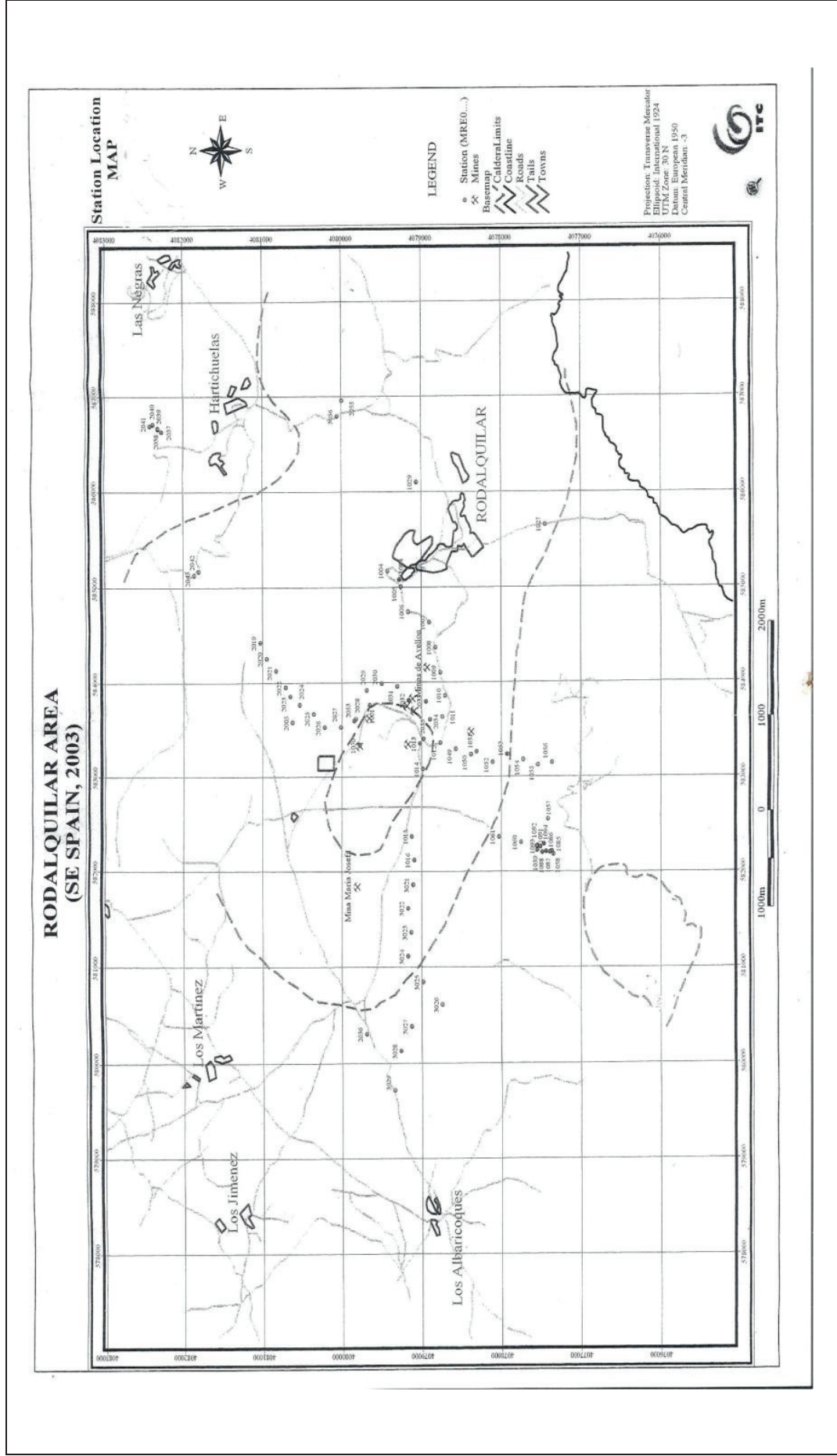
Portable (PXRF) instrumentation, Sampling and analysis procedures

XRF data collection and analysis utilizes low-level x-ray sources to irradiate sample material. When a sample is irradiated by x-rays, part of this radiation can be absorbed by sample atoms, when the incoming radiation evicts an electron from an inner electron orbit. The empty electron orbit is filled up by a higher energy electron from an electron orbit further away from the atom nucleus. The energy difference of the two orbits is released in the form of characteristic electromagnetic radiation. This radiation is element specific and its intensity is proportional to the quantity of a specific atom. The resulting fluorescent emissions can be used to identify the elements present and estimate their concentrations. In general, XRF can be used for metals with an atomic number of 12 (Magnesium) or heavier. Detection limits for any individual element depend on a variety of factors, including atomic weights, counting times, excitation source and strength, sample preparation packing, matrix effects, and inter-element spectral interferences (Kalnicky & Singhvi, 2001)

XRF systems can be deployed in a laboratory setting or as field portable instruments (PXRF). A limitation of the latter is the lower energy levels which affects the lower limits of detection limits compared to a laboratory instrument. Measurements can be made on prepared samples, or in situ on the soil/rock surface; in both cases, the detector window is pressed against a sample's (or subsample's) surface. An XRF instrument typically measures concentrations in a very small subsample of an original sample; proper sample homogenization is critical to ensuring replicability and adequate precision in measurements. Measurement times typically range from 60 to 600 seconds. Although the XRF instrument is not measuring radioactivity of material, the measurement analysis involves the same type of spectroscopy as radionuclide measurements ; therefore, the same principals of counting errors and counting statistics as a function of count times apply (EPA, 2007)

The general conduct and standard operating procedures of an PXRF analyzer in the field and lab are established by protocols of both the USGS and by the SOPs of the manufacturer- Thermo-Fisher Scientific ((US EPA, 2006); EPA 2007)

GEOCHEMICAL AND SPECTRAL CHARACTERIZATION OF HYDROTHERMAL ALTERATION FACIES AT THE EPITHERMAL GOLD MINERALIZATION AT RODALQUILAR, SPAIN



In this research a Niton XL3t GOLDD+ PXRF was used with an 8 mm diameter measuring spot. The instrument was used in combination with a Helium gas purge in order to obtain good results for the lighter elements Mg, Al and Si. The rock sample powders were analysed with the PXRF fixed in a Niton Lab-Mate which provides extra shielding and which allows measurement operation via a connected laptop. The Niton PXRF was used in its “Mining Mode” using a He-gas flush. Four filters were used, Main (Ti, V, Cr Mn, Fe, Ni Co, Ni,Cu, Zn, As Se, Rb, Sr, Zr, Nb, Mo, Pd, Cd, Sn, Hf, Ta, W, Ba, Sb ,Re, Au, Pb and Bi, low (K, Ca , Ti , V and Cr), high (Pd, Ag, Cd, Sn, Sb and Ba) and light filter (Mg, Al, Si, P and Cl) which needs Helium purging for its optimal performance. In total each measurement took 90 seconds. All measurements were made in duplicate or up to five fold to obtain a good average.

Quality Assurance and Quality Control in XRF Data Collection

Interferences and potential problems

The total method error for XRF analysis is a combination of both instrument precision and user- or application-related error. The precision of the element error is least significant as compared to user or application related errors, which is more significant as it varies with site and method used. (US EPA 2006)

Specific QA/QC procedures were designed and applied to minimize user- and (or) application-related errors include the following:

1. This is among the potential sources of error, since the X-ray signals decreases with the increase of distance from the source. The error can be minimized by maintaining the distance for each sample, and by using flat sample surfaces, and by homogenizing samples to the greatest extent possible.

2. Representativeness: In order to characterize the site conditions accurately, samples which are collected must be representative of the area under investigations. This will ensure that the samples reflects the concentrations of the concern at a given time and location.

Sample representation can be affected by geologic variability of the area concerned, the variability of the concentrations concerned, sampling and preparation, and the analytical procedures.

Representativeness will generally be established by a regular grid over the site area that may be augmented by additional samples in areas of potential contamination as determined from the preliminary analysis of the site history.

3. Reference analysis: One of the most effective methods of quality control in the use of FPXRF technology is the use of reference analysis of samples by laboratory ICP/AES or equivalent laboratory methods. Kaolinite and Basalt were used as reference materials in this study. Some 18 samples were also sent to Utrecht University laboratory for XRF analysis on a larger laboratory XRF, so that these samples could be compared with the results obtained by the ITC Niton PXRF. These 18 measurements were carried out on pressed rock powder tablets.

4. Calibration Check: Instrument calibrations were done prior to starting of any analysis, and were repeated several times during the analysis procedures to ensure maximum and efficient performance of an instrument.

In order to improve data quality, the dataset were calibrated using the results from the Utrecht University, which are assumed to be correct. All factors were linear except for Zr and Ca. See table 4.1 for the calibration factors.

Table 4.1: Calibration correction factors for some of the elements, to improve the data quality of Niton readings.

Niton	Zr	Ca	Rb	As	Cr	Fe	Ti	Ba	Sr	Pb	K	Al%	Si	S	Mg
Calibration factor	18+25 (ppm)	1.56+0.05	2.23	1.6	1	1	1.25	1.33	1.78	1	1	1.35	1	0.75	1.5

The above procedures allowed quality control of the data in terms of both precision and accuracy. See figure 4.3 and 4.4.

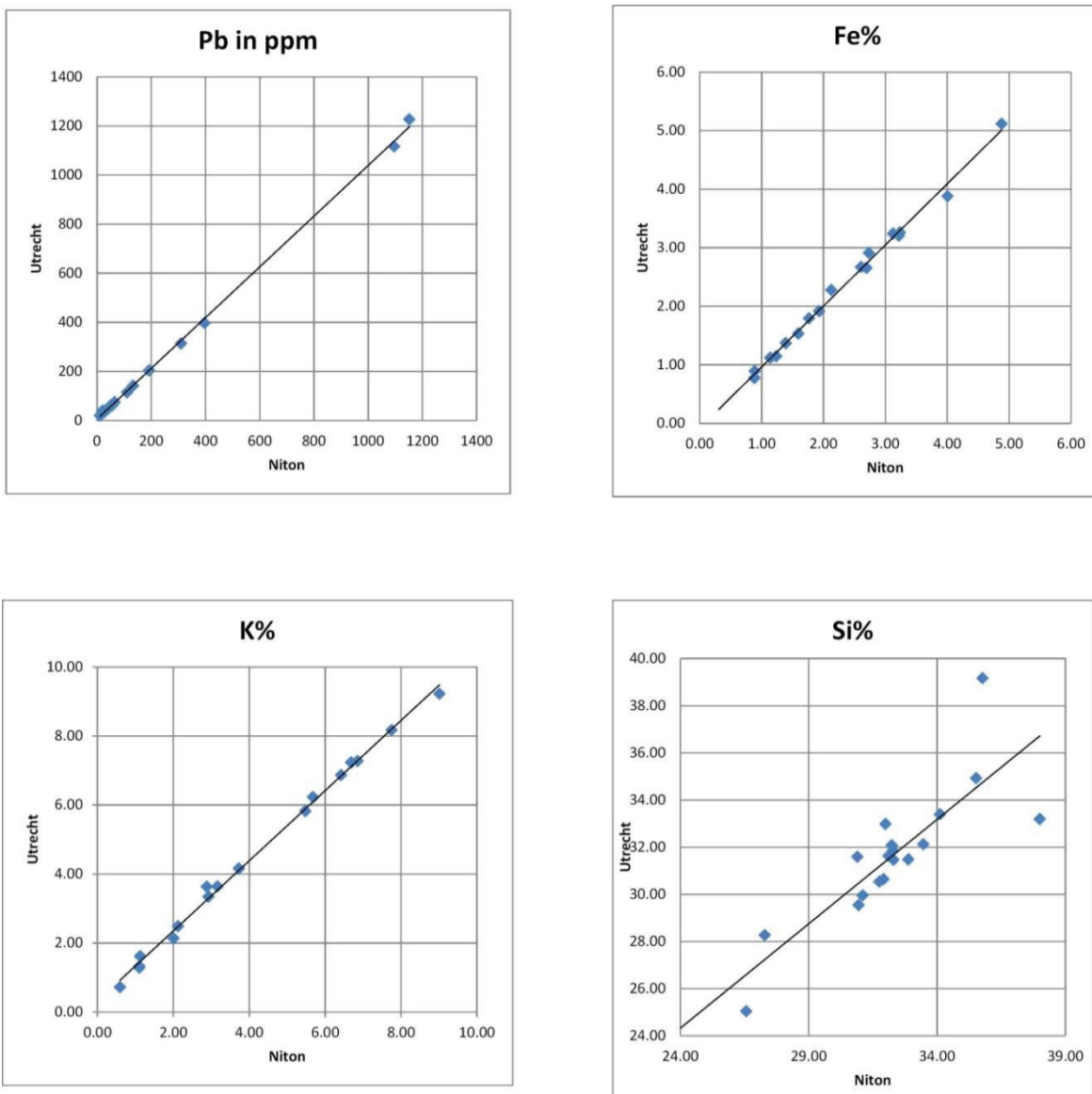


Figure 4.3: Plots of ITC Niton PXRf (Horizontal) against Utrecht lab XRF results (Vertical) for some elements

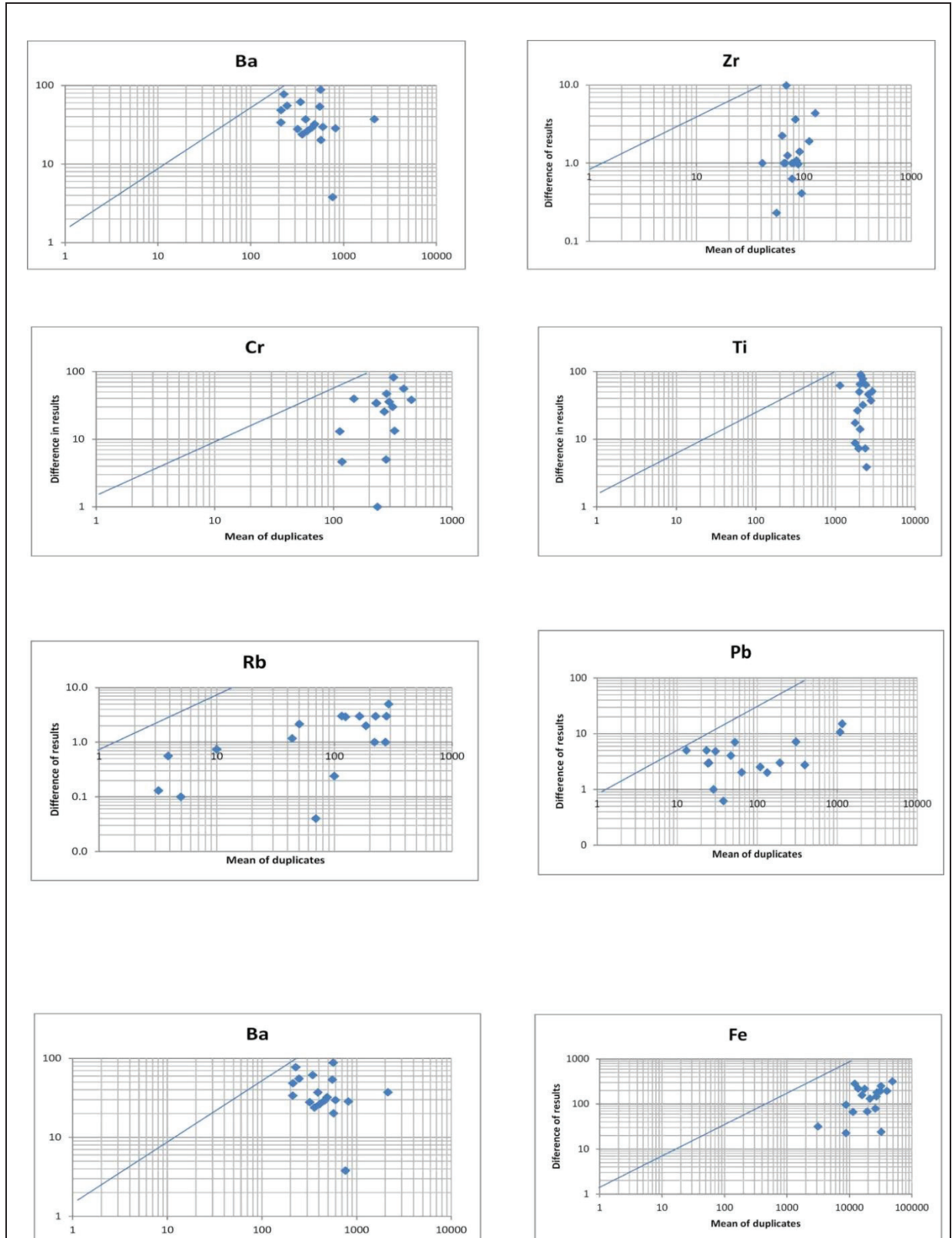


Figure 4.4: Thompson and Howarth plots of duplicate measurements on 18 pressed rock powder tablets First set measured on 1st Nov, 2011 Repeat measurement on 15th Nov, 2011, under the same settings. The line represents the 90% precision condition

The precision of the PXRF results is acceptable, as can be seen in the Thomson-Howarth plots (figure 4.3). Almost all results fall below 90% precision line in the graph.

Accuracy of the portable PXRF is, also acceptable, as the results for elements like Cr, Pb, K, Si and Fe, matches the results of the Utrecht XRF lab results, and thus, in this case, they were not calibrated. The PXRF results are also fairly good for some elements like Ti and Ba. (figure 4.2), although for some elements, the calibration has to be done (table 4.1). Sulphur is the only element measured which had higher values than the Utrecht XRF lab results.

4.2.1. Univariate statistical analysis.

Before any statistical tests, all those elements with more than 25% reported values below detection limit were discarded. The dataset was then transformed through a centred logratio transformation procedure to overcome the data closure problems. Several studies (Carranza, 2011; Filzmoser, Hron, & Reimann, 2010; Peter Filzmoser, 2009) have shown that centred logratio transformation (Clr) transformation is very useful for the opening up of a closed data set.

Centred log transformation, ideally it takes each component variable and divides it with the geometric mean of the component (centering) and then takes the log ratio of each quotient.

The results are the transformation of the data into “real components adding up to Zero”, which is called “openings”.

Transformation of the PXRF data was performed using the CodaPack software, using standard procedures as explained by (Peter Filzmoser, 2009).

Exploratory data analysis (Histograms, Box plots and QQ plots) were applied to the transformed data, as explained by (Chiprés, Castro-Larragoitia, & Monroy, 2009), to allow data exploration and defining the threshold between geochemical background and anomaly.

Different software packages (R, SPSS, X-cell and Grapher) were used to treat the data in order to get the required outputs.

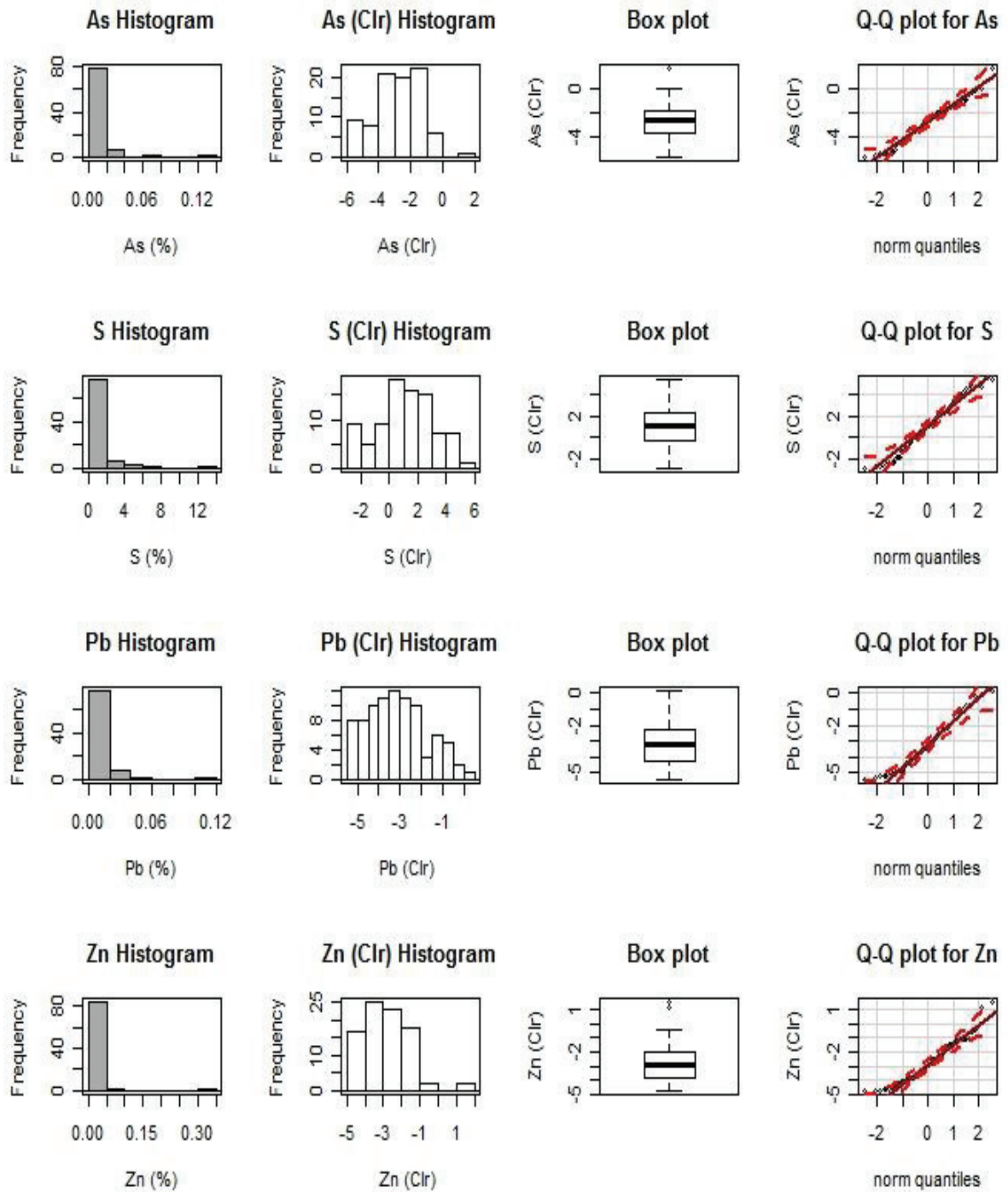


Figure 4.5: Exploratory data analysis. Histograms (both non transformed and Clr transformed) with Box plots and QQ plots for the Clr transformed data, of the mineralization related elements within Rodaquilar area.

Plots of the elements (Exploratory Data Analysis-EDA) shows that Clr is good in opening up the compositional datasets (resulting into an approximate Gaussian distribution), and hence we can apply the statistical measures to the data set. The resulting Histograms (approximate Gaussian distribution) and the QQ plots confirm this.

4.2.2. Mapping of Uni-elements populations.

Histograms, box plots and QQ plots (EDA) were examined to define populations groups in the dataset. Standard procedures as explained by (Carranza, 2010; Chiprés et al., 2009; Reimann, Filzmoser, & Garrett, 2005), were applied to come up with the threshold values of different elements, based on formula

$$\text{Threshold} = \text{Median} + 2 \text{ MAD} \dots\dots\dots (I)$$

In which MAD is the absolute deviations of all values from the data median.(Tukey, 1977)

4.2.2.1. Arsenic, Sulphur, Zn and Pb distribution

The histogram of the Clr transformed As, S, Zn and Pb data approximate a Gaussian distribution, with two populations.

As and S are spatially associated with areas of known gold mineralization see figures 4.7 and 4.8. Arsenic distribution can be explained as a pathfinder element for the epithermal gold deposit, while the high S concentrations within the area can be associated with mining activities not only for Au but also Pb-Ag which were taking place within the area. Zn and Pb show high values, which is common as it is known, they are associated with the epithermal systems. Rodalquilar was famous for the base metal mining before the discovery of the gold deposit.

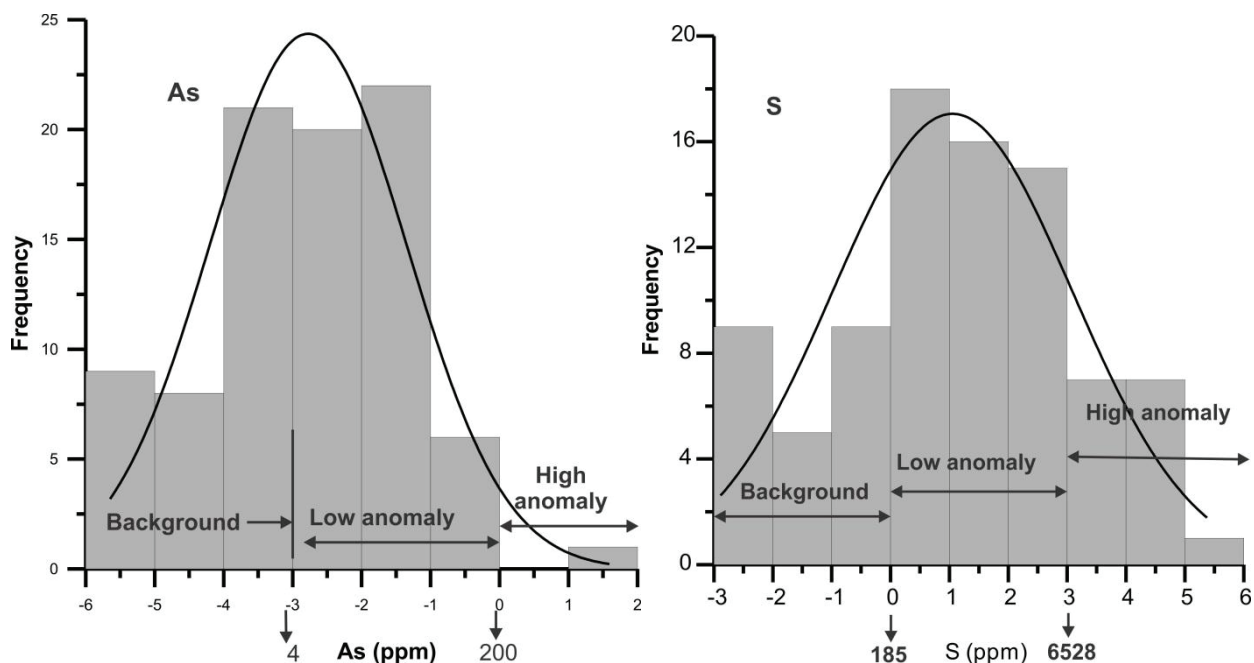


Figure 4.6: Histograms of Clr transformed data for As left and S right, showing approximate Gaussian distribution

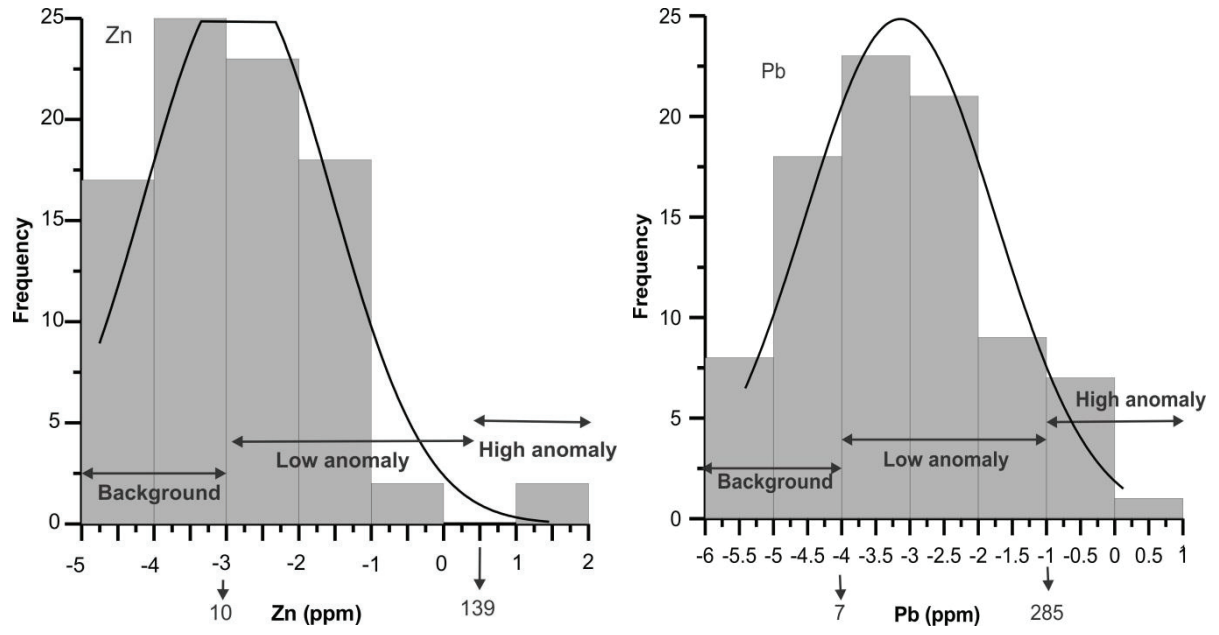


Figure 4.7: Histograms of Clr transformed data for Zn left and Pb right, showing approximate Gaussian distributions with two populations.

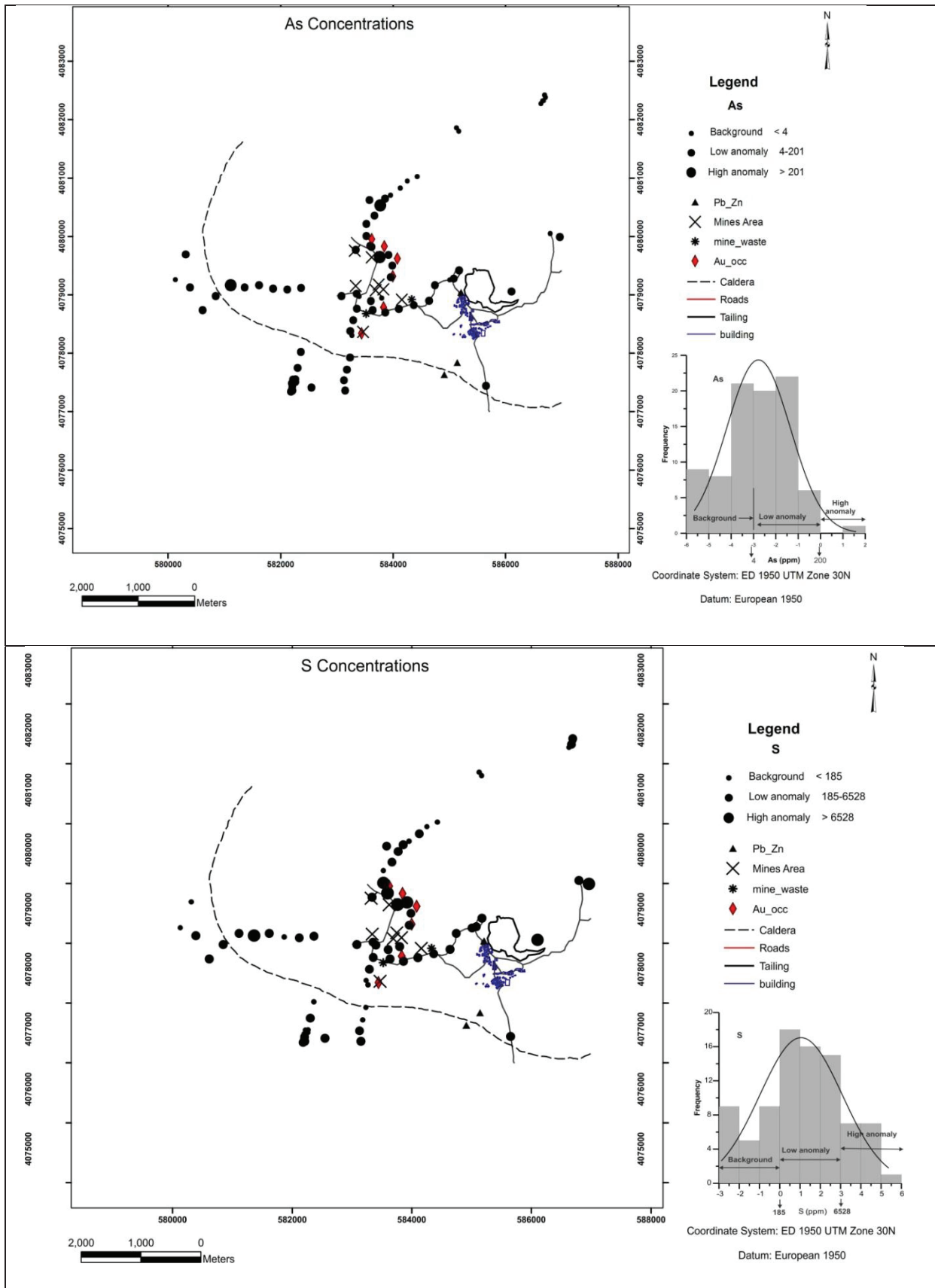


Figure 4.8: Geochemical map of As and S distribution within Rodalquilar gold deposits.

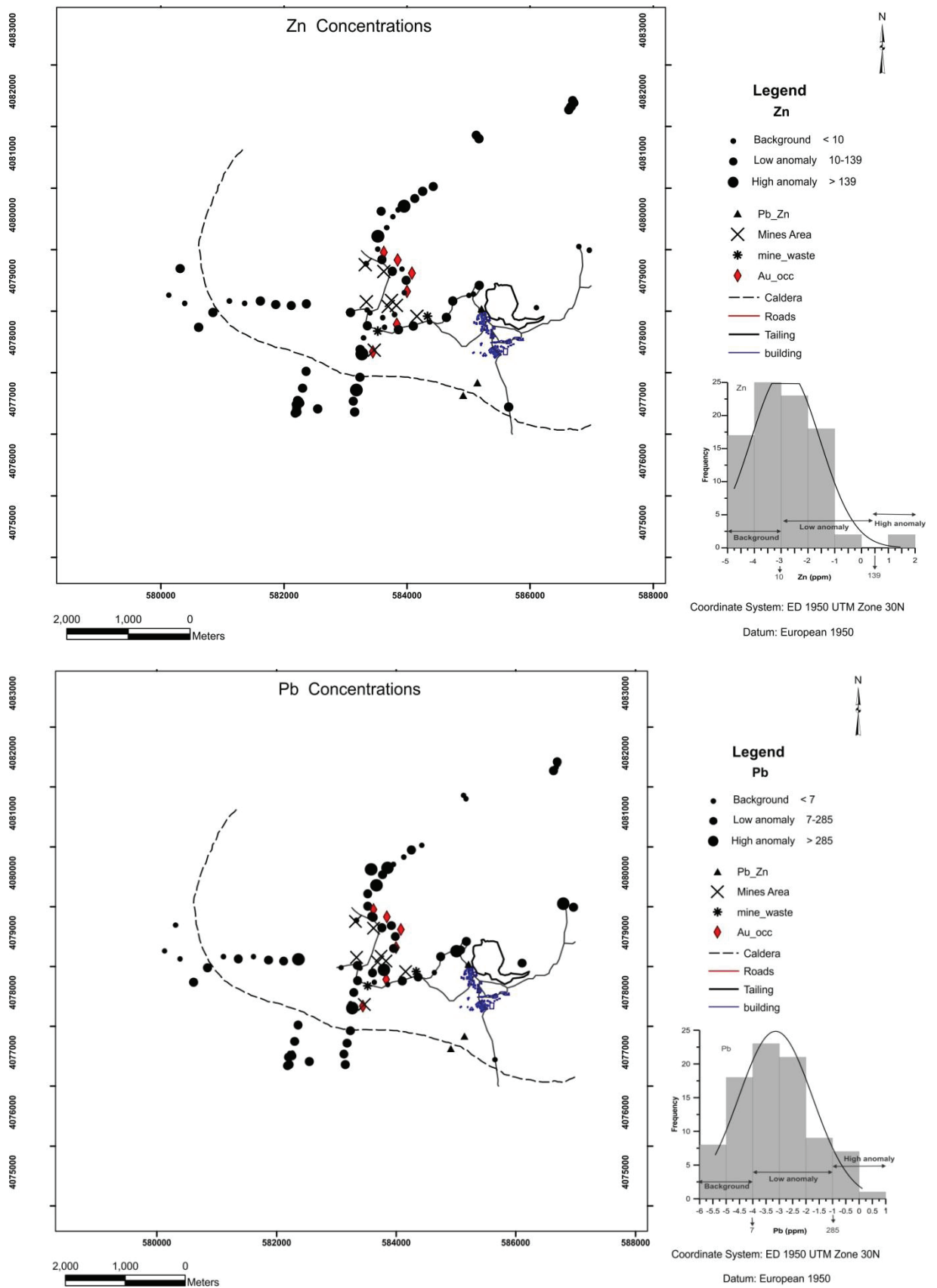


Figure 4.9: Geochemical map of Zn distribution within Rodalquilar gold deposit

4.2.3. Multi-variate statistical analysis.

Correlation analysis were applied to the dataset to reveal the relation between elements

Table 4.2: Correlation matrix of the Clr transformed data.

Clr transformed data correlation matrix																	
	Clr- Al2O3	Clr- CaO	Clr- FeO	Clr- K2O	Clr- MgO	Clr- SiO2	Clr- TiO2	Clr- As	Clr- Ba	Clr- Cl	Clr- Cr	Clr- Nb	Clr- Pb	Clr- Rb	Clr- S	Clr- Sr	Clr- Zn
Clr- Al2O3	1.00																
Clr- CaO	-0.29	1.00															
Clr- FeO	-0.43	0.15	1.00														
Clr- K2O	-0.27	-0.04	0.00	1.00													
Clr- MgO	-0.46	0.23	0.05	0.21	1.00												
Clr- SiO2	0.60	-0.48	-0.12	-0.36	-0.54	1.00											
Clr- TiO2	0.68	-0.20	-0.17	-0.42	-0.62	0.73	1.00										
Clr- As	0.11	-0.49	0.11	-0.10	-0.60	0.31	0.22	1.00									
Clr- Ba	0.02	-0.27	-0.10	0.46	-0.16	0.03	-0.12	0.11	1.00								
Clr- Cl	0.38	-0.19	-0.29	-0.51	-0.29	0.27	0.34	0.20	-0.40	1.00							
Clr- Cr	0.31	-0.40	0.07	-0.23	-0.19	0.38	0.16	0.17	0.21	0.00	1.00						
Clr- Nb	0.56	-0.32	-0.18	-0.45	-0.57	0.81	0.84	0.27	-0.18	0.35	0.21	1.00					
Clr- Pb	0.09	-0.48	-0.23	-0.03	-0.26	0.13	0.08	0.15	0.24	-0.04	0.08	0.17	1.00				
Clr- Rb	-0.36	0.13	-0.02	0.82	0.42	-0.42	-0.44	-0.30	0.32	-0.48	-0.28	-0.44	-0.09	1.00			
Clr- S	0.16	-0.40	-0.11	-0.31	-0.52	0.22	0.15	0.49	0.02	0.40	0.14	0.14	0.31	-0.60	1.00		
Clr- Sr	0.53	-0.18	-0.20	-0.60	-0.59	0.54	0.58	0.26	-0.22	0.50	0.31	0.58	-0.01	-0.76	0.46	1.00	
Clr- Zn	-0.22	0.20	0.11	0.18	0.22	-0.21	-0.16	-0.24	-0.02	-0.48	-0.22	-0.16	-0.10	0.30	-0.56	-0.28	1.00
Clr- Zr	0.64	-0.33	-0.14	-0.42	-0.62	0.83	0.86	0.32	-0.19	0.42	0.19	0.90	0.05	-0.51	0.22	0.63	-0.19

Al₂O₃, SiO₂, TiO₂, Zr, Nb and Sr, shows very high positive correlations between them, which can be linked to lithological associations. Dataset also shows high correlations between Rb and K₂O and between Zr and both SiO₂ and TiO₂. There is observed a strong correlation between Zr and Nb (0.90). The association of Nb with the rest of the elements is not clearly understood.

In order to reveal more information about the relationship between the elements, and reveal hidden multivariate data structures, factor analysis was applied to the dataset. Two major factors scores (factors 1: SiO₂, TiO₂, Nb and Zr; factors 2: As and S) reveal the elements associations related to lithology and mineralization respectively. See table 4.4. Scatter plots of the factors (fig.4.11) reveal an unclear clustering of elements between factor 1 and factor 2, factor 1 and factor 3, and factor1 and factor4 respectively. Since Zn and Pb are known to be associated with epithermal gold systems, clustering in factor 1 vs. factor 2 and factor1 and factor4 plots could be assumed to be related to mineralization within the area. This is however hard to explain as factor2 elements (S and Sr), assumed to be related to mineralization, belongs to different clusters in all plots.

Table 4.3: Factor scores of the Clr transformed data.

	Clr transformed data-factor scores									
	Component									
	1	2	3	4	5	6	7	8	9	10
clr- Al2O3	0.62	0.11	-0.02	-0.06	0.09	0.38	0.28	0.01	0.04	0.53
clr- CaO	-0.24	0.02	-0.26	-0.07	-0.10	-0.10	-0.25	-0.29	-0.82	-0.01
clr- FeO	-0.11	-0.02	0.09	-0.06	-0.05	-0.95	0.08	-0.12	-0.06	-0.05
clr- K2O	-0.30	-0.71	0.03	0.42	-0.05	-0.03	-0.22	-0.07	0.19	0.27
clr- MgO	-0.54	-0.28	-0.62	-0.19	-0.11	0.01	0.02	-0.18	0.14	-0.32
clr- SiO2	0.86	0.18	0.06	0.09	0.08	0.01	0.18	-0.01	0.29	-0.06
clr- TiO2	0.90	0.16	0.08	-0.07	0.05	0.07	0.02	0.04	-0.10	0.15
clr- As	0.16	0.12	0.90	0.02	0.10	-0.09	0.06	0.03	0.25	-0.07
clr- Ba	-0.07	-0.22	0.14	0.87	0.06	0.14	0.18	0.12	0.06	-0.01
clr- Cl	0.22	0.26	0.22	-0.58	0.46	0.37	0.00	-0.09	0.05	0.04
clr- Cr	0.14	0.18	0.04	0.15	0.08	-0.08	0.91	0.02	0.17	0.05
clr- Nb	0.92	0.15	0.11	-0.13	0.02	0.08	0.05	0.11	0.05	-0.11
clr- Pb	0.06	0.05	0.07	0.11	0.04	0.11	0.02	0.96	0.18	0.00
clr- Rb	-0.29	-0.87	-0.11	0.22	-0.13	0.05	-0.12	-0.05	-0.01	-0.02
clr- S	-0.02	0.63	0.35	0.08	0.48	0.02	-0.14	0.21	0.31	0.17
clr- Sr	0.47	0.71	0.14	-0.08	0.08	0.17	0.13	-0.13	0.02	0.21
clr- Zn	-0.10	-0.14	-0.07	0.01	-0.96	-0.04	-0.10	-0.03	-0.05	-0.01
clr- Zr	0.91	0.20	0.14	-0.13	0.06	0.04	0.00	-0.04	0.12	0.06
Total	6.78	2.34	1.95	1.40	1.12	0.96	0.83	0.63	0.39	0.35
% Variance	37.68	13.00	10.82	7.79	6.20	5.36	4.64	3.53	2.19	1.95
Cumulative %	37.68	50.68	61.51	69.30	75.50	80.85	85.49	89.01	91.20	93.16

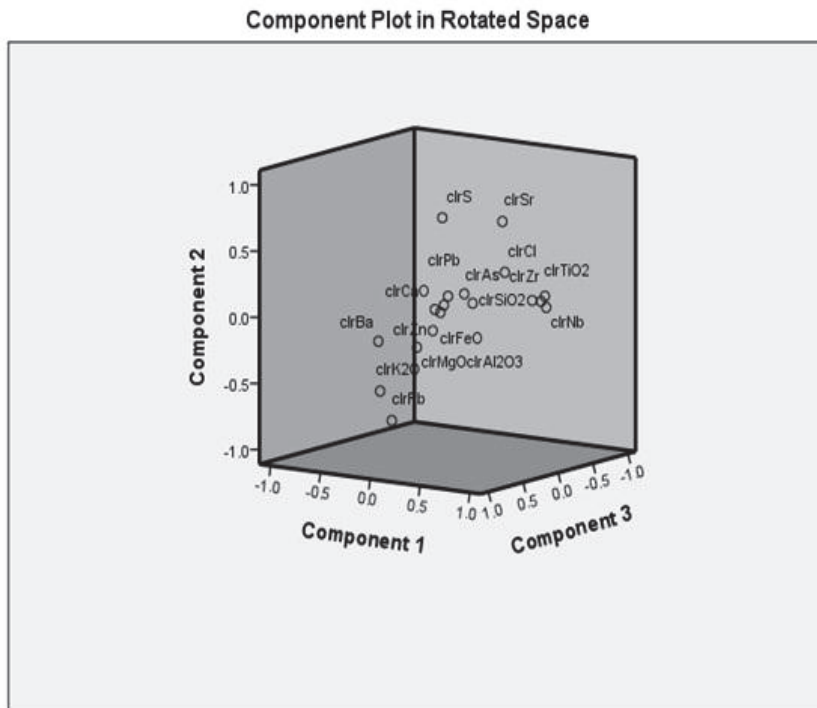


Figure 4.10: Components plot of the scores for the Clr transformed data

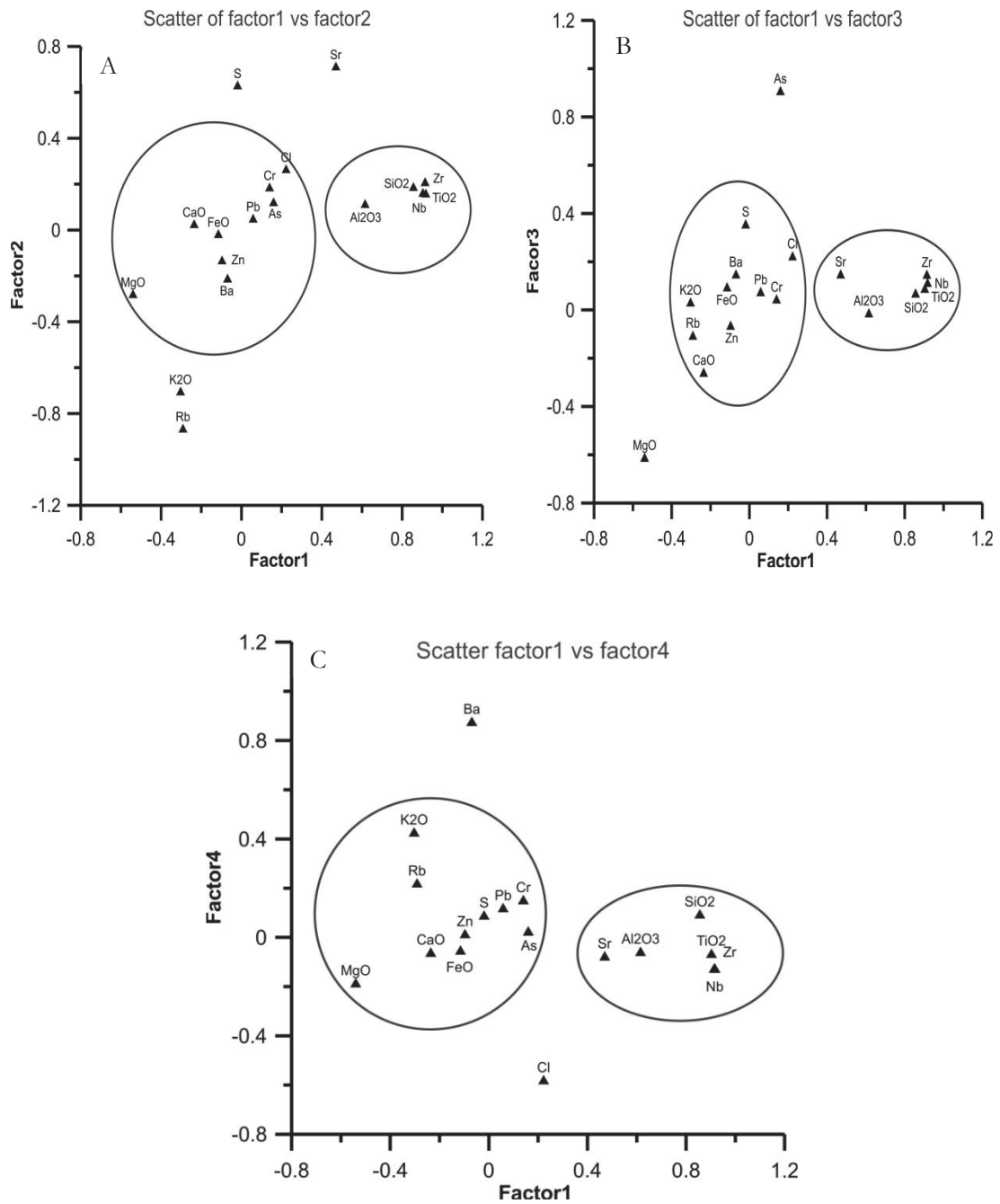


Figure 4.11: A, B and C scatter plots of factor1 against factor2, factor3 and factor4 respectively.

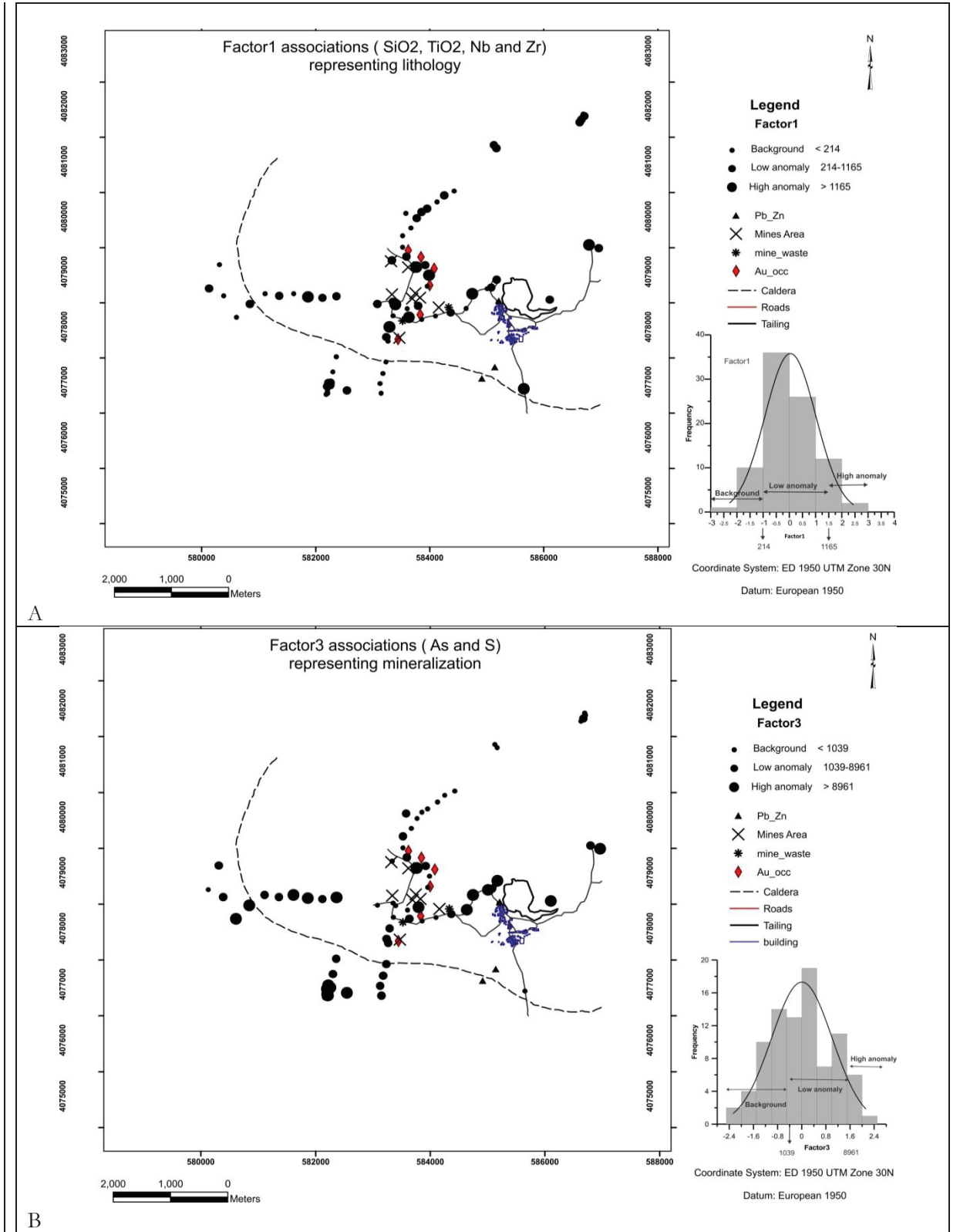


Figure 4.12: A and B Geochemical map of factor 1 and factor 3 scores, representing lithology and mineralization respectively

4.2.4. Litho geochemistry.

4.2.4.1. Trace elements geochemistry.

Elements of demonstrated immobility in hydrothermal alteration and metamorphism can provide useful litho geochemical parameters for mineral exploration. Immobile elements can yield precise identifications of precursor volcanic rock type and magmatic affinity, and quantitative estimates of mass, volume and mineralogical changes (M.A. Booden, J. L. Mauk, & Simpson, 2011; MacLean & Barrett, 1993; Pearce & Norry, 1979; Warren et al., 2007; Winchester & Floyd, 1977)

In this research immobile incompatible element (Zr) together with TiO₂, SiO₂ and Al₂O₃ are used to characterize the altered volcanic rocks. Data from Arriba's 1995 is used as part of this research for comparison and for calibration purposes. See table 4.5. and the figures.

Table 4.4: Samples from Arriba's 1995. Showing chemical composition of selected rocks types representative of the study area.

Alteration zone	Black chalcodony		Vuggy silica		Advanced argillic		Intermediate argillic		Sericitic		Propylitic		Unaltered rock	
	87A171b	87A284a	87A230	87A285	87A169	SRT185	S3-27	SRT378	SRT595	87A14	S2-125	S3-418	87A344	HPOR
Sample no.	1	2	3	4	5	6	7	8	9	10	11	12	13	14
SiO ₂ (wt %)	86.2	86.8	95	93.4	82	70.4	67.7	69.8	70.6	74.4	61.1	53.4	67.2	60.4
Al ₂ O ₃	1.66	0.97	1.19	0.78	6.84	16.8	18.7	16.4	15.3	14.7	15.6	15.3	14.4	15
Fe ₂ O ₃	4.51	5.07	0.85	2.58	0.98	2.53	4.17	3.79	3.14	1.81	5.49	9.14	2.37	6.85
MgO	0.1	0.1	0.1	0.1	0.1	0.16	0.32	0.1	1.07	0.78	3.38	6.73	1.44	4.5
CaO	0.1	0.05	0.03	0.02	0.03	0.1	0.05	0.06	0.17	0.04	2.78	4.16	2.97	7.79
Na ₂ O	0.17	0.17	0.15	0.17	0.31	0.32	0.15	0.24	0.2	0.32	3.18	3.48	2.71	2.29
K ₂ O	0.24	0.31	0.12	0.21	0.99	0.69	1.91	0.48	4.35	4.06	3.62	0.34	2.71	1.52
TiO ₂	0.25	0.4	0.38	0.38	0.4	0.42	0.62	0.47	0.46	0.29	0.54	0.61	0.25	0.53
P ₂ O ₅	0.37	0.14	0.09	0.05	0.12	0.16	0.05	0.11	0.12	0.09	0.11	0.13	0.09	0.1
MnO	0.02	0.02	0.02	0.02	0.02	0.02	0.02	0.02	0.02	0.02	0.1	0.39	0.05	0.12
L.O.I. 925°C	3.94	4.15	1.22	2.21	7.48	7.66	6.59	7.8	4.06	3.09	3.84	4.89	5.97	1.31
Rb (ppm)	90	22	10	10	14	16	96	10	182	152	132	14	196	52
Sr	2700	880	500	134	880	440	28	144	10	18	138	132	170	130
Y	22	10	10	10	10	10	24	10	26	24	34	28	24	12
Zr	130	110	116	102	142	120	140	120	125	120	104	82	122	78
Cu	910	2600	20	50	20	20	20	42	98	20	20	20	20	20
Zn	20	20	20	20	20	20	152	20	20	20	255	540	42	60
As	11800	130	100	2200	83	260	72	132	45	20	80	150	80	80

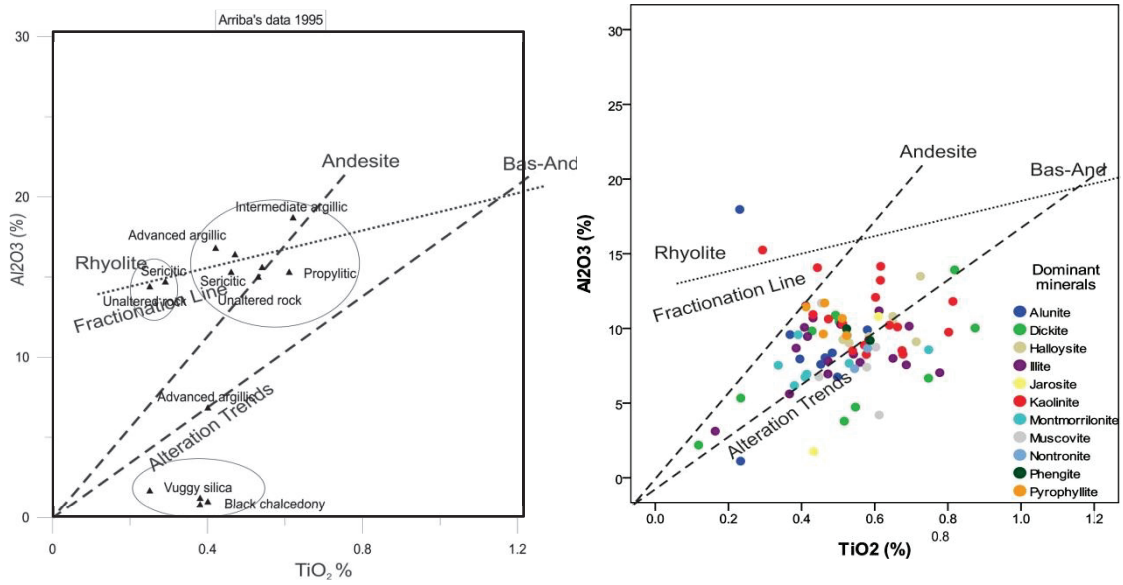


Figure 4.13: TiO_2 vs. Al_2O_3 for Arriba's 1995 dataset left and Niton readings right.

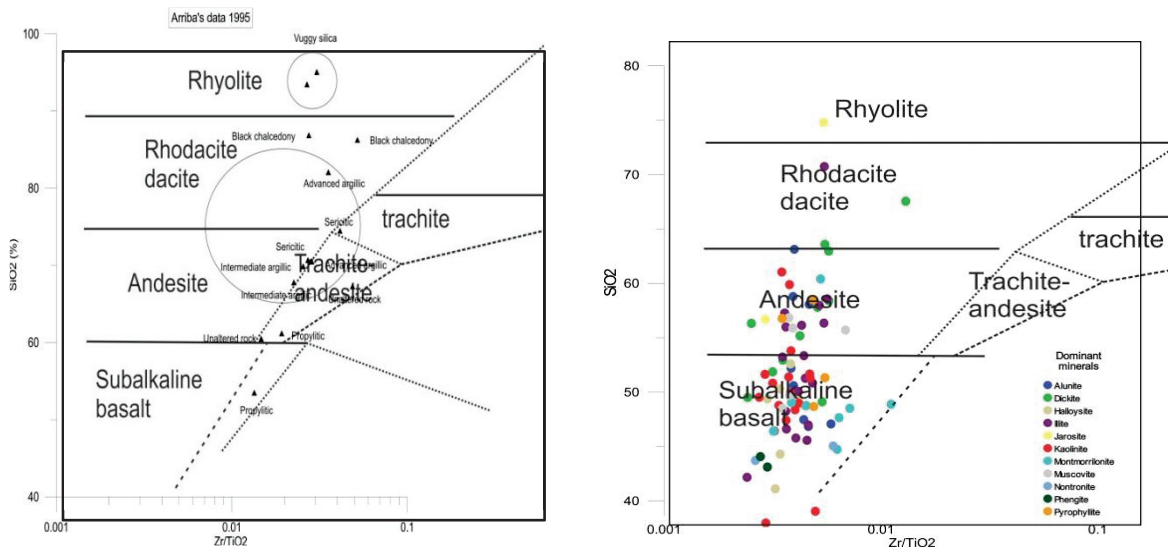


Figure 4.14: Zr/TiO_2 vs. SiO_2 for Arriba's 1995 dataset, left and Niton readings right.

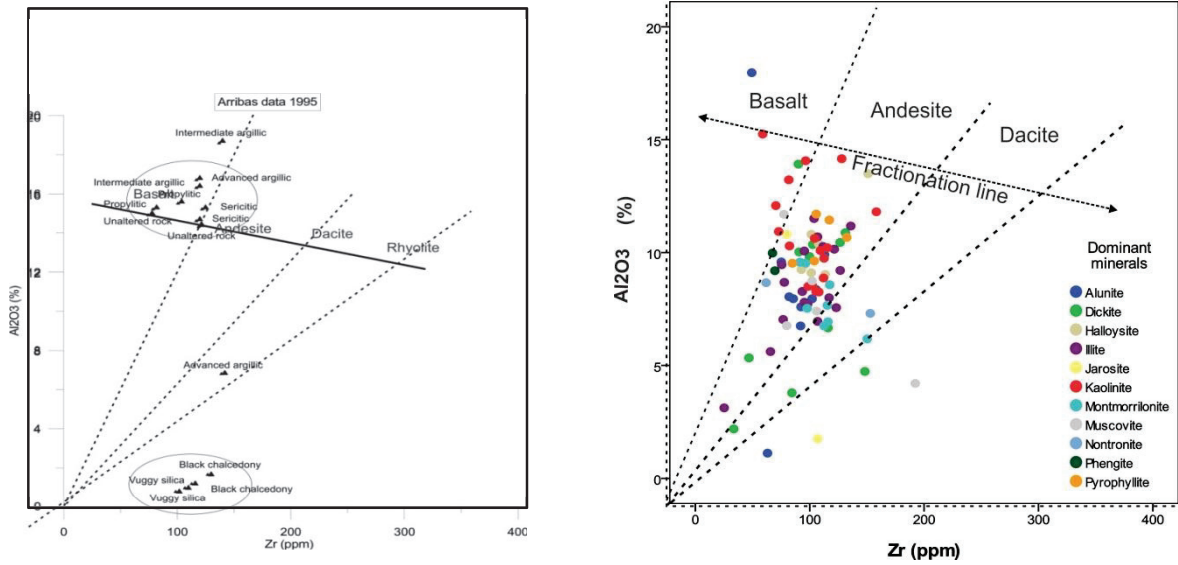


Figure 4.15: Zr (ppm) vs. Al₂O₃% for Arribas 1995 dataset, left and Niton readings right.

Arriba's data, 1995

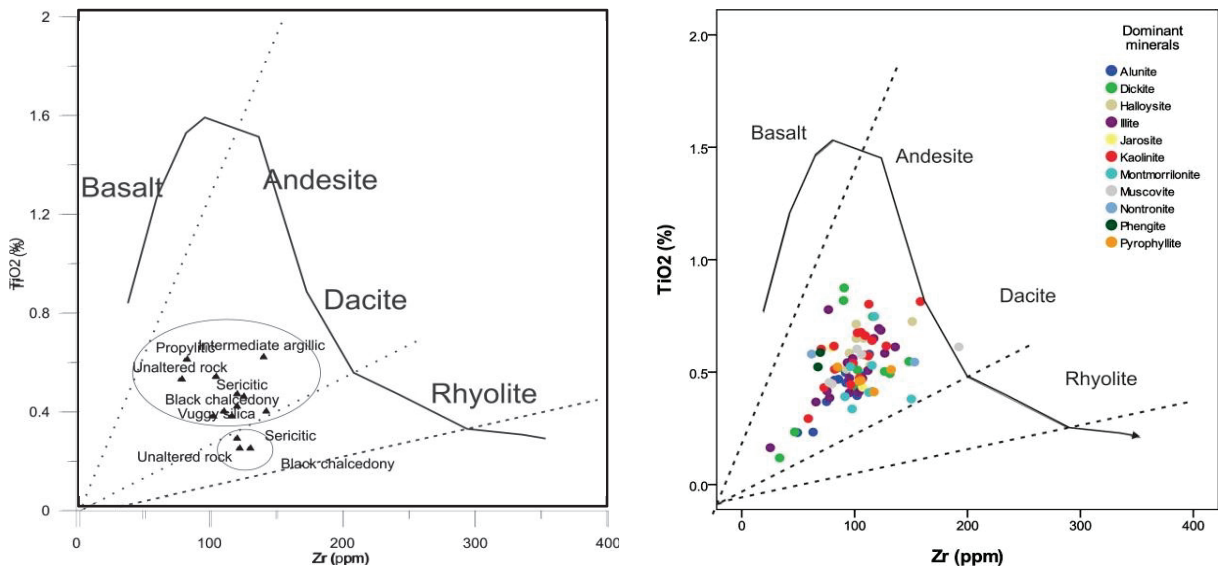


Figure 4.16: Zr (ppm) vs. TiO₂% for Arribas 1995 dataset, left and Niton readings right

The distribution of the elements within the area is very complex, as we are dealing with an intricate mineralized system. Many factors are controlling the geochemical variations within the area, these includes the lithology, alteration styles and the supergene enrichment. Among, all elements, Zr and TiO₂ seem to be more effective in discriminating the volcanic lithologies of the area, as the results range from Andesitic to Rhyolitic compositions, which ties with what the literatures reports about the area.

Zr and TiO₂ have contrasting behaviour during differentiations, hence the Zr/TiO₂ is preserved during K-metasomatism, and thus, theoretically, they should be able to show the extent of differentiation and alteration (M.A. Booden et al., 2011). The other elements show a wide variation of rock types, from Mafic

to Rhyolitic in compositions, which is quite contrary to the literature as well as field/ hand specimens. These contradictions can be attributed to the fact that we are dealing with a complex alteration system as stated earlier.

4.2.4.2. Alteration Indices

Alteration indices like the (modified) chlorite-carbonate-pyrite-index CCPI and Ishikawa alteration indices (AI) were used to produce the alteration box plots (Large, Gemmell, Paulick, & Huston, 2001). Such alteration box plots have been widely used for VMS deposits, and recently have also been applied to epithermal gold deposits (Gemmell, 2007). The method can provide mineralogical and geochemical features, which can be applied as a set of exploration vectors (Gemmell, 2007). Other alteration indices like the Hashigushi and Silicification indices, can also be used (Franklin, 1977) in graphs. From the results obtained; all indices proved to be capable of discriminating samples in terms of alteration intensities.

Modified Ishikawa Alteration Index takes care of the intensity of chlorite and sericite alteration

$$AI = 100 * (MgO + K_2O) / (MgO + CaO) \dots \dots \dots (2)$$

Modified chlorite-carbonate-pyrite-index takes care of chlorite, carbonate and pyrite alterations

$$CCPI = 100 * (MgO + FeO) / (MgO + FeO + K_2O) \dots \dots \dots (3)$$

Silicification index takes care of the enrichment of Si and the depletion of Al.

$$SI = 100 * SiO_2 / (SiO_2 + Al_2O_3) \dots \dots \dots (3)$$

The Hashigushi index takes care of the enrichment of Mg components and the depletion of Fe

$$HI = Fe_2O_3 / (Fe_2O_3 + MgO) \dots \dots \dots (4)$$

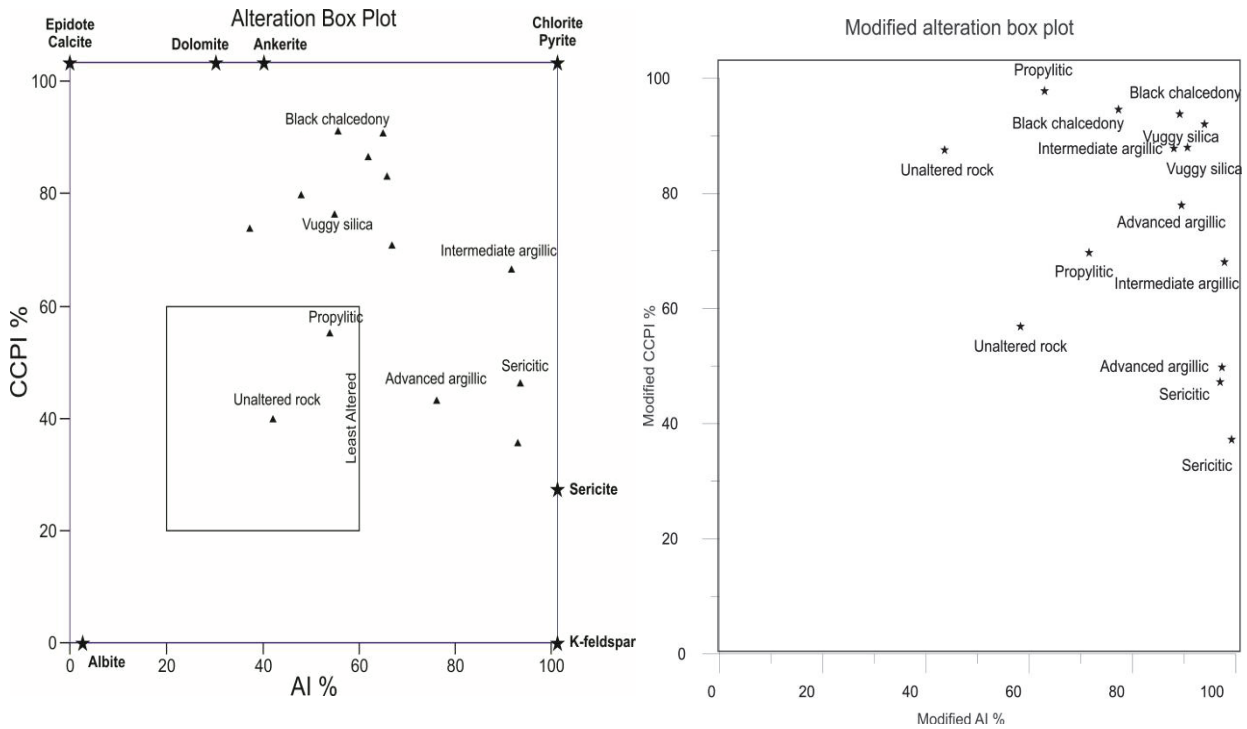


Figure 4.17: Box plot and modified box plot, left and right respectively, for Arriba's 1995 dataset.

There is a clear shift of the alteration intensities when comparing the conventional alteration box plot and the modified box plot for the Arriba's 1995 dataset .although there are few exceptions. Na_2O is very crucial in the hydrothermal alteration processes. Shallow hydrothermal systems are characterized by the gain of K and the loss of Na and Ca.(M.A. Booden et al., 2011) Missing Na_2O in the database has great consequences and this can be taken as one of the serious disadvantages of the PXRf instrument in lithological measurements., hence need to work on other alteration indices. Quantification of the shift, is not possible , as the shifting is not systematic in all directions/alteration styles, and also due to the fact that we are missing a key element, which counts for the mass transfer.

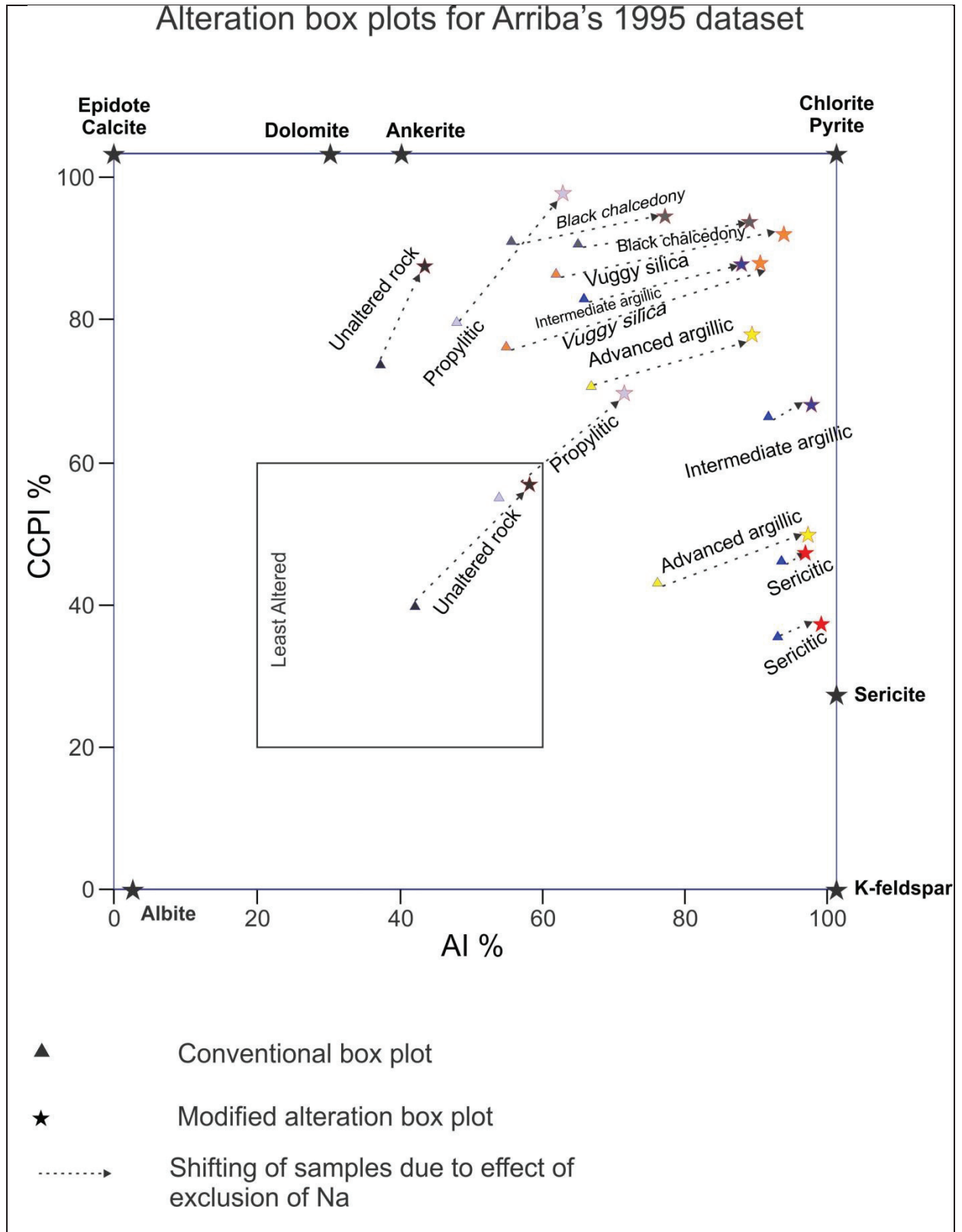


Figure 4.18: Plot of conventional alteration box plot overlaid to modified alteration box plot data from Arribas.

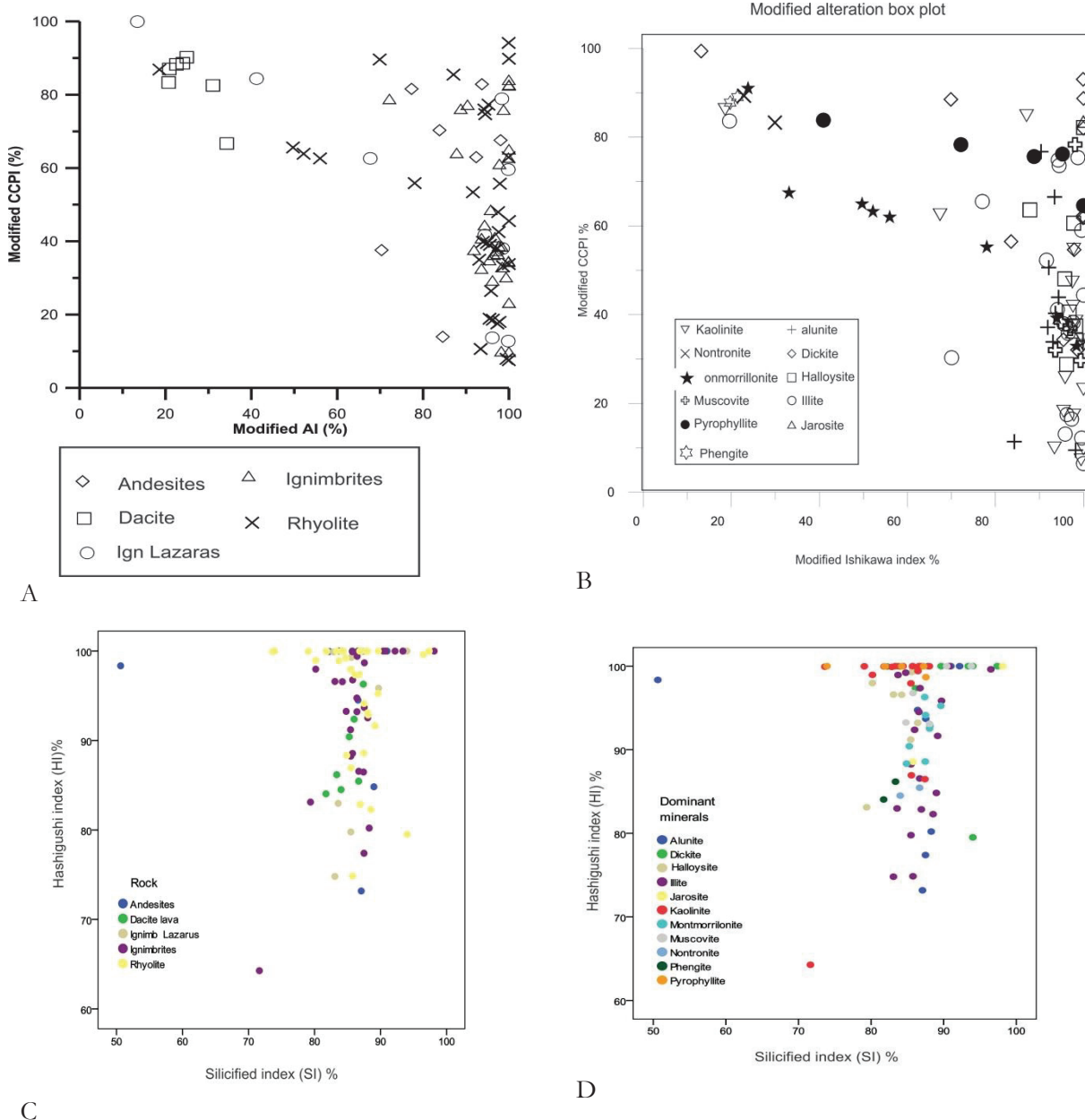


Figure 4.19: Plots of modified alteration box plot index (A) and (B) grouped by lithology type and by dominant mineralogy respectively compared to Silicified versus Hashigushi indices grouped by lithology and dominant mineralogy, respectively. (C) and (D).

The four modified box plots, shows a shift in position of alteration intensities as the result of the exclusion of the Na. To a certain extend the plots can still be used to delineate the alteration style and intensity of the epithermal gold system. The plot no. 4-19 D of Silicification index against Hashigushi index seems to be better than the modified alteration box plot in describing the alteration intensity. The results show that the rocks are highly altered as explained from the literatures and also observed from the hand specimens.

4.3. Concluding remarks.

In this chapter, different techniques have been applied to the geochemical dataset in order to get information about the lithology and hydrothermal alteration within the Rodalquilar epi-thermal gold deposit.

Trace and major elements were used to try to answer the research questions, in order to achieve the objectives of this research.. Based on the results from the trace elements geochemistry, it is possible to deduce different lithologies using the PXRF, and also it is shown that Zr and Ti are the most effective element in discriminating these lithologies.

The modified alteration box plots ,with certain level of uncertainty (due to the effects of the exclusion of Na) together with the Silicified and Hashigushi Indices calculated from the whole rock geochemistry, proved to be effective in delineating alteration styles and intensities for the epithermal deposits.

That it is possible to differentiate lithologies, different alteration styles and intensities, as well identifying the suitable elements which can be used to characterize different volcanic lithologies in and around of Rodalquilar epithermal gold deposit by using the portable XRF.

5. ANALYSIS OF ASD SPECTRAL DATA FOR IDENTIFICATION OF ALTERATION MINERALOGY

5.1. IR spectra data collection, processing and interpretation

An Analytical Spectral Devices (ASD Field Spec) full-range field spectrometer was used to collect hyperspectral data in laboratory on the rock powders. ASD FieldSpec Pro is a full computer controlled spectrometer with a spectral range of 350-2500 nm. It is designed to collect solar reflectance, radiance and irradiance measurements of materials. The full technical and quality-control considerations for operation of the ASD full-range spectrometer can be found in (Hatchell, 1999). Significant operational QA/QC considerations for the ASD spectrometer are primarily internal calibration, instrument optimization, white-reflectance Spectralon reference collection, and multiple spectral data collections per target. ASD FieldSpec Pro is compact and easy to set up, thus allowing much data collection. The device has a contact reflectance probe (see picture Fig. 5.1), which can be fixed to the fibre optic cable to provide spectral capabilities measurements. ASD allows collections of high quality reflectance spectra over a wide range of surfaces, with improved signal to noise ratio, making it ideal for a wide range of applications.

Detailed and simplified simplifications of ASD FielsSpec Pro is provided in table 5 (5.1) and figure (5.1) show the ASD Fieldspec Pro diagram.

Table 5.1: ASD Fieldspec Pro instrument specifications.


Spectral Range	350-2500 nm	
Spectral Resolution	3 nm @700nm 10 nm @1400 -2100 nm	
Sampling Interval	1.4 nm @ 350-1050 nm 2 nm @ 1000-2500 nm	
Scanning Time	100 milliseconds	
Detectors	One 512 element Si photodiode array 350-1000nm Two separate, graded index InGaAs photodiodes 1000-2500 nm	
Input	2 m. fibre optic (25° field of view) Optional foreoptics available	
Weight	7.2 kg. (excluding batteries, notebook and optional accessories)	

Figure 5.1: ASD FieldSpec Pro diagram

Laboratory spectra of rocks and rock powders were acquired using the ASD field Spectra by taking three measurements per rock samples and one measurement per rock powder sample. Significant operational QA/QC considerations for the ASD spectrometer are primarily internal calibration, instrument optimization, white-reflectance reference collection, and multiple spectral data collections per target. The pre-processing of the ASD data was done by applying the Splice correction, using the View Spec – Pro software, to correct for the shifting in spectrum. (3 detectors).

The corrected files were then exported as ASCII files, so that they could be used in other software (e.g. Envi or Spectral geologist), followed by building up the spectra library in Envi environment. The spectra were then processed by Spectral geologist software, by application of the standard techniques based on the standard formula for relative reflectance, using a linear interpolation technique for the hull-quotient reflectance spectrum derived by taking the ratio of the band reflectance spectrum to the enveloping upper convex Hull. (Hatchell, 1999) The technique is used to quantify the spectral absorption features that are related to a certain mineral, in terms of wavelength position, width, depth, asymmetry and slope of the upper convex hull. These spectral parameters are controlled by the crystal structure and chemical composition of the minerals, and hence they can be used to identify different volcanic rock types (Van der Meer, 2004)

5.2. The reflectance properties of minerals

Causes of Absorption: Electronic Processes

Application of visible-infrared spectroscopy in geology is primarily based on the fact that minerals do have unique spectral absorption features in the solar reflected spectrum. Study by Green (1998) utilized the use of imaging spectra in the visible-infrared region to determine the distribution of minerals in different scales (Green et al., 1998).

Minerals formed as a result of hydrothermal alterations, clays, carbonates and iron oxides can be mapped by using reflectance spectroscopy because they have characteristic strong molecular absorption features, which can best be seen in the short wave infrared wavelength region around $2.20\mu\text{m}$ (Van der Meer, 2004). Identification of hydrothermally altered minerals from hyperspectral images can help in understanding the geology and alteration pattern of the area (Debbas, van Ruitenbeek, van der Meer, Carranza, & Stein, 2005). When subjected to a mineral, photons may be reflected or refracted (scattered) from grain surfaces, pass through the grain, or absorbed by the grain surface. Scattered photons can be detected and measured. Light is absorbed in minerals by several processes, these processes and the wavelength dependency can allow derivation of different information about the chemistry of the minerals.

The ASD spectrometer can be used to measure absorptions due to these processes (Clark, 1995, 1999)

Electronic and vibrational processes are the two well-known causes of absorption in the VNIR and SWIR. Detailed information about reflectance of different minerals can be found in the website of USGS. <http://speclab.cr.usgs.gov/PAPERS.refl-mrs/refl4.html>

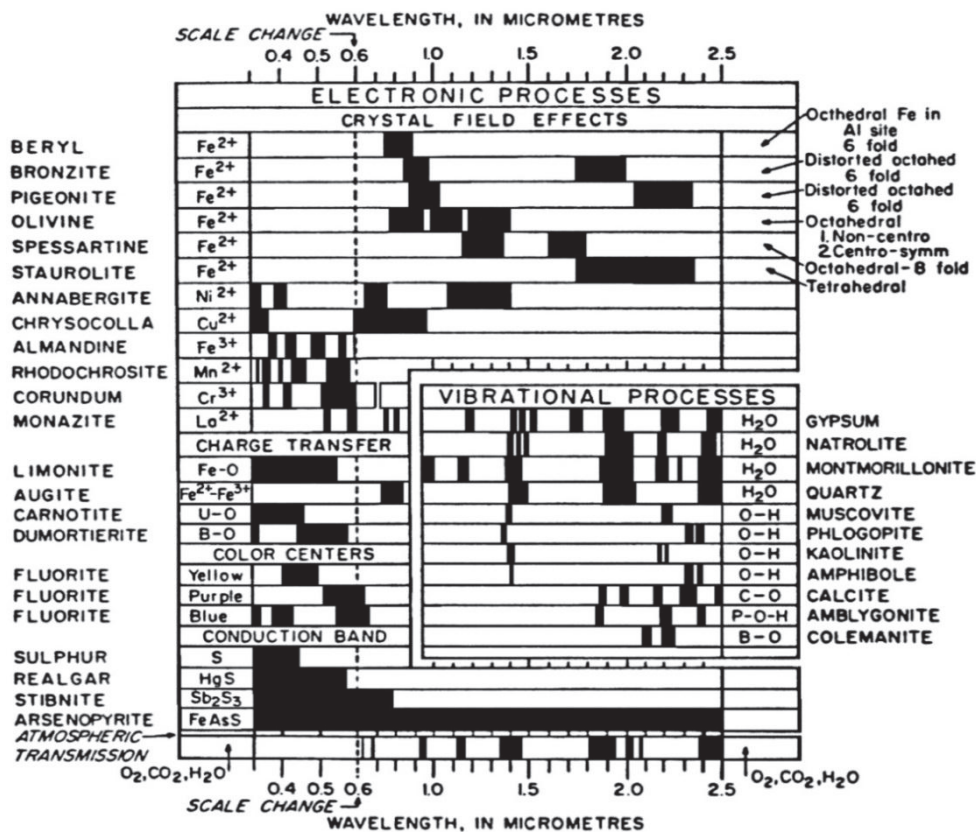


Figure 5.2: Spectra signature diagram. The width of the black bars indicate the relative widths of absorption bands (adapted from Clark, 1999)

High sulphidation epithermal deposits are characterized by advanced and intermediate argillic alterations. The following paragraphs will try to explain the alteration minerals associated with advanced and intermediate argillic alterations, and their spectral characteristics.

The spectral characteristics features of some clay and hydrous silica minerals are summarized in the following paragraphs, from help document of spectral software of CSIRO (Sasha, 2004).

Copied from (Yirgu, 2008)

Alunite: a sulphate minerals with a chemical formula of $(K, Na)Al_3(SO_4)_2(OH)_6$. Spectrally alunite can be classified into K-alunite or Na-alunite. The doublet near 2165nm and 2175nm is a diagnostic feature of both K-alunite and Na-alunite. In a multiphase mixture a spectral feature near 1765nm and 1475nm is usually the only recognizable features of alunite.

Pyrophyllite $Al_2Si_4O_{10}(OH)_2$

the presence of small quantities of pyrophyllite gives very sharp spectral features. The sharp features near 2188nm and 1388nm are the two characters features of pyrophyllite. A doublet occurs near 2070nm and 2080nm with additional small features near 2222nm, 2320nm and 2348nm. A minor shoulder occurs on the short-wavelength side of the major 2188nm feature.

Kaolinite ($Al_2Si_2O_5(OH)_4$) is spectrally characterized by a pair of doublets centered near 1400nm and 2200nm where 1450nm feature is being deeper than 1400nm features in the first doublet. The second doublet is composed of 2166 and 2206 features with 2206 is being the stronger. The relative sharpness and depth of the two doublets is caused by variation in crystallinity thus the poorly crystalline becomes more of shoulder in the two doublets. Additional features occur near 1360nm and a triplet near 2320nm, 2350nm and 2380nm and small feature can be visible near 1850nm. Kaolinite may be discriminated from dickite by the fact that the 1400nm doublet is closer together, typically 10-15nm in kaolinite, whereas it exceeds 20nm in dickite and halloysite.

Halloysite $Al_2Si_2O_5(OH)_4$: it shows doublet features around 1400nm and 2200nm like other kaolin. However the doublet structures are less well defined in halloysite than kaolinite. The 1400nm doublet consists of 1412nm and 1390nm features with the former is being the deeper whereas the second doublet consists of a 2175nm and 2210nm features usually with the latter the deeper. The wave length in both doublets is wider than kaolinite and slightly narrower than dickite. Unlike dickite and most kaolinites, the 1910 nm water absorption is a major feature.

Dickite $Al_2Si_2O_5(OH)_4$: is found in association with alunite and quartz in intensely acid-leached part of hydrothermal alteration systems. It belongs to kaolin group of clay minerals with pair of doublets centred near 1400nm and 2200nm.

Illite : $(K,H_3O)(Al,Mg,Fe)_2(Si,Al)_4O_{10}[(OH)_2,(H_2O)]$

the major diagnostic, fairly sharp features of illite are located near to 1408, 2200, 2348, 2442 nm. A broad "dimple" can occur near 2100 nm. Illite differs from muscovite/sericite spectra by its relative deep water bands at 1910 and 1460 nm. Research suggests that short-wavelength absorptions near 2190 are likely to be more sodic and those at longer wavelengths, near 2206, are more potassic. Fe-bearing illites have been known to have absorptions near 2240 nm. Mixed layer smectite/illites have shoulders near 1455, deep 1910 nm water features.

Montmorillonite $((Na,Ca)_{0.33}(Al,Mg)_2(Si_4O_{10})(OH)_2 \cdot nH_2O$: it is some time called smectite. It shows a great absorption features near 2208 nm, along with intense and asymmetric features at 1410 nm and 1910 nm. Both the 1410 and 1910 nm features are obviously asymmetric. The asymmetric feature is occurring due to a shoulder developed near 1460 nm and due to intense water absorption at 1940 nm.

5.3. Identified minerals and their diagnostic absorption features.

This section describes different alteration minerals identified in the 87 rock powders after interpretation with spectra interpretation field manual (Pontual, Merry, & Ganson, 1997) and comparison with USGS spectral library from the ENVI software..

Analysis of the field data is based on interpretation from TSG and spectral interpretation field manual as well as comparison with USGS spectral library. Results of the method applied show the presence of several SWIR –active alteration minerals which includes: alunite, dickite, halloysite, illite, jarosite, K_alunite, kaolinite, montmorillonite, muscovite, prophyllite and mixture of these minerals. Some samples have pure spectra of the identified mineral, while others occur as a mixture with other minerals. Spectral parameters such as absorption depth, position and crystallinity index were derived from the spectra , so that we can get the information about the relative abundance and crystallinity of the rocks.

5.3.1. Kandite minerals group

Kaolinite and halloysite are common minerals that belong to kandite group in the alteration system of the study area. Some dickite is also observed with some variation. These minerals are not easy to differentiate because they have similar spectral shape and absorption features and they often occur together as mixture in samples.

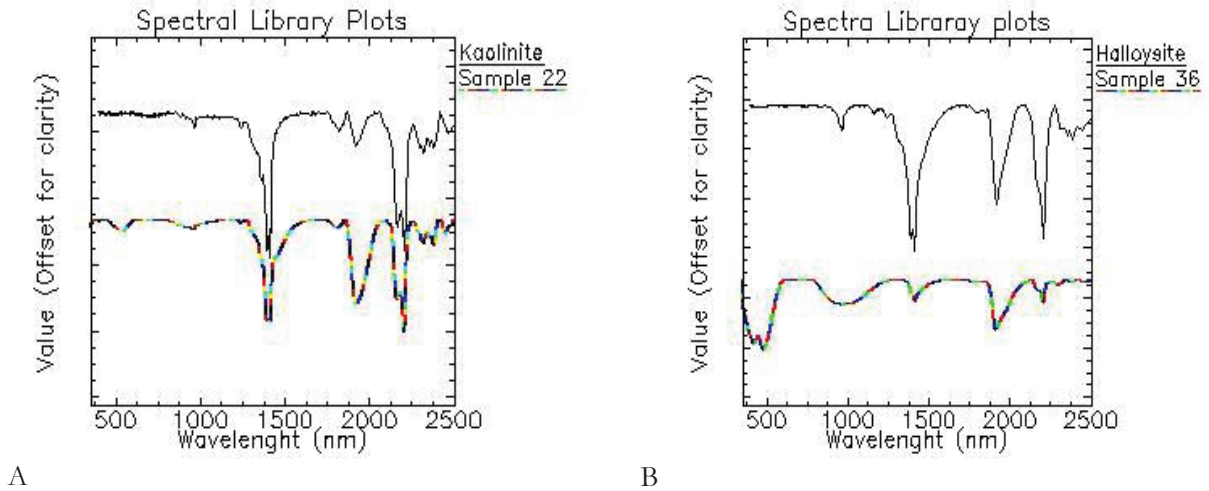


Figure 5.3: Spectra showing kandite minerals group observed , Kaolinite A and Halloysite B.

5.3.1.1. Crystallinity for Kaolinite.

Kaolinite crytallinity indicates (KCI) a degree of structure order in a solid and therefore this parameter can give a clue about which environment we are dealing with (Pontual, Merry, & Ganson, 1997b). Kaolinite crystallinity can be described in terms of slope of the spectrum in the 2160-2180 nm region. The slope 2160 and slope 2180 parameters are calculated as the ratio at 2160 nm over 2177 nm and ratio at 2184 nm over 2190 nm respectively. The slopes are analysed based on the shape and wavelength spacing of the Al-OH band doublets absorption feature.

Kaolinite crystallinity can also be expressed by combining the two slope parameters (2160 and 2180 slopes), using the formula:

$$KCI = (2180 \text{ slope} - (2160 \text{ slope} - 2180 \text{ slope}))$$

where KCI = Crystallinity Index for Kaolinite

The KCI increases in value with increasing kaolinite crystallinity. The Index has an advantage over the slope parameters in the sense that, it can be presented as histogram or line profile.

The kaolinite crystallinity index ranges between 0.789 and 1.063. Most of the indices fall between 0.996 to 1.063, with the exception of one sample (sample number 76) which has the lowest crystallinity value of 0.789.

KCI is plotted spatially (Figure 5.4) to find out if there is a pattern in kaolinite crystallinity over the area and to see the variation in their values.

From the plot, a pattern was observed for the kaolinite crystallinity within the study area. The moderately and highly crystalline are found outside the highly altered area, while the highly altered area, in this case the mineralized area is characterized by low values of crystallinity index as compared to the periphery area. In this case, we simply conclude that, the mineralization within the study area is associated with low crytallinity kaolinites.

GEOCHEMICAL AND SPECTRAL CHARACTERIZATION OF HYDROTHERMAL ALTERATION FACIES AT THE EPITHERMAL GOLD MINERALIZATION AT RODALQUILAR, SPAIN

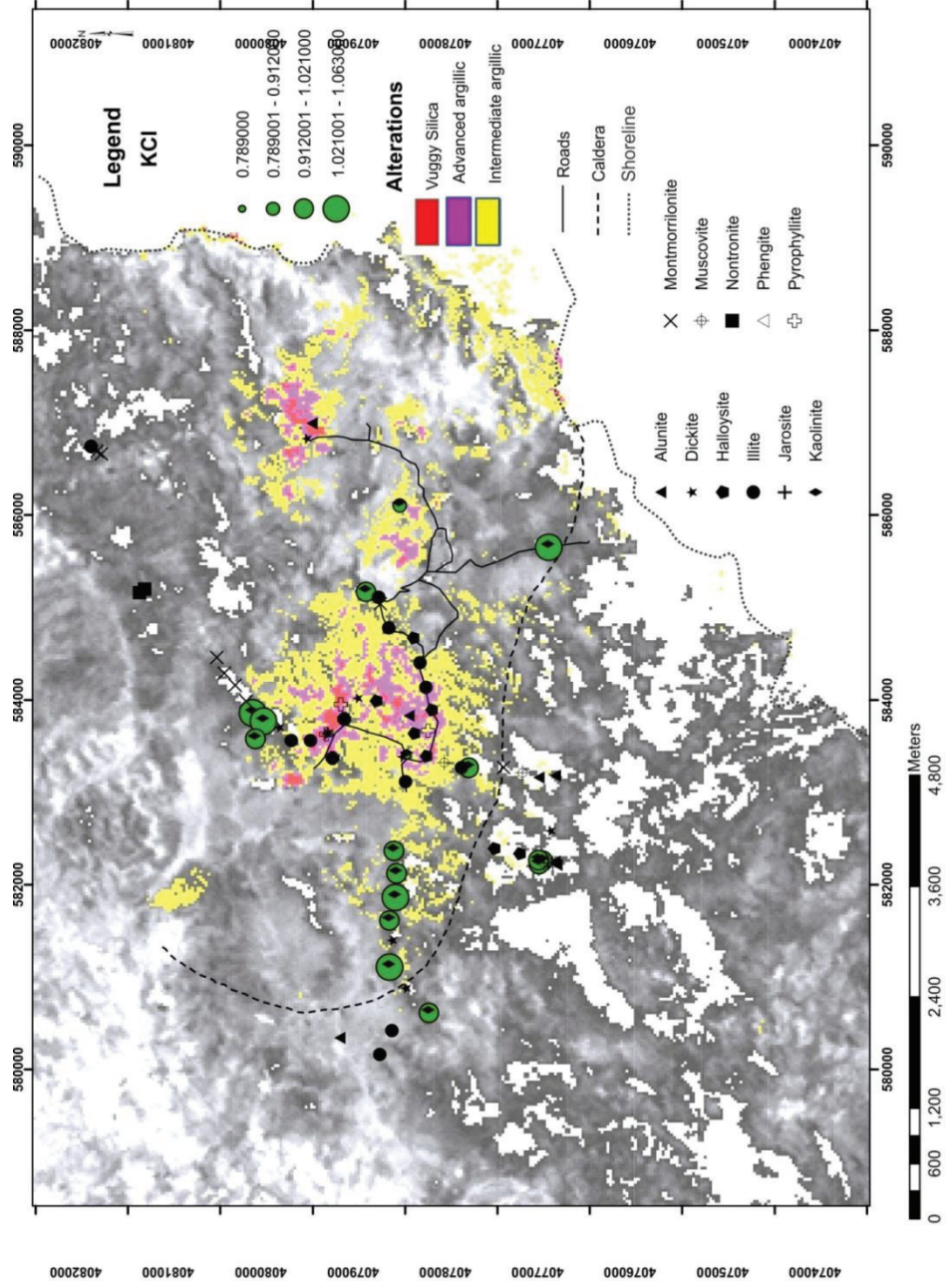


Figure 5.4: Spatial variation of dominant mineralogy overlaid on the alteration Map of Aster band ratio modified after Arribas 1990 alteration Map .

Table 5.2: Spectra parameters of kaolinite , a subset of samples observed to have kaolinite as the dominant mineralogy.

Original Number	Powder_ID	X	Y	Rock_Name	Dominant_min	Secondary_min	D_1900	D_2200	R_2160	R_2177	slope 2160	R_2184	R_2190	Slope 2180	KCI	P_2200
01004pm1_p.FOS	P_08	585171	4079421	Ignimbrites	Kaolinite	Montmorillonite	0.277	0.125	0.96	0.943	1.017	0.935	0.924	1.012	1.007	2208
01015pm1_p.FOS	P_20	582368	4079119	Rhyolite	Kaolinite	Alunite	0.132	0.0929	0.965	0.956	1.01	0.951	0.944	1.008	1.006	2208
01016pm1_p.FOS	P_21	582122	4079090	Rhyolite	Kaolinite	Illite	0.111	0.127	0.964	0.945	1.019	0.935	0.922	1.014	1.009	2208
01027pm_p.FOS	P_22	585652	4077444	Rhyolite	Kaolinite		0.252	0.337	0.766	0.779	0.983	0.783	0.771	1.016	1.049	2207
01029pm_p.FOS	P_23	586103	4079058	Rhyolite	Kaolinite	K_Alunite	0.0859	0.285	0.775	0.741	1.046	0.749	0.765	0.979	0.912	2207
01051pm_p.FOS	P_26	583267	4078307	Rhyolite	Kaolinite		0.273	0.0819	0.981	0.978	1.002	0.974	0.964	1.01	1.018	2208
01059pm_p.FOS	P_34	582225	4077549	Ignimbrites	Kaolinite		0.0927	0.0459	0.987	0.975	1.013	0.97	0.965	1.005	0.997	2207
01091pm_p.FOS	P_48	582261	4077509	Ignimbrites	Kaolinite		0.0796	0.0414	0.985	0.975	1.011	0.97	0.967	1.004	0.997	2208
01093pm_p.FOS	P_50	582267	4077554	Ignimbrites	Kaolinite		0.098	0.0583	0.98	0.967	1.014	0.962	0.957	1.005	0.996	2207
03021pm_p.FOS	P_51	581866	4079105	Rhyolite	Kaolinite		0.171	0.261	0.867	0.86	1.008	0.852	0.834	1.022	1.036	2207
03022pm_p.FOS	P_52	581616	4079167	Rhyolite	Kaolinite	Alunite	0.2	0.146	0.937	0.933	1.005	0.927	0.915	1.013	1.021	2207
03024pm_p.FOS	P_54	581113	4079167	Rhyolite	Kaolinite		0.279	0.234	0.886	0.874	1.015	0.862	0.844	1.022	1.029	2207
03026pm_p.FOS	P_56	580615	4078739	Andesites	Kaolinite	Jarosite	0.125	0.0507	0.988	0.979	1.009	0.975	0.97	1.006	1.003	2208
02005pm1_p.FOS	P_60	583581	4080620	Rhyolite	Kaolinite	K_Alunite	0.302	0.302	0.796	0.786	1.012	0.782	0.773	1.012	1.012	2207
02023pm1_p.FOS	P_65	583858	4080649	Rhyolite	Kaolinite		0.288	0.336	0.79	0.797	0.991	0.793	0.772	1.027	1.063	2207
02024pm1_p.FOS	P_66	583770	4080531	Rhyolite	Kaolinite		0.301	0.244	0.849	0.849	0.999	0.847	0.835	1.015	1.031	2208
02035pm1_p.FOS	P_76	583398	4078972	Ignimb Lazarus	Kaolinite	Nacrite	0.165	0.348	0.788	0.695	1.135	0.698	0.725	0.962	0.789	2206

5.3.2. Smectite

This is another clay minerals group present in the samples analysed. The minerals include montmorillonite and nontronite. In analysed samples, both montmorillonite and nontronite are observed in some of the samples. Montmorillonite is an alteration product of volcanic tuffs and ash, it is formed as a late-hydrothermal formation in various rocks. In high sulphidation epithermal system, montmorillonite is typical of the periphery of the alteration zonation (quartz-alunite-kaolinite-illite-montmorillonite-Chlorite)(Robb, 2005)

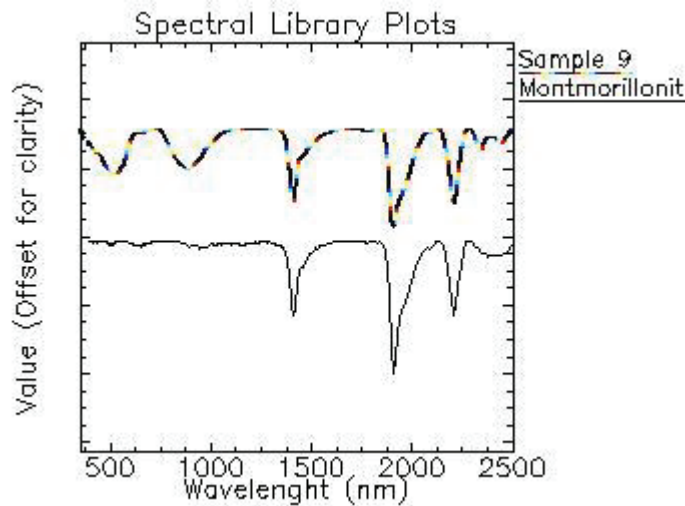


Figure 5.5: Spectra of montmorillonite observed in the study area

5.3.3. Sulphate group

K alunite, alunite and jarosite are common minerals in this group. K₂alunite, is the dominant mineral in the area, spectra of K₂alunite is observed in most of samples, though alunite and jarosite spectra, also exist in analysed samples. In general, alunite occurs as veins and replacement masses in trachyte, rhyolite, and similar potassium rich volcanic rocks. Alunite is formed by the action of sulphuric acid bearing solutions on these rocks during the oxidation and leaching of metal sulphide deposits.

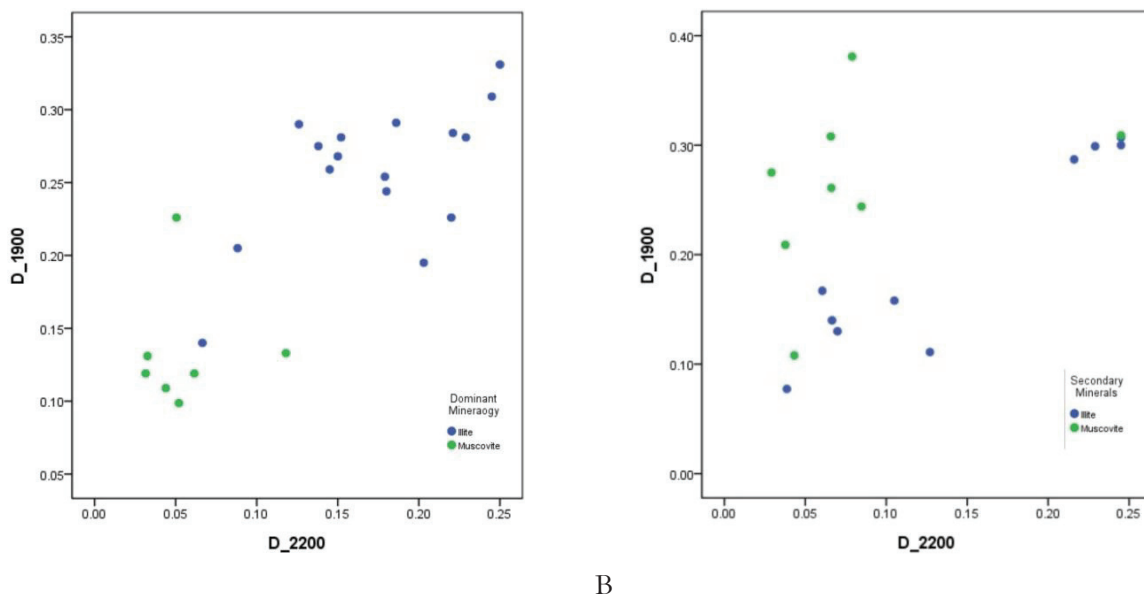
5.3.4. Illite-Sericite-Muscovite group

This is a group of mica minerals observed within the area. Illite and muscovite spectra are observed in analysed samples. Illite is typically found as extremely fine-grained masses of greyish-white to silvery-grey, sometimes greenish-grey, material. Illite can be found in a wide variety of environments, formed as a result of either weathering or hydrothermal alteration of muscovite-phengite, Illite can also be authigenic or could be derived from alteration of K-feldspars or recrystallization of smectites.(Meunier, 2005). In the study area, very few samples indicate the presence of phengite minerals as the dominant or secondary alteration mineral.

5.3.4.1. Crystallinity of illite and muscovite

The crystallinities of illite, muscovite and kaolinite, were studied in combination with mineral chemistry to see whether it is possible to characterize the lithology, and alteration style of the Rodalquilar gold deposit area using the ASD data.

The relationship between depth parameters for the Al-OH and H₂O/OH are plotted to try to show how the crystallinity of the illite /muscovite varies within the study area. The illite/muscovite crystallinity can be observed by looking on increasing sharpness of the AlOH, increasing depth of AlOH relative to H₂O, and weakening of H₂O feature(Pantual, Merry, & Ganson, 1997).



A

B

Figure 5.6: Plots of the crystallinity of illite and muscovite (A), grouped by dominant mineralogy, and crystallinity of illite and muscovite (B) grouped by secondary mineralogy

Plot shows that, the illite and muscovite relationship, can better be addressed with the secondary mineralogy rather than the dominant mineralogy. Plot A gave a bit of strange result, while plot B, gave a pattern which is known for the crystallinity of illite and muscovite.

5.3.5. Pyrophyllite group

This is the last group of minerals observed within the area. Pyrophyllite spectra are observed in few samples. Pyrophyllite is found mainly as a hydrothermal alteration product derived from feldspar in typically higher temperature alteration assemblages.

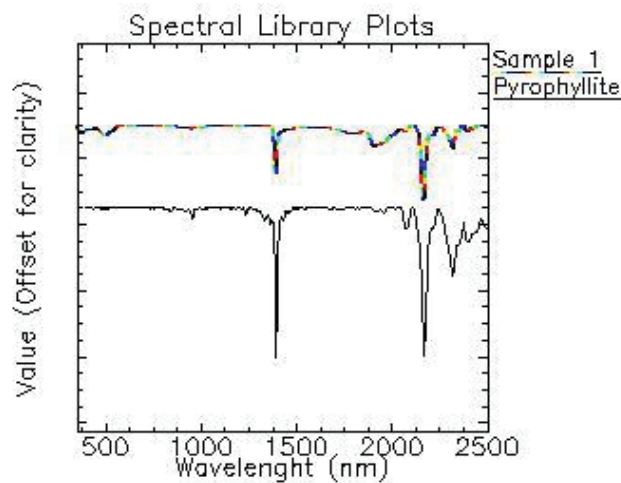


Figure 5.7: Spectra of pyrophyllite mineral observed within the study area

In most of the analysed samples, spectra of minerals occur as a mixture with other minerals, with no pure spectra to describe their diagnostic features. Some minerals like kaolinite, pyrophyllite and alunite were identified by their diagnostic features.

From the results of the dominant and secondary mineralogy observed within the study area, the most prevalent alteration minerals observed belongs to sericite, argilization and silicification which are typical for the high sulphidation epithermal system. Looking on the mineral map (fig 5.11), it can be observed also, that there is a kind of mineral zoning (quartz-alunite-kaolinite-illite- montmorillonite), which is a typical zoning for the high sulphidation epithermal system, though in the zoning sequence, chlorite mineral is absent (chlorite has not been observed in the study area)

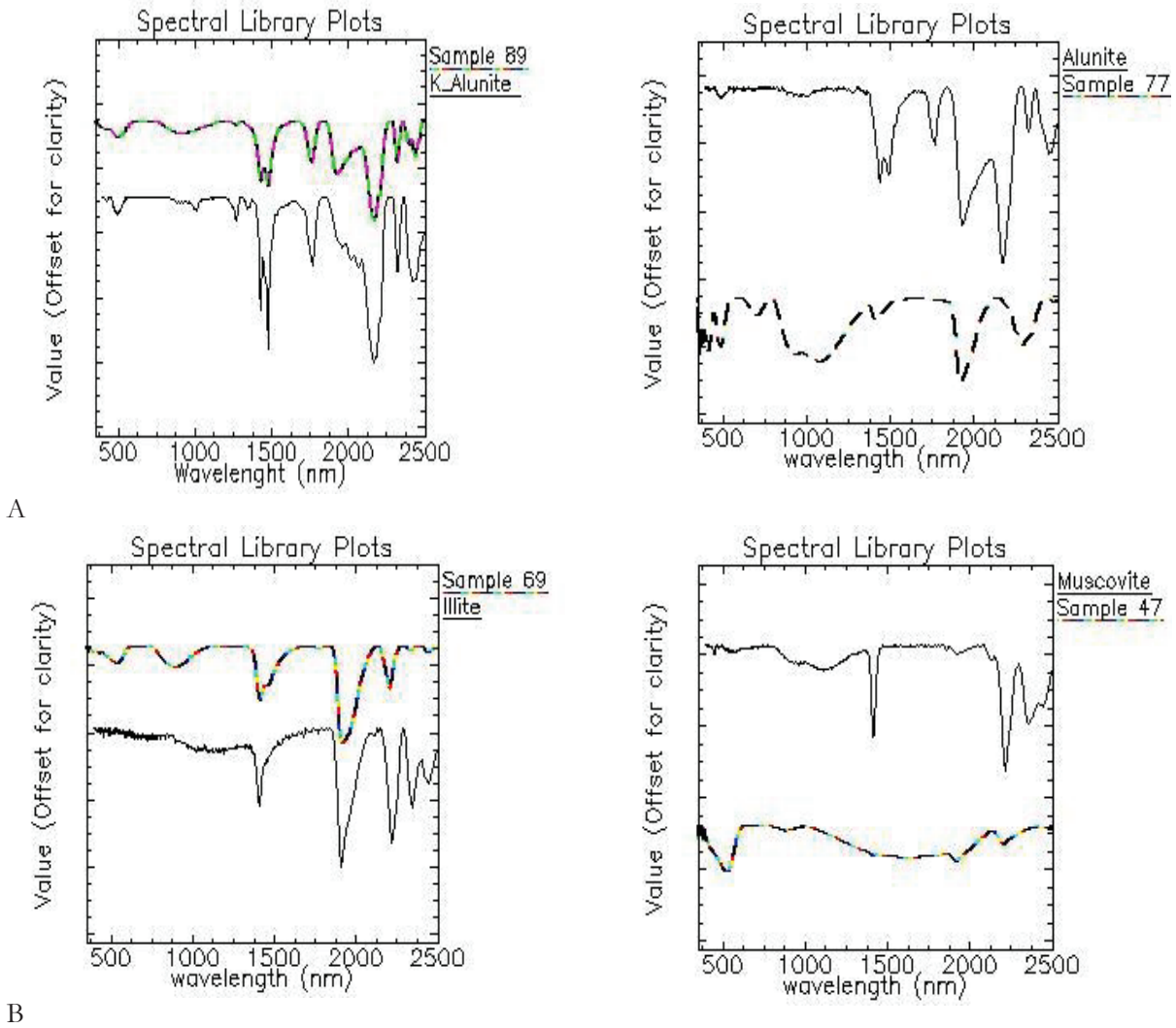


Figure 5.8: Spectra of sulphate minerals, K-Alunite and alunite (A) and illite-sericite-muscovite minerals, illite and muscovite (B).

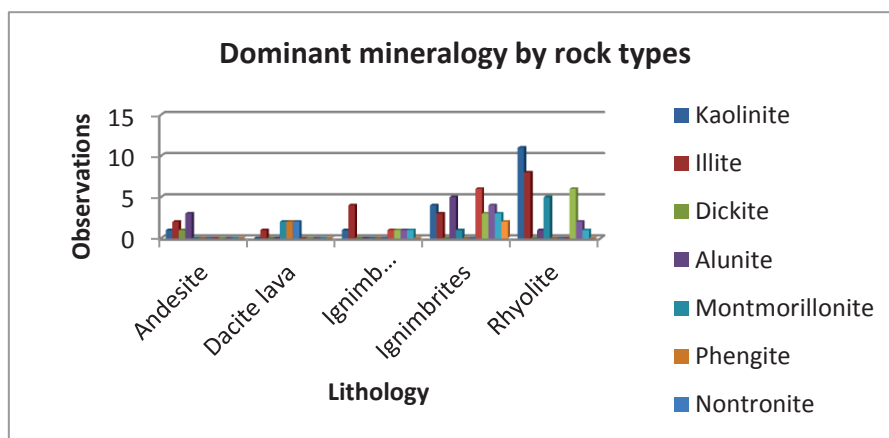


Figure 5.9: Histogram of alteration minerals grouped by lithology

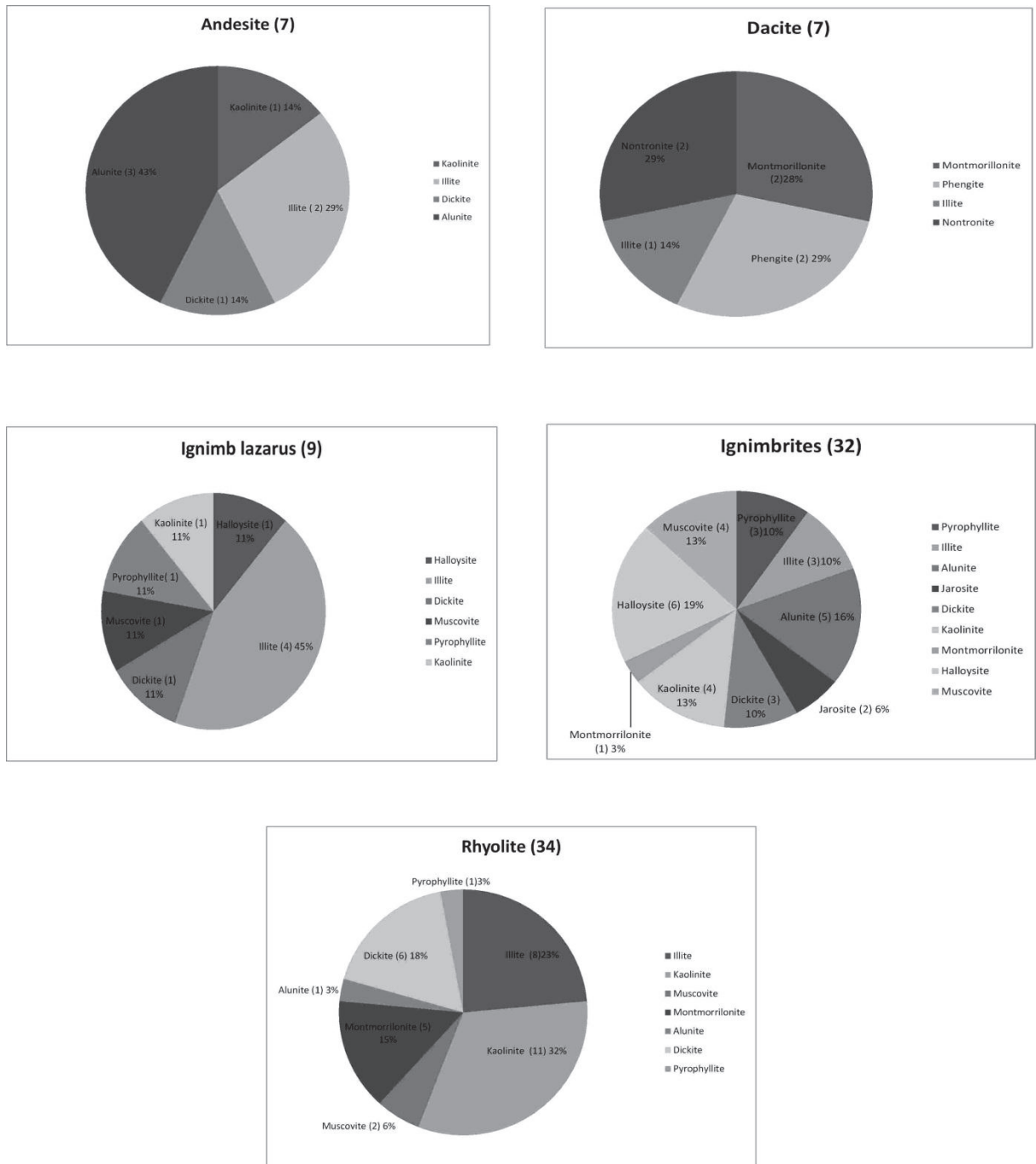


Figure 5.10: Minerals observed in the area, grouped according to their host rocks, based on the interpretations of the dominant minerals.

GEOCHEMICAL AND SPECTRAL CHARACTERIZATION OF HYDROTHERMAL ALTERATION FACIES AT THE EPITHERMAL GOLD MINERALIZATION AT RODALQUILAR, SPAIN

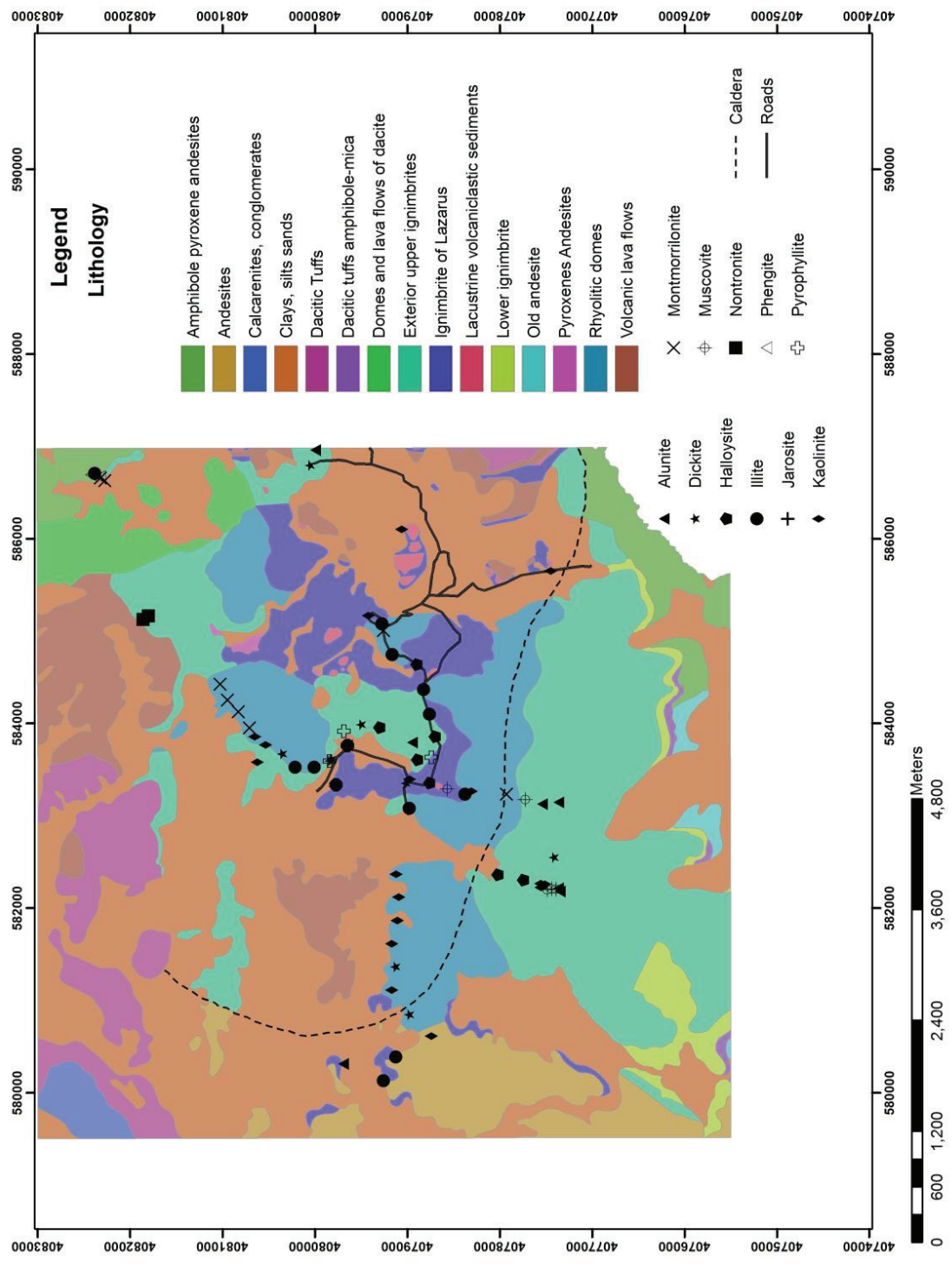


Figure 5.11: A location plot showing dominant mineralogy overlain to geological map of the study area.

As is shown in the plots, there is no direct association between alteration minerals and lithology, as almost all alteration minerals are found in all lithologies found within the area, with few exceptions. The dacitic lava contains very few near-infrared active minerals, while Ignimbrites and Rhyolites contain a variety of alteration minerals.

5.4. Distribution of alteration minerals.

The hydrothermal alteration mineral within the study area show a zonation pattern with kaolinite, illite and alunite dominating over other alteration minerals and thus covers larger part of the area. Montmorillonite and illite, as expected in a high-sulphidation epithermal system, are observed on the periphery of the zonation pattern. Kaolinite, illite and alunite exist as pure spectra, although in most cases, they occur as mixed spectra with other minerals. Halloysite and dickite spectra are also abundant, making the kandite group the dominant within the area. Montmorillonite, muscovite and pyrophyllite follows in the group, while Jarosite is the last, with just two samples were observed to have jarosite as a dominant mineral.

The spatial distribution of the clay minerals within the area, vary from location to location, and this can be associated with the fact that, they results from different sources.

5.5. Concluding remarks.

Spectral NIR detectable parameters such as crystallinity and mineral chemistry combined, have indicated the possibility of the potential application of reflectance spectroscopy in the characterizing alteration and elements associations within the Rodalquilar study area.

Kaolinite crystallinity shows a special pattern, whereby the, highly altered mineralized areas are characterized by low value of the KCI index, and the least altered, peripheral zone is characterized by high values of KCI. Kaolinite crystallinity can thus be used as an inverse vector to the orezone of the deposit.

On the other hand, based on the results of this study there is no clear or direct association between lithology and mineralogy in the area covered by the investigated rock samples, because the mineralization within the study area is not lithologically controlled.

6. DATA INTEGRATION

6.1. Introduction

This chapter compares the geochemical parameters determined by PXRF with the ASD mineralogical data and parameters of rock samples. Scatter plots of different geochemical, mineralogical and spectral parameters have been utilized to show the relationship between the alterations, mineralization and lithology within the Rodalquilar gold deposit. In some cases, the integration involves the overlying of maps and images

6.2. Mineralization

Relationship between geochemical elements related to mineralization within the study area such as As, S, Pb, Zn, Sr and the factor analysis scores of factor 3(= S and As) and the dominant mineral composition were evaluated by using the box plots and scatter diagrams.. If any apparent relationship exists, this can be used in discriminating and characterizing the mineralization within the area based on the dominant mineralogy found within the study area Figure 6.1

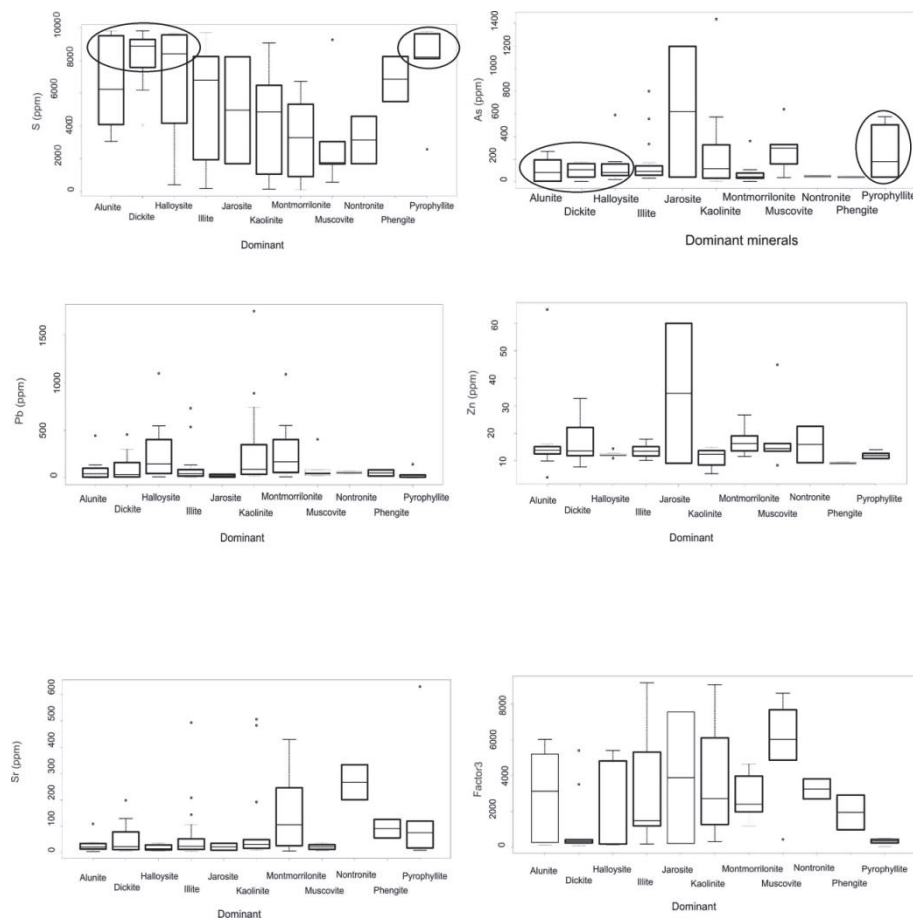


Figure 6.1: Box plot of geochemical parameters associated to mineralization related to dominant spectrally detectable mineralogy

The box plots in figure 6.1 show large overlap and therefore poor separation between alterations detected minerals for most elements associated with mineralization within area. As and S has good contrasting behaviour for the argillic –advanced argillic alteration minerals (alunite, dickite, halloysite, kaolinite and prophyllite) in which, they have high values for S and low values for As. This contrasting behaviour between As and S for the argillic-advanced alteration minerals, makes factor 3 scores, the best in discriminating the mineralization within the study area, and giving a link between mineralization and alteration. In general purpose two groups can be picked one with high values and the other one with low values of the scores, prophyllite and muscovite can be taken as a marker, representing low values (argillic – advanced argillic) and high values (prophylic).

There is a clear link between factor3 scores with alterations minerals; low values representing the argillic to advanced argillic alteration while high values representing the prophylic alterations. The trend shows a clear zonation. Figure 6.2

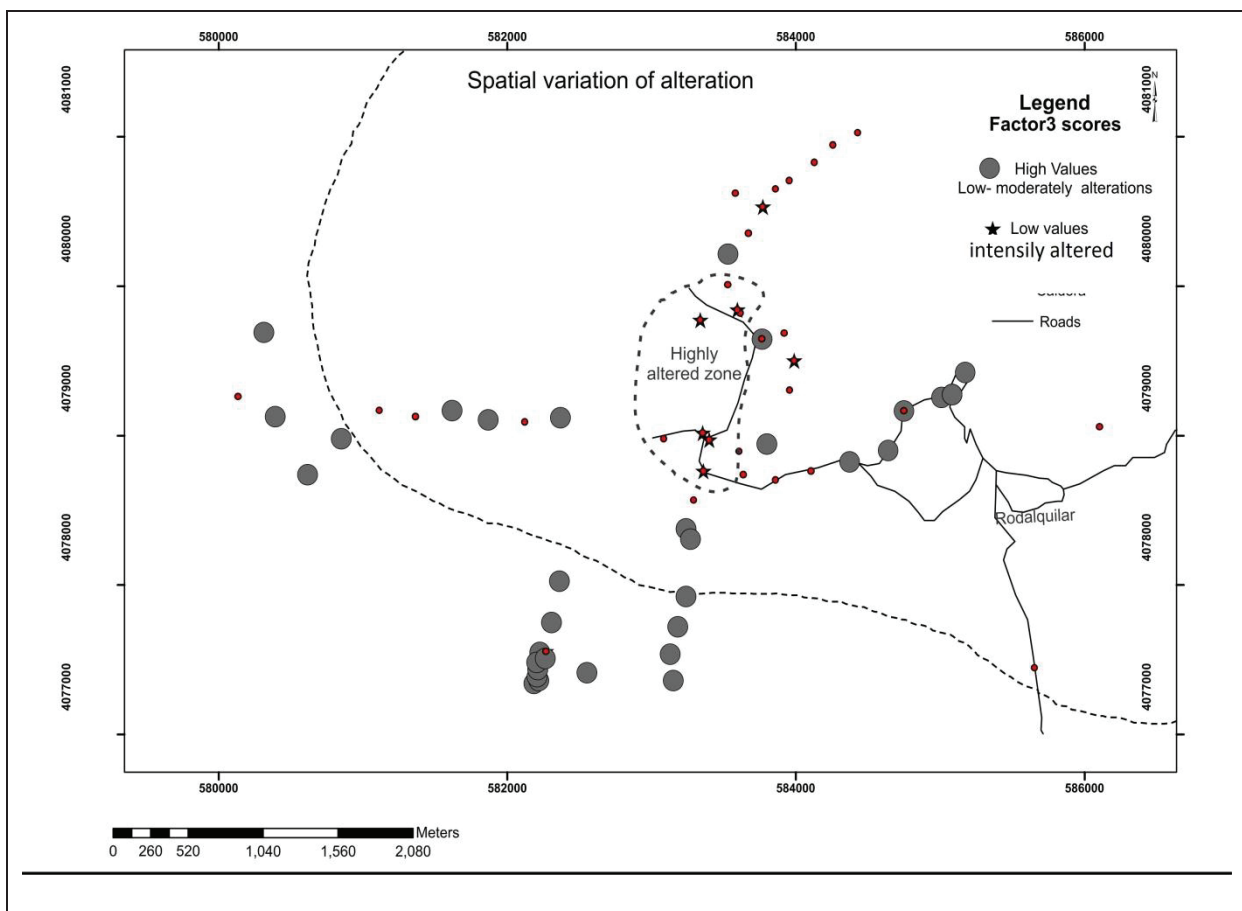


Figure 6.2: The spatial variation of scores of factor3 related to hydrothermal alteration. The plot shows a clear zonation of alteration intensity within Rodalquilar gold deposit.

The scatter plot of As against S (figure 6.3) shows no proper trend with the alteration minerals, but again we can differentiate the zones of argillic to advanced argillic (high S, low As) from the rest, with some interference of illites and muscovites. The clustering of different alteration mineralogy, with high S and low as represents the argillic to advanced argillic zones.

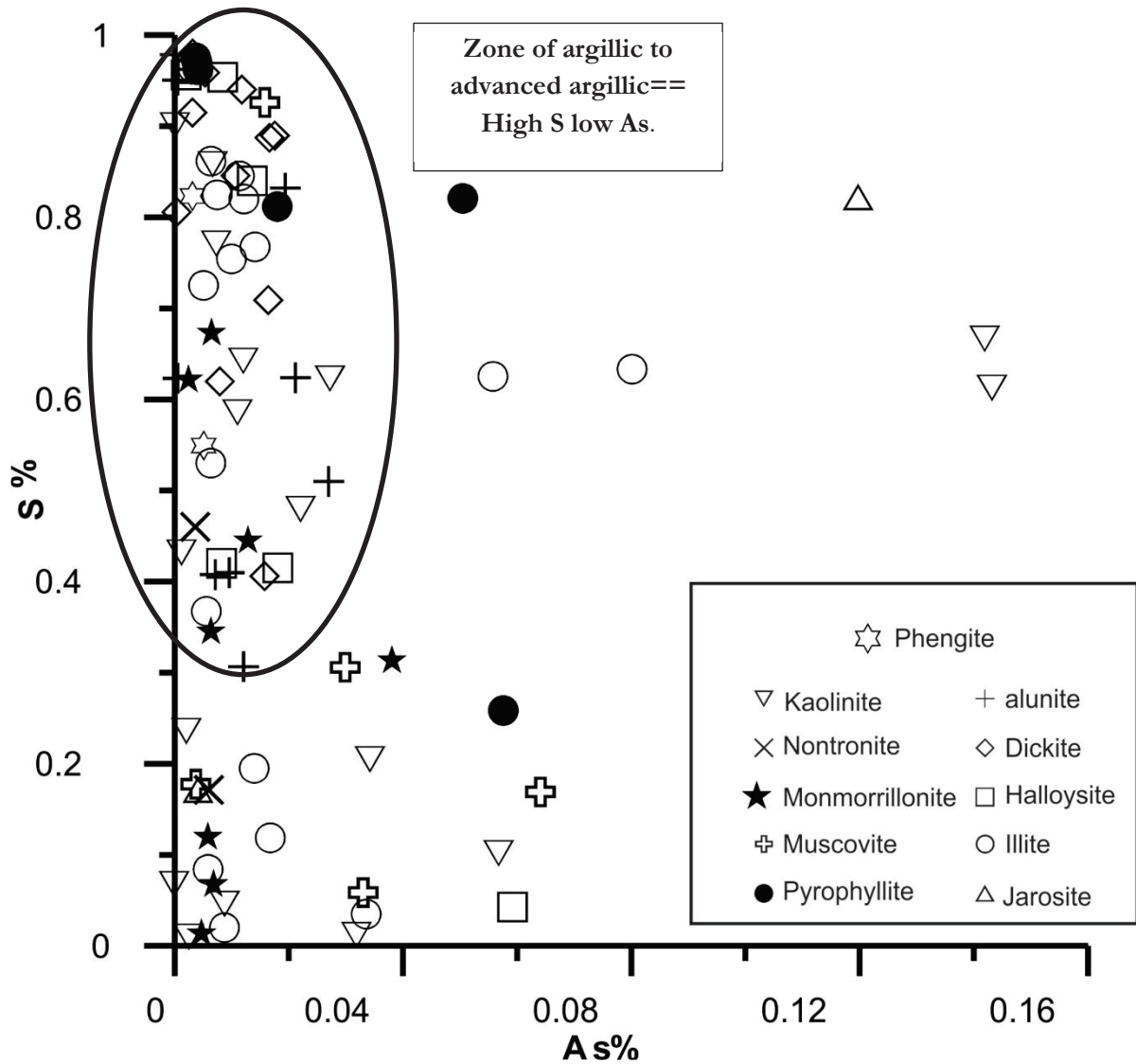


Figure 6.3: Scatter plot of As versus S within Rodalquilar gold deposit, grouped by the dominant spectrally detectable mineralogy. Plot shows no proper trend between As and S with the alteration mineralogy.

6.3. Alterations

Relationship between geochemical parameters indicative for alterations, the Silicified Index (SI) and Hashigushi Index (HI), were also evaluated by overlying the parameters to the Hymap ratio color-composite image of the area. Aim is to see whether the Silicified Index and Hashigushi Index, can reveal the same information about the mineralogy as the one known from the ratio color-composite images. The Hymap image (ratio color composite RGB) have the following combinations;

$$\mathbf{R}: R_{2100\text{nm}}/R_{2171\text{nm}}, \quad \mathbf{G}: R_{2171\text{nm}}/R_{2206\text{nm}}, \quad \mathbf{B}: R_{2357\text{nm}}/R_{2258\text{nm}}$$

The resulting image has the following color interpretations, magenta: Alunite, Red: Pyrophyllite, Yellow: Kaolinite, Orange: Alunite/Dickite mixture, Green: Illite/Montmorillonite and Blue: Unaltered minerals.

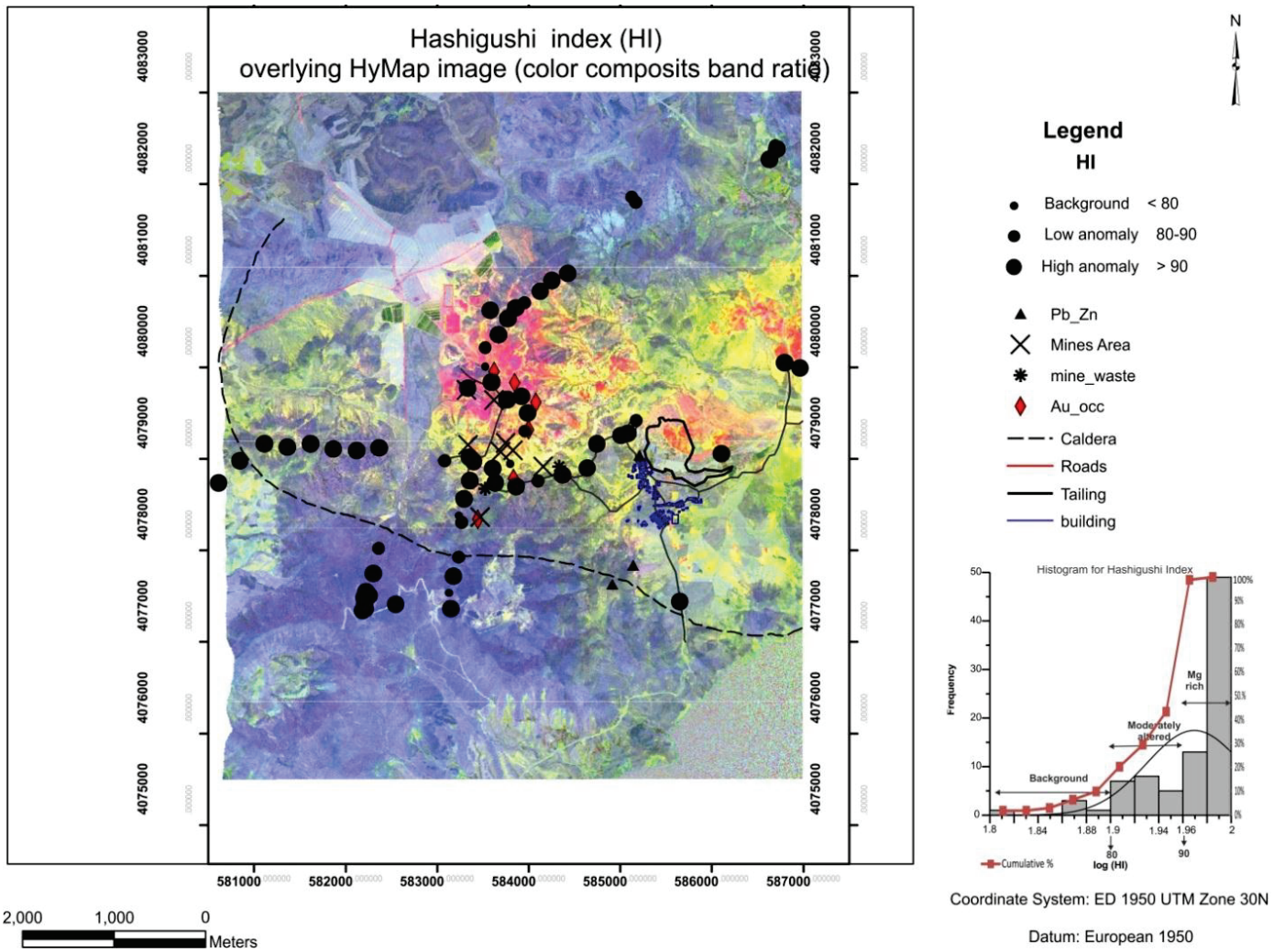


Figure 6.4a : (A). Hashigushi (HI) index overlaid to the HyMap ratio color composite image of the area. Magenta and yellow illustrates alunite and kaolinites respectively

A

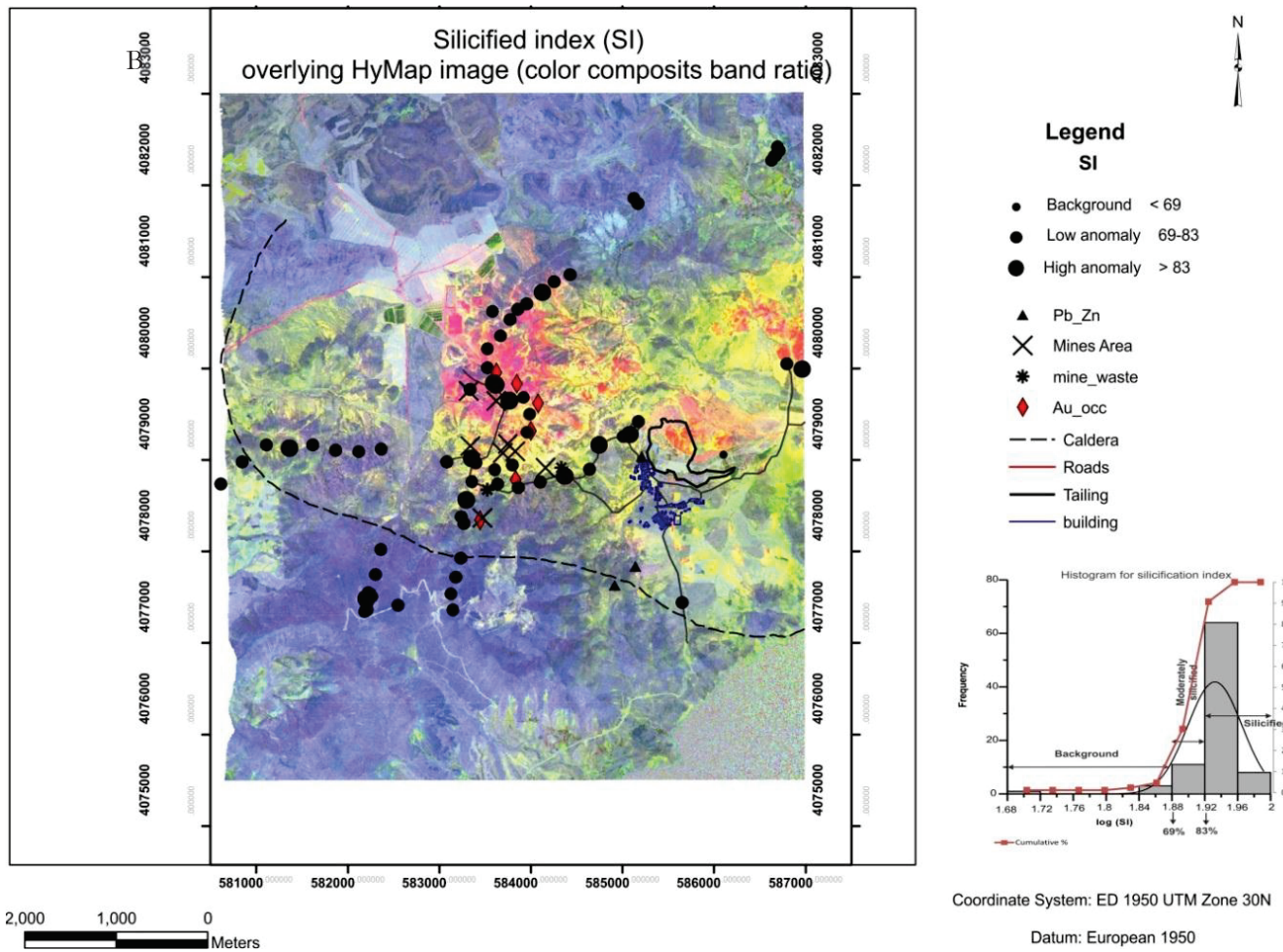


Figure 6. (B) Silicified (SI) indices overlaid to the HyMap ratio color-composite image of the area. Magenta and yellow illustrates Alunite and Kaolinites respectively..

In combination the relationship between the areas of mineralization and of hydrothermal alterations were evaluated by again, overlying the geochemical map responsible for mineralization expressed by the scores of factor 3 with the Hymap ratio color-composite image. Figure 6.4 (A) illustrates that the mineralized area is dominated by alunite and kaolinite as dominant mineral.. There is also a strong relation between mineralization and the alteration within the area. The latter is because the mineralized area is highly silicified and rich in Mg.

The results show that, the Hashigushi- and Silicified Index, can be used to characterize the hydrothermal alteration system of the study area, as the results matches with the Hymap images and the existing information from various publications. Previous studies (Arribas et al., 1995; Rytuba et al., 1990) from the area, reported that, the gold mineralization within Rodalquilar is restricted to the zones of intensely alterations, and more specifically in zones of silicic alterations.

6.4. Lithology.

The relationship between lithology and spectrally detectable minerals is evaluated by the scatter plots of elements which proved to be suitable for discriminating lithology within the study area (TiO_2 , Zr and to the lesser extent the Al_2O_3) and by simply overlying the spectrally detectable mineralogy map with the geological map of the area. Figure 6.5 illustrates that, there is no clear relation between lithology and alteration minerals, All alteration minerals are scattered in one zone, with few exceptions of samples with high TiO_2 and Zr contents.

The combination plot of geological map of the area with the spectrally detectable dominant mineralogy of the area (figure 5.11 in chapter 5) also shows that, there is no direct association between hydrothermal alteration minerals and lithology, as almost all alteration minerals are found in all the different lithological units occurring within the area, with few exceptions. In general the dacitic lava has few near-infrared active alteration minerals, while ignimbrites and rhyolites contains a variety of alteration minerals, as compared to other lithological units . It is also observed from the plot, that montmorillonite as a dominant mineral is only found in the older andesite formation within the study area.

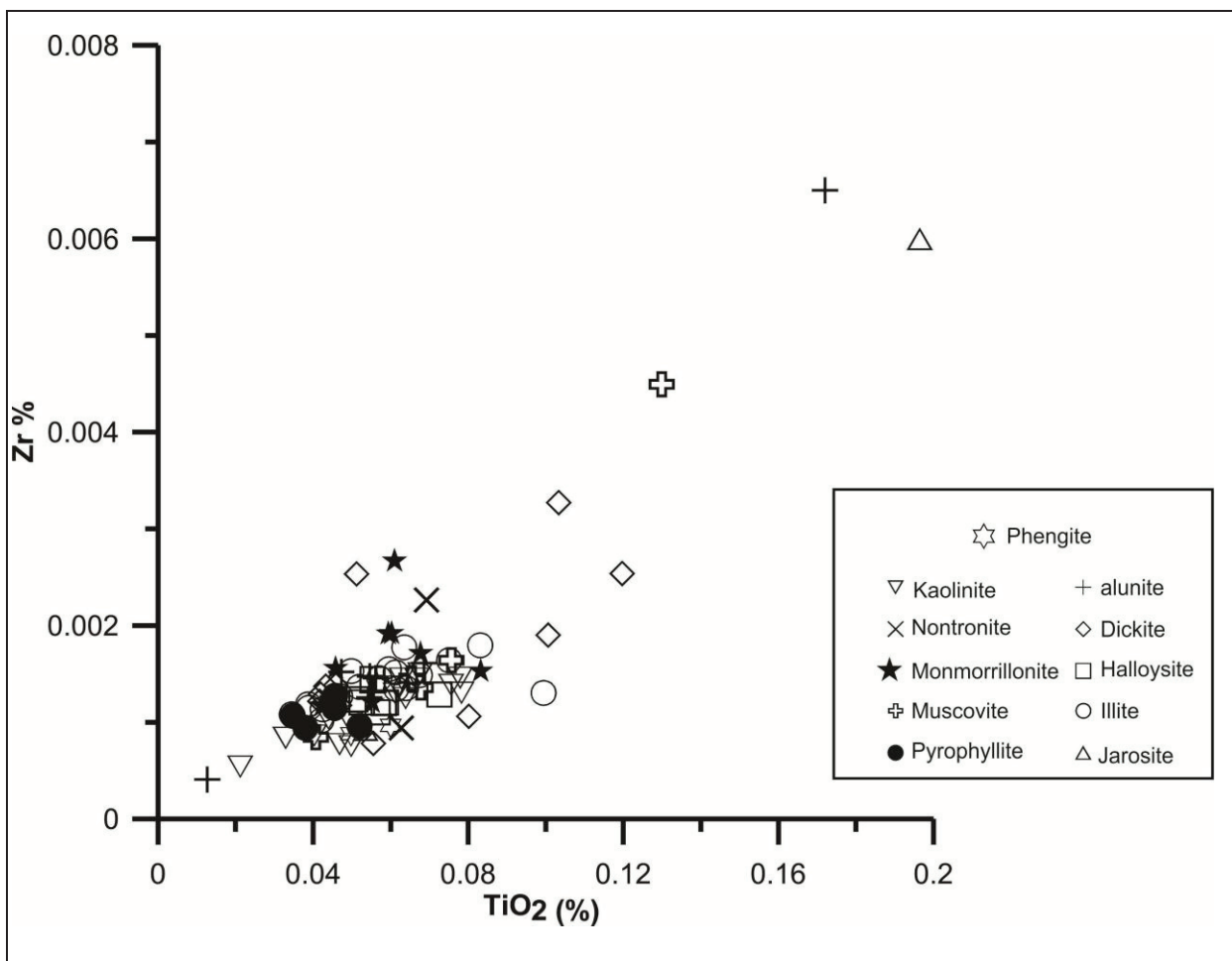


Figure 6.5: Scatter plots of geochemical elements which are useful in discriminating the lithology within the Rodalquilar gold deposit, grouped by dominant mineralogy.

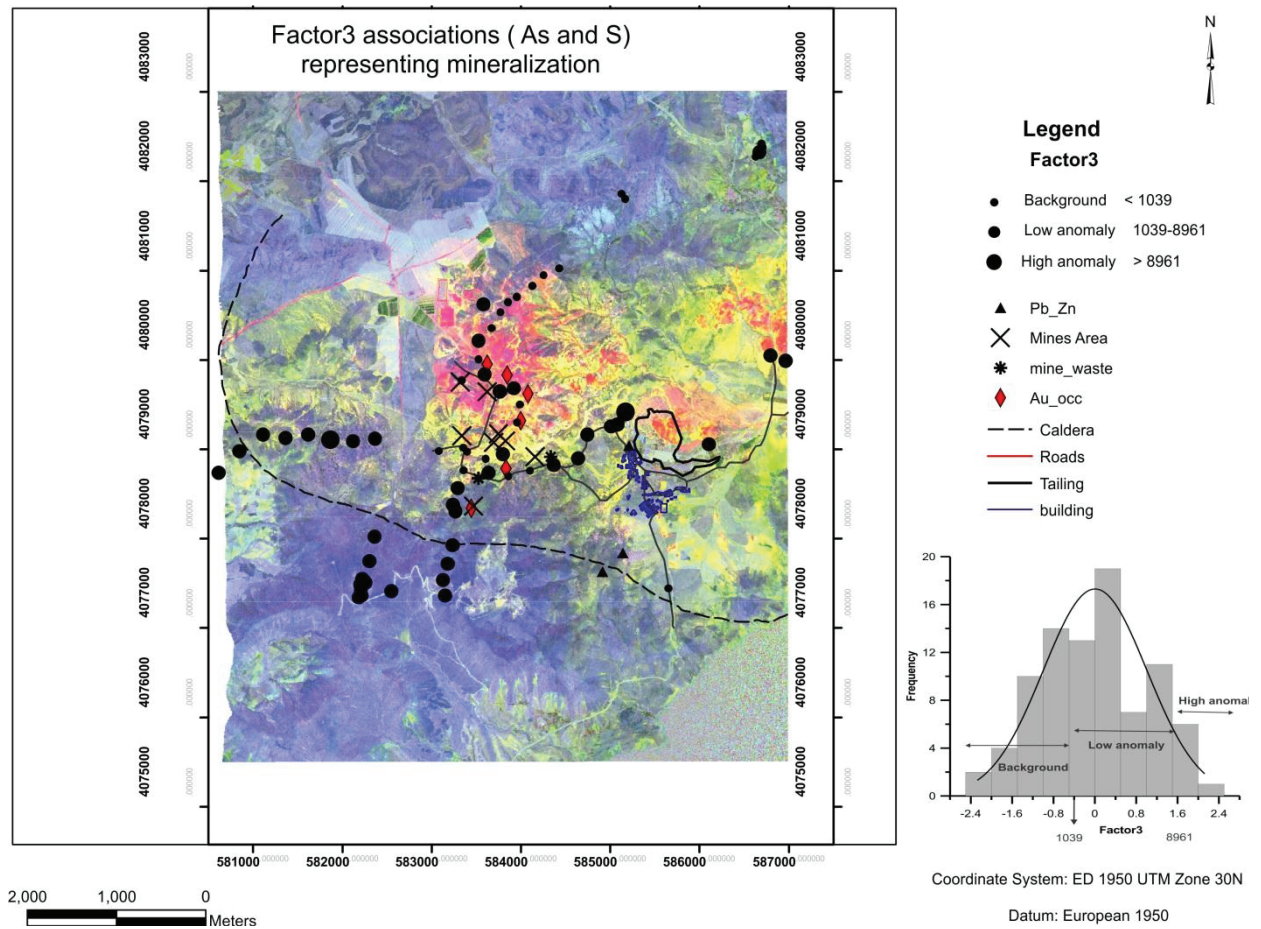


Figure 6.6: Factor3 geochemical map overlying the HyMap ratio color-composite image, showing the mineralized area being dominated by alunite and kaolinite minerals.

6.5. Geochemical parameters in relation to ASD parameters

6.5.1. Alteration indices and Al-OH absorption features

Relationship between Modified Ishikawa and CCPI index (Geochemical parameters) with the ASD parameters (wavelength and depth of Al-OH features) were examined by using scatter plots (variation analysis). Since the element composition affects the spectra of minerals, knowing the relationship between elements might be of great help in discriminating the area in terms of mineralogical compositions and or abundance.

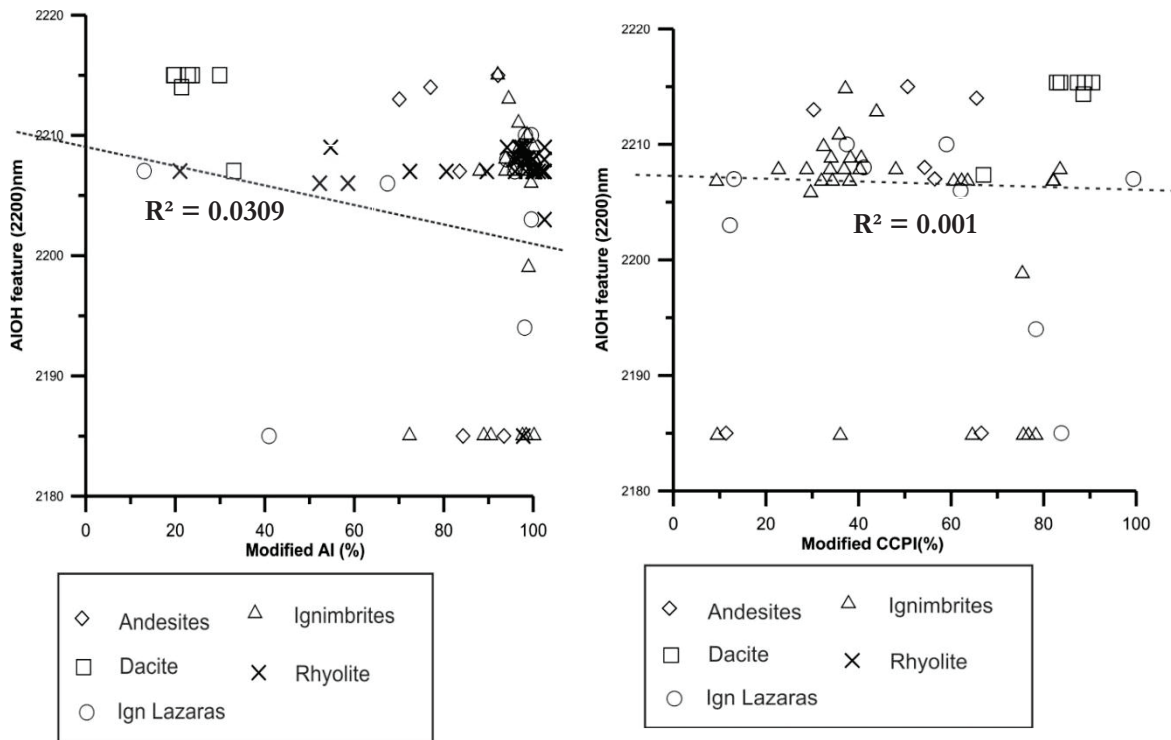


Figure 6.7: Scatter Plots of modified Ishikawa index (AI) versus wavelength position of Al-OH absorption feature near 2200 nm (left) and modified CCPI index versus wavelength position of Al-OH absorption feature near 2200 nm (right).

The plots show a negative correlation between the wavelength position and both modified indices. In both plots most samples plot in higher wavelength positions. Two major clusters can be observed in plots, the dominant cluster of rhyolites and ignimbrites with only few andesites, and a cluster of dacitic lava. With the exception of few scattered sample points, located in lower wavelength region, in both plots, there is a negative correlation between the wavelength positions of Al-OH feature and the alteration indices. Both plots shows a shift towards higher wavelength positions, which can be correlated with the higher degree of alterations. Recent studies e.g. (Mateer, 2010), have shown that , the shift of Al-OH absorption features towards higher wavelengths, is the result of decreasing in Al content, which in this case can be related to the hydrothermal alteration. The plot figure 6.7 does not show a clear relation between the Al-OH feature (wavelength position) and the modified alteration intensities , or between the modified Ishikawa (AI) and modified CCPI.

On the other hand, the results show that, to some extent we can use the modified hydrothermal alteration indices together with the wavelength position of 2200 nm Al-OH absorption feature to characterize different lithological units depending on their mineralogical compositions.

6.5.2. Lithology and Al-OH absorption features

Relationship between Al-OH absorption features (depth and position in nm) and lithology was studied by simply using box plots to see the variations of these parameters within different lithologies. The objective is to see whether the Al-OH features can reveal any information about the hydrothermal processes within the area.

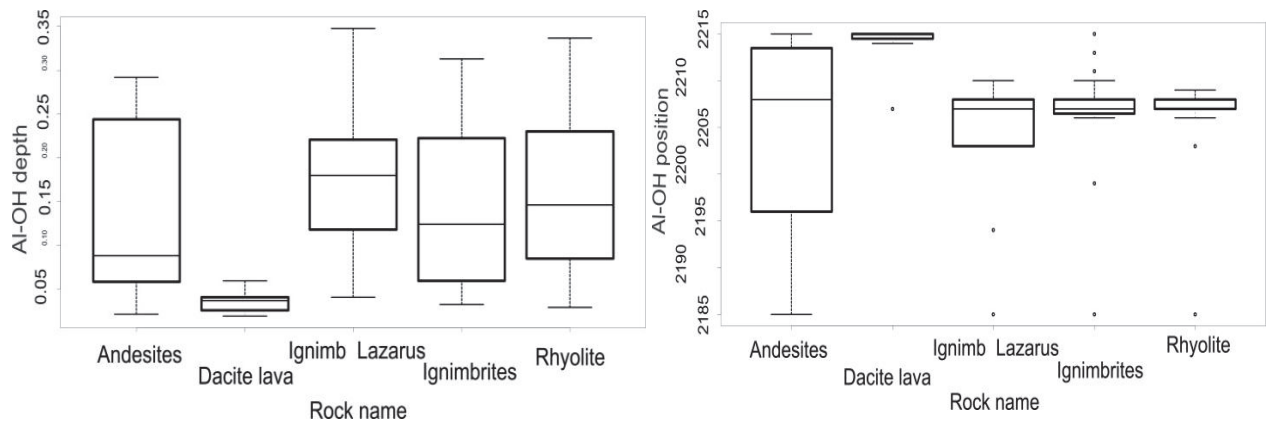


Figure 6.8: Box plots of Al-OH features , depth of Al-OH absorption feature in nm (right) and wavelength position of the absorption feature near 2200 (nm) (left) , grouped by lithology.

Andesites have the widest range of observations in terms of both depth and position of Al-OH features. Rhyolite has almost a normal distribution of depth feature (with wide variations also), and it has low variations in terms of wavelength position. The variations of the parameters with lithology seem to have no clear pattern and therefore little information could be derived in terms of alteration processes within the study area.

To get more information about the relationship between Al-OH feature and lithology, the point map of depth parameters is overlaid to the geological map of the area. This combination map shows that the central part, which is the highly mineralized part of the study area, is dominated by higher depth of the Al-OH feature as compared to the surrounding area.(See figure 6.6)

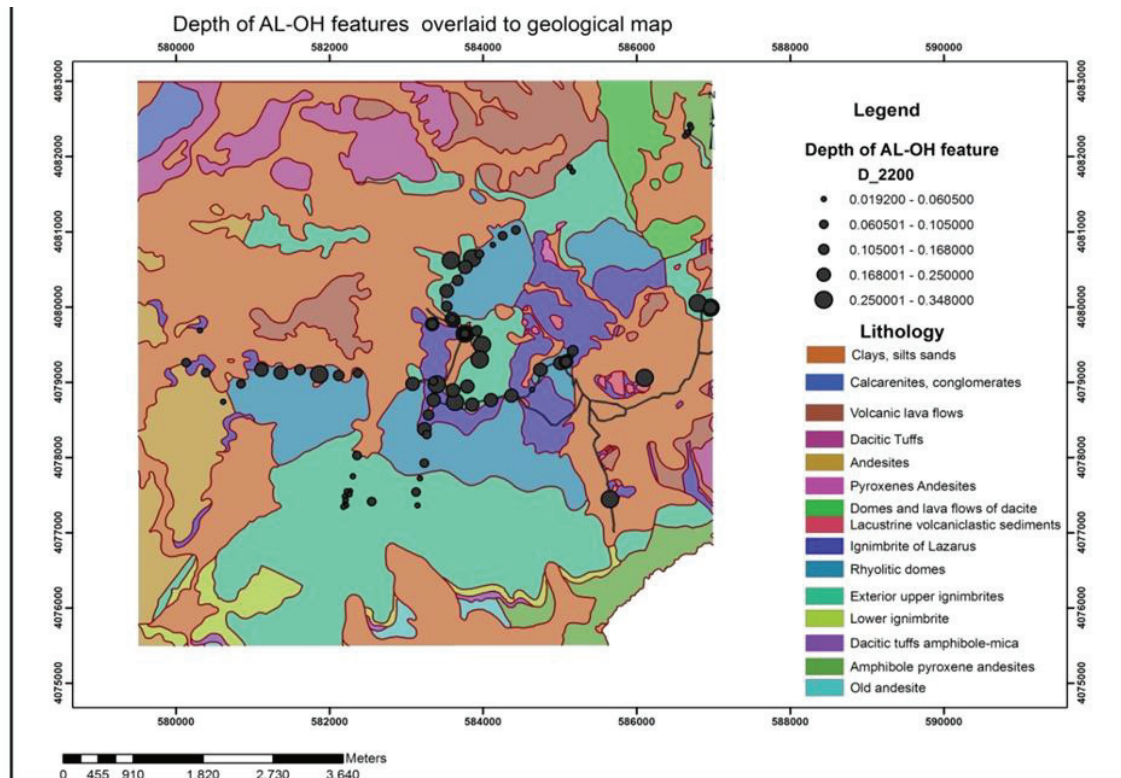


Figure 6.9: Point Map of depth of Al-OH absorption feature overlaid on the geological map of the area.

Concluding remarks

The results obtained from different integration methods are in most cases consistent with the information from literature or with the results from the geochemical as well as spectral analysis.

Data integration has been found useful in identifying areas which are hydrothermally altered, and these identified zones, can in turn give information about the mineralization, e.g. (Ranjbar & Honarmand, 2004).

Thus, it is evident that we can improve exploration efforts in targeting the epithermal gold systems in an area such as Rodalquilar gold deposit by combining the results of alteration mineralogy, crystallinity, alteration, lithology and geochemical anomalies.

Combination or comparison of satellite imagery with geochemical and mineralogical data can enhance the areas which are hydrothermally altered with more confidence and hence reducing the chance of enhancing false anomalies. Published studies by (Arribas et al., 1995; Rytuba et al., 1990) show that the Rodalquilar gold deposit is closely associated with the zones of advanced argillic alteration, characterized by dominant alunite alteration mineralogy, which coincides with the results of the current research, obtained by the integration and comparison of the PXRF data with the ASD data.

Based on the results above, it is shown that data integration of geochemical and ASD is very effective in characterizing the area of study in terms of lithology and mineralogical compositions.

7. CONCLUSIONS AND RECOMMENDATIONS

7.1. Conclusion

The objective of this research was to test whether a direct field data of major and trace elements (PXRF) can be used in combination with mineralogical IR information for the exploration of the epithermal gold deposits. Research questions were formulated to achieve this objective, which could be addressed as follows:

Can different lithologies be deduced from the whole rock geochemistry using the PXRF in Rodalquilar area?

Trace and major elements were used to answer the research questions. It is possible to deduce different lithologies using the PXRF by using the results from the trace elements geochemistry.

Figure 4.16 (page 36) shows that, it is possible to deduce different lithologies from the whole rock geochemistry using the PXRF.

Can different alteration styles be deduced by using the PXRF in Rodalquilar?

The modified alteration box plots, with certain level of uncertainty due to the effects of the exclusion of Na, together with the Silicified and Hashigushi Indices calculated from the whole rock geochemistry, proved to be effective in delineating alteration styles and intensities for the epithermal deposits.

Factor analysis reveals one factor in which the scores for As and S show most efficient in discriminating between less and highly hydrothermally altered rocks within the area. High values of S and low values of As represents areas of argillic to advanced argillic alteration. Muscovites and pyrophyllite can be taken as markers for the high scores of the As-S factor (factor no. 3) for less altered and low scores for highly altered rocks respectively. See figure 4.19 (page 29), and figures 6.2 and 6.3 (page 58 and 59)

Which elements measured by PXRF can be used to characterize the lithology in the Rodalquilar epithermal alteration system?

Zr and TiO₂ proved to be most efficient in discriminating the lithologies in Rodalquilar gold deposit area, followed to the lesser extent by Zr and Al₂O₃. The ratio of the two element remains constant as the immobile elements are conserved in the alteration processes, despite the loss in mobile constituents the more immobile elements are conserved in the alteration processes. The concentration of the immobile elements changes, but their ratio does not.

In general the results show that the mineralization area is dominated by intense alunite and kaolinite alteration. This is in general consistent with the results from previous studies, e.g.(Arribas et al., 1995). There is also a good consistency between results from the geochemistry and results from ASD as far as the styles and intensity of hydrothermal alteration are concerned.

Results show that the central part of the study area is highly altered (dominated by higher depth of the Al-OH absorption feature at 2200nm) as compared to the surrounding area. Figure 6.6 illustrates the link between mineralization and alteration. There is no direct association between hydrothermal alteration minerals and lithology, concluding that, the mineralization within the area is not lithologically controlled.

7.2. Recommendations.

In view of future exploration for epithermal Au deposits the following recommendations are made :

A grid sampling scheme is recommended for future exploration of epithermal systems using PXRF and a representative number of altered and unaltered samples should be taken into consideration.

Portable XRF field measurements required multiple readings to account for the effects of grain size and the 8mm diameter measuring spot. It should be noted that Helium gas purging is required for the optimal measurements of light elements, and thus, for field measurements this should be taken into considerations as well.

Data integration is important, especially the incorporation of geological and geophysical datasets such as aeromagnetic, resistivity and gamma ray spectrometry (K, U and Th). Clay minerals resulted from pervasive hydrothermal alterations are characterized by low –resistivity and low magnetic anomalies. Gamma-ray is suggested because of the high concentration of potassium minerals such as illite in the study area.

LIST OF REFERENCES

- Arribas, A., Cunningham, C. G., Rytuba, J. J., Rye, R. O., Kelly, W. C., Podwysocki, M. H., . . . Tosdal, R. M. (1995). Geology, Geochronology, Fluid Inclusions, and Isotope Geochemistry of the Rodalquilar Gold Alunite Deposit, SPAIN. [Article]. *Economic Geology and the Bulletin of the Society of Economic Geologists*, 90(4), 795-822.
- Bedini, E., van der Meer, F., & van Ruitenbeek, F. (2009). Use of HyMap imaging spectrometer data to map mineralogy in the Rodalquilar caldera, southeast Spain. *International Journal of Remote Sensing*, 30(2), 327 - 348.
- Carranza, E. J. M. (2010). Mapping of anomalies in continuous and discrete fields of stream sediment geochemical landscapes. *Geochemistry: Exploration, Environment, Analysis*, 10(2), 171-187. doi: 10.1144/1467-7873/09-223
- Carranza, E. J. M. (2011). Analysis and mapping of geochemical anomalies using logratio-transformed stream sediment data with censored values. *Journal of Geochemical Exploration, In Press, Corrected Proof*. doi: 10.1016/j.gexplo.2011.05.007
- Chiprés, J. A., Castro-Larragoitia, J., & Monroy, M. G. (2009). Exploratory and spatial data analysis (EDA–SDA) for determining regional background levels and anomalies of potentially toxic elements in soils from Catorce–Matehuala, Mexico. *Applied Geochemistry*, 24(8), 1579-1589. doi: 10.1016/j.apgeochem.2009.04.022
- Clark, R. N. (1995). Reflectance Spectra. *AGU Handbook of Physical Constants* 178-188.
- Clark, R. N. (1999). Spectroscopy of Rocks and Minerals, and Principles of Spectroscopy *Manual of Remote Sensing, Volume 3* (Remote Sensing for the Earth Sciences,), 3- 58.
- Corbett, G. (2002). Epithermal Gold for Explorationists. [Paper 2002-01,]. *Applied geoscientific practice and research in Australia*.
- Debba, P., van Ruitenbeek, F. J. A., van der Meer, F. D., Carranza, E. J. M., & Stein, A. (2005). Optimal field sampling for targeting minerals using hyperspectral data. *Remote Sensing of Environment*, 99(4), 373-386. doi: 10.1016/j.rse.2005.05.005
- Dill, H. G. (2010). The “chessboard” classification scheme of mineral deposits: Mineralogy and geology from aluminum to zirconium. *Earth-Science Reviews*, 100(1-4), 1-420. doi: 10.1016/j.earscirev.2009.10.011
- EPA. (2007). Method 6200, Field portable x-ray fluorescence spectrometry for the determination of elemental concentrations in soil and sediment. *Washington, D.C., U.S. Environmental Protection Agency*.
- Estifanos, S. (2006). *Spectral indicators for assessing pollution in the epithermal gold mining area of Rodalquilar, South East Spain*. MSc Thesis, ITC, Enschede. Retrieved from http://www.itc.nl/library/papers_2006/msc/ereg/samuel.pdf
- Filzmoser, P., Hron, K., & Reimann, C. (2010). Bivariate statistical analysis of environment (compositional) data *Science of the Total Environment*, 408, 4230-4238.
- Franklin, J. M. (97). Lithogeochemical and Mineralogical Methods for Base Metal and Gold Exploration. *Exploration Geochemistry, Paper 28*.
- Gemmell, J. B. (2007). Hydrothermal Alteration Associated with the Gosowong Epithermal Au-Ag Deposit, Halmahera, Indonesia: Mineralogy, Geochemistry, and Exploration Implications. *Economic Geology*, 102(5), 893-922. doi: 10.2113/gsecongeo.102.5.893
- Green, R. O., Eastwood, M. L., Sarture, C. M., Chrien, T. G., Aronsson, M., Chippendale, B. J., . . . Williams, O. (1998). Imaging Spectroscopy and the Airborne Visible/Infrared Imaging Spectrometer (AVIRIS). *Remote Sensing of Environment*, 65(3), 227-248. doi: 10.1016/s0034-4257(98)00064-9

- H.Macdonald, E. (2007). *Handbook of gold exploration and evaluation*. Cambridge England: Woodhead Publishing.
- Hatchell, D. C. (1999). Analytical Spectral Devices, Inc. (ASD) [Technical Guide]. *4th Ed*.
- Hedenquist, A'NTONIO ARRIBAS R., & GONZALEZ-URIEN, E. (1996). Exploration for Epithermal Gold Deposits. *Society of Economic Geology*.
- Kalnicky, D. J., & Singhvi, R. (2001). Field portable XRF analysis of environmental samples. *Journal of Hazardous Materials*, 83(1-2), 93-122. doi: 10.1016/s0304-3894(00)00330-7
- Large, R. R., Gemmeil, J. B., Paulick, H., & Huston, D. L. (2001). The Alteration Box Plot: A Simple Approach to Understanding the Relationship between Alteration Mineralogy and Litho-geochemistry Associated with Volcanic-Hosted Massive Sulfide Deposits. *Econ Geol*, 96(5), 957-971. doi: 10.2113/gsecongeo.96.5.957
- M.A. Booden, J. L. Mauk, & Simpson, M. P. (2011). Quantifying Metasomatism in Epithermal Au-Ag Deposits: A Case Study From the Waitekauri Area, New Zealand. *Economic Geology, in press*.
- MacLean, W. H., & Barrett, T. J. (1993). Litho-geochemical techniques using immobile elements. *Journal of Geochemical Exploration*, 48(2), 109-133. doi: 10.1016/0375-6742(93)90002-4
- Mateer, M. A. (2010). Ammonium illite at the Jerritt Canyon district and Goldstrike property, Nevada: Its spatial distribution and significance in the exploration of Carlin-type deposits Great Basin evolution and metallogeny (pp. 26). Wyongming: Geological Society of Nevada.
- Meunier, A. (2005). Clays (pp. 476).
- Misra, K. C. (1999). Understanding Mineral Deposits
- Mixa, P., Dobes, P., Zacek, V., Lukes, P., & Quintanilla, E. M. (2011). Epithermal gold mineralization in Costa Rica, Cordillera de Tilaran - exploration geochemistry and genesis of gold deposits. *Journal of Geosciences*, 56(1), 81-104. doi: 10.3190/jgeosci.090
- Morgan Poliquin. (2011). Vein system & type of deposits Retrieved 3/10, 2011, from <http://www.almadenminerals.com/geoskool/vein-systems.html>
- Noel C. White, J. W. H. (1995). Epithermal Gold Deposits: Styles, Characteristics and Exploration. *SEG Newsletter*, No. 23,, 1, 9-13.
- Oepen, P. S.-v., Friedrich, G., & Vogt, J. H. (1989). Fluid evolution, wallrock alteration, and ore mineralization associated with the Rodalquilar epithermal gold-deposit in southeast Spain. *Mineralium Deposita*, 24(4), 235-243. doi: 10.1007/bf00206385
- Pantual, S., Merry, N., & Ganson, P. (1997). *Practical Application Handbook*. G_MEX, Vol 2, AUSPEC INTERNATIONAL.
- Pearce, J. A., & Norry, M. J. (1979). Petrogenetic implications of Ti, Zr, Y, and Nb variations in volcanic rocks. *Contributions to Mineralogy and Petrology*, 69(1), 33-47. doi: 10.1007/bf00375192
- Peinado, F. M., Ruano, S. M., González, M. G. B., & Molina, C. E. (2010). A rapid field procedure for screening trace elements in polluted soil using portable X-ray fluorescence (PXRF). *Geoderma*, 159(1-2), 76-82. doi: 10.1016/j.geoderma.2010.06.019
- Peter Filzmoser, K. H., Clemens Reimann. (2009). Univariate statistical analysis of environmental (compositional) data: Problems and possibilities. *Science of the Total Environment*, 11466, 9.
- Pirajno, F. (2008). *Hydrothermal processes and mineral systems*. DE: Springer Verlag.
- Pontual, S., Merry, N., & Ganson, P. (1997). Epithermal Alteration Gold Systems. *G-MEX , AUSPEC INTERNATIONAL*, 4, 1-44.
- Pontual, S., Merry, N., & Ganson, P. (1997b). Spectral Intepretation field manual, Spectral Analysis, Guide for Mineral Expoloration. *G_MEX, Vol 1, AUSPEC INTERNATIONAL*.

- Queralt, I. (1996). Adularia-sericite type wallrock alteration at the María Josefa gold mine: An example of low sulfidation epithermal ore deposit, within the volcanic Rodalquilar Caldera (SE, Spain). *ACTA GEOLOGICAHISPANICA*, v. 30 (1995), p. 91-100.
- Ranjbar, H., & Honarmand, M. (2004). Integration and analysis of airborne geophysical and ETM+ data for exploration of porphyry type deposits in the Central Iranian Volcanic Belt using fuzzy classification. *International Journal of Remote Sensing*, 25(21), 4729-4741. doi: 10.1080/01431160410001709011
- Reed, M. H. (1997). Hydrothermal alterations and its relationship to ore fluid composition, *Geochemistry of Hydrothermal Ore deposits*. Vol. 1, Chapter 7. (pp. 303-365).
- Reimann, C., Filzmoser, P., & Garrett, R. G. (2005). Background and threshold: critical comparison of methods of determination. *Science of the Total Environment*, 346(1-3), 1-16. doi: 10.1016/j.scitotenv.2004.11.023
- Robb, L. (2005). Introduction to Ore-forming Processes (pp. 373).
- Robert, F. (1997). Gold Deposits and Their Geological Classification. *Exploration Geochemistry, Paper 29*.
- Robert, F. (2007). Models and Exploration Methods for Major Gold Deposits types. *Ore Deposits and Exploration Technology, Paper 48*, 691-711.
- Rytuba, J., Arribas, A., Cunningham, C., McKee, E., Podwysocki, M., Smith, J., & Kelly, W. (1990). Mineralized and unmineralized calderas in Spain; Part II, evolution of the Rodalquilar caldera complex and associated gold-alunite deposits. *Mineralium Deposita*, 25(0), S29-S35. doi: 10.1007/bf00205247
- Taylor, B. E. (2007). Epithermal Gold Deposits. *Mineral Deposits Division, Special Publication No. 5*, p. 113-139.
- Tukey, J. W. (1977). *Exploratory Data analysis*. Reading: Addison-Wesley.
- US EPA. (2006). XRF Technologies for Measuring Trace Elements in Soil and Sediment. [Innovative Technology Verification Report]. *Niton XLt 700 Series XRF Analyzer*.
- Van der Meer, F. (2004). Analysis of spectral absorption features in hyperspectral imagery. *International Journal of Applied Earth Observation and Geoinformation*, 5(1), 55-68. doi: 10.1016/j.jag.2003.09.001
- Warren, I., Simmons, S. F., & Mauk, J. L. (2007). Whole-Rock Geochemical Techniques for Evaluating Hydrothermal Alteration, Mass Changes, and Compositional Gradients Associated with Epithermal Au-Ag Mineralization. *Economic Geology*, 102(5), 923-948. doi: 10.2113/gsecongeo.102.5.923
- Werner F, G. (1981). Geothermal mineral equilibria. *Geochimica et Cosmochimica Acta*, 45(3), 393-410. doi: 10.1016/0016-7037(81)90248-9
- Winchester, J. A., & Floyd, P. A. (1977). Geochemical discrimination of different magma series and their differentiation products using immobile elements. *Chemical Geology*, 20(0), 325-343. doi: 10.1016/0009-2541(77)90057-2
- Xia, Q. L., Cheng, Q. M., Lu, J. P., Xiao, W., Sang, H., Yuan, Z. X., . . . Qiu, J. L. (2011). Application of portable XRF technology to identification of mineralization and alteration along drill in the Nihe iron deposit, Anhui, East China. *Diqiu Kexue - Zhongguo Dizhi Daxue Xuebao/Earth Science - Journal of China University of Geosciences*, 36(2), 336-340.
- Yirgu, D. (2008). *Geochemical and spectral characterization of heavy metal pollutants using stream sediment at Rodalquilar gold mining area, SE Spain*. MSc, ITC, Unpublished MSc Thesis.

APPENDICES

Appendix 1. A simple field classification of the material is given together with the sample location coordinates obtained by GPS

Station Name	Powder ID	x_coord	y_coord	Field descriptions
MRE01002	P_02	581280	4085101	Abundant gypsum and probably kaolinite. Colour anomaly in 468 Aster bands combination.
MRE01004	P_04	585171	4079421	Volcaniclastic with Qtz xls and possibly kaol-alunite. (P_08 as well)
MRE01005	P_05	585007	4079255	Felsic volcaniclastic with Qtz Xls and probably kaolinite in crystals. Slightly silicified.
MRE01006	P_06	584747	4079164	Felsic volcaniclastic with silicification + Qtz veinlets and disseminated sulfides. (P_09, P_10 and P_11) as well
MRE01007	P_07	584639	4078901	Ignimbrite or lithic tuff. Felsic. Probably slightly weathered. Some small Qtz veinlets with good crystals. (P_12) as well
MRE01008	P_13	584370	4078824	Felsic volcaniclastic. Crossed by abundant veinlets with FeOx in some parts. Locally with magnetite or oxidized Pyrite. Alteration Probably Kaolinite-Alunite.
MRE01009	P_14	584104	4078762	Volcaniclastic rock with Qtz crystals, and advanced argillic alteration. Part of the sample has a piece of a vein of Alun-Kaol, the rest is pervasively altered to kaolinite-Alunite.
MRE01010	P_15	583859	4078703	Completely altered rock with some Qtz eyes and argillized feldspars. Advance argillic alteration with Alun-Kaol?
MRE01011	P_16	583636	4078738	Breccia and volcanic brecciated rock. Silicified and crossed by some silica veinlets. Some disseminated sulfides.
MRE01012	P_17	583358	4078762	Volcanic rock. In general very silicified and int part vuggy. This rock is surrounded by less silicified material that is very argillized. Could be a feeder zone surrounded by argillized rock.
MRE01013	P_18	583352	4079016	Volcanic gray-red color. Locally silicified or very silicified. Crystaloclast of Qtz and feldspars altered to clays. All is stained partially with FeOx (hematite?). Sample at some distance from road and probably over a structure zone (silicified) of about

continuation

MRE01014	P_19	583084	4078979	Last sample on the road before going out to the valley (to the west). Volcaniclastite with abundant Qtz crystals and argillic alteration. Could have some sericite-illite as feldspar alteration.
MRE01015	P_20	582368	4079119	Volcaniclastic with Qtz xls and argillized feldspars. Felsic rock. Pervasive alteration. Probably kaol-illite. The rock is silicified and with some very small Qtz veinlets and some FeOx.
MRE01016	P_21	582122	4079090	Volcanite with Qtz and felds xls. Slightly silicified with some white Qtz veinlets. Soft pervasive argillization. Locally brecciated. Sample close to a shaft. Probably Kaol, and some disseminated FeOx (prob. Hematite).
MRE01049	P_24	583292	4078567	Very silicified rock with some hematite. Small outcrops.
MRE01050	P_25	583237	4078377	Volcaniclastic with Qtz Xls. White color because of argillization to Kaol-Alun.
MRE01051	P_26	583267	4078307	Probably a lithic tuff with siliceous fragments and greenish color. Probably propylitic alteration
MRE01052	P_27	583155	4078106	Volcaniclastite of fine to medium grain. FeOx stain and some greenish alteration not very strong.
MRE01053	P_28	583236	4077924	Ryolitic tuff or ignimbrite with abundant Qtz and Felds Xls and some micas. Almost unaltered. Just plagioclases are whitish
MRE01054	P_29	583180	4077721	Volcaniclastic with just slight alteration. Qtz+Felds+some micas Xls.
MRE01055	P_30	583128	4077539	Volcaniclastic (Qtz+Plag+Micas). Some disseminated points of hematite. Plagioclase slightly argillized.
MRE01056	P_31	583148	4077361	Volcaniclastite. Part of the plagioclase crystals are argillized but most are fresh.
MRE01057	P_32	582550	4077414	Pyroclastite with abundant Qtz Xls and Plagioclases. The plagioclases are argillized to kaolinite or illite
MRE01058	P_33	582183	4077342	Pyroclastic rocks. Lithic tuff or ignimbrite. Some veinlets of Qtz. With crustiform texture.
MRE01059	P_34	582225	4077549	Volcaniclastic rock that is the host of a Qtz vein and stockwork (possibly of low sulfidation). Wide of about 2 to 3 m (vein+stockwork). There are crustiform textures with Qtz probably after calcite or adularia. Azimuth of vein=aprox 355°.
MRE01060	P_35	582305	4077748	Volcaniclastic with Qtz+Palg Xls. Part of the plagioclases are altered to white clay. The zone is an area of abundant veins and veinlets of Qtz (prob of low sulfidation).

continuation

MRE01061	P_36	582361	4078025	Pyroclastic, locally brecciated. Slightly altered.
MRE01070	P_37	583336	4079772	Argillized rock In open pit (P_38) as well
MRE01084	P_39	585080	4079274	Outcrop that could be a fragment in the pyroclastic rock (P-40, P_41, P_42 and P_43) as well
MRE01085	P_44	582216	4077362	Silicified rock with some Qtz veinlets
MRE01086	P_45	582206	4077387	Silicified volcanoclastic with Qtz veins. Colloform textures. Host rock slightly argillized.
MRE01087	P_46	582210	4077435	Volcanoclastite. Crossed by Qtz veinlets. Slightly argillized.
MRE01088	P_47	582202	4077484	Volcanoclastite. Silicified. Slightly argillized.
MRE01091	P_48	582261	4077509	Volcanoclastic crossed by Qtz veinlets.
MRE01092	P_49	582270	4077545	Volcanoclastic. Silicified.
MRE01093	P_50	582267	4077554	Volcanoclastic with scarce Qtz veinlets.
MRE02005	P_60	583581	4080620	Soil is greyish in colour and rocks are highly altered.
MRE02019	P_61	584428	4081025	Neogene volcanics which are felsic extrusives. The alteration is pervasive
MRE02020	P_62	584256	4080946	Strongly altered felsic extrusive volcanics with pervasive alteration. Chlorite, epidote, and feldspars present. Probably a propylitic alteration
MRE02021	P_63	584127	4080828	Strongly altered felsic extrusive volcanics with pervasive alteration. Chlorite, epidote, and feldspars present. Probably a propylitic alteration
MRE02022	P_64	583953	4080707	Highly altered felsic volcanics. Show pervasive alteration
MRE02023	P_65	583858	4080649	Highly altered volcanics. Possibly alunite. Show pervasive alteration and biotite is also present.
MRE02024	P_66	583770	4080531	Felsic altered volcanics showing pervasive alteration
MRE02025	P_67	583670	4080354	Felsic altered volcanics showing pervasive alteration
MRE02026	P_68	583527	4080215	Felsic altered volcanics showing pervasive alteration
MRE02027	P_69	583528	4080008	Highly altered felsic volcanics. Alteration is pervasive. Sample was taken from open pit and there are several underground workings around.
MRE02028	P_70	583614	4079820	Highly altered felsic volcanics. Alteration is pervasive. Sample was taken from open pit and there are several underground workings around. Quartz veins and chalcedony observed
MRE02029	P_71	583918	4079684	Highly altered felsic volcanics. Alteration is pervasive. Sample was taken from open pit and there are several underground workings around. Quartz veins and chalcedony observed

continue

MRE02030	P_72	583987	4079500	Highly altered felsic volcanics. Alteration is pervasive. Sample was taken from open pit and there are several underground workings around. Quartz veins and chalcedony observed
MRE02031	P_73	583956	4079303	Highly altered felsic volcanics. Alteration is pervasive. Sample was taken from open pit and there are several underground workings around. Quartz veins and chalcedony observed
MRE02033	P_74	583796	4078944	Felsic altered volcanics with pervasive alteration.
MRE02034	P_75	583607	4078893	Alteration is strong and pervasive. The felsic volcanics have a lot of quartz veins.
MRE02035	P_76	583398	4078972	Felsic altered volcanics with pervasive alteration.
MRE02036	P_77	580313	4079691	Weakly altered felsic intermediate volcanics. Conglomeritic heterogenous rocks
MRE02037	P_78	586630	4082274	Highly altered volcanoclastic rocks. Show pervasive alteration.
MRE02038	P_79	586660	4082319	Brecciated altered volcanics showing pervasive alteration.
MRE02039	P_80	586671	4082323	Weakly altered volcanics. Dark in colour with a lot of quartz grains. Show pervasive alteration
MRE02040	P_81	586711	4082384	Weakly altered volcanics. Dark in colour with a lot of quartz grains. Show pervasive alteration
MRE02041	P_82	586694	4082422	Weakly altered volcanics. Dark in colour with a lot of quartz grains. Show pervasive alteration
MRE02042	P_83	585168	4081803	Weakly altered volcanics. Dark in colour with a lot of quartz grains. Show pervasive alteration
MRE02043	P_84	585128	4081859	Weakly altered volcanics. Show pervasive alteration
MRE02053	P_85	583595	4079841	Altered felsic volcanics. Alteration is pervasive. Sample was taken from open pit and there are several underground workings around. (P_86 and P_87) as well
MRE02055	P_88	586962	4079992	Highly altered felsic volcanics. Alteration is pervasive. Sample was taken from open pit and there are several underground workings around. (P_89) as well